Vol. 158 No. 1, April 1, 1984 ISSN 0003-2670

ANALYTICA CHIMICA ACTA

International journal devoted to all branches of analytical chemistry

ELSEVIER

ANALYTICA CHIMICA ACTA

International journal devoted to all branches of analytical chemistry
Revue internationale consacrée à tous les domaines de la chimie analytique
Internationale Zeitschrift für alle Gebiete der analytischen Chemie

PUBLICATION SCHEDULE FOR 1984

	J	F	M	A	M	J	J	A	S	O	N	D
Analytica Chimica Acta	156	157/1	157/2	158/1 158/2	159	160	161	162	163	164	165	166

Scope. *Analytica Chimica Acta* publishes original papers, short communications, and reviews dealing with ever aspect of modern chemical analysis, both fundamental and applied.

Submission of Papers. Manuscripts (three copies) should be submitted as designated below for rapid and efficien handling:

Papers from the Americas to: Professor Harry L. Pardue, Department of Chemistry, Purdue University, West Lafayette IN 47907, U.S.A.

Papers from all other countries to: Dr. A. M. G. Macdonald, Department of Chemistry, The University, P.O. Box 363 Birmingham B15 2TT, England. Papers dealing particularly with computer techniques to: Professor J. T. Clerc Universität Bern, Pharmazeutisches Institut, Baltzerstrasse 5, CH-3012 Bern, Switzerland.

Submission of an article is understood to imply that the article is original and unpublished and is not being considere for publication elsewhere. Upon acceptance of an article by the journal, authors will be asked to transfer the copyrigh of the article to the publisher. This transfer will ensure the widest dissemination of information.

Information for Authors. Papers in English, French and German are published. There are no page charges Manuscripts should conform in layout and style to the papers published in this Volume. Authors should consul Vol. 150/2 for detailed information. Reprints of this information are available from the Editors or from: Elsevier Editoria Services Ltd., Mayfield House, 256 Banbury Road, Oxford OX2 7DH (Great Britain).

Reprints. Fifty reprints will be supplied free of charge. Additional reprints (minimum 100) can be ordered. An orde form containing price quotations will be sent to the authors together with the proofs of their article.

Advertisements. Advertisement rates are available from the publisher.

Subscriptions. Subscriptions should be sent to: Elsevier Science Publishers B.V., Journals Department, P.O. Bo 211, 1000 AE Amsterdam, The Netherlands. Tel: 5803 911, Telex: 18582.

Publication. *Analytica Chimica Acta* appears in 11 volumes in 1984. The subscription for 1984 (Vols. 156–166) i Dfl. 2145.00 plus Dfl. 231.00 (p.p.h.) (total approx. U.S. $950.40). All earlier volumes (Vols. 1–155) except Vols. 2 and 28 are available at Dfl. 200.00 (U.S. $80.00), plus Dfl. 15.00 (U.S. $6.00) p.p.h., per volume.

Our p.p.h. (postage, packing and handling) charge includes surface delivery of all issues, except to subscribers i Australia, Brasil, Canada, China, Hong Kong, India, Israel, Japan, Malaysia, New Zealand, Pakistan, Singapore, Soutl Africa, South Korea, Taiwan and the U.S.A. who receive all issues by air delivery (S.A.L. — Surface Air Lifted) at n extra cost. For the rest of the world, airmail and S.A.L. charges are available upon request.

Claims for issues not received should be made within three months of publication of the issues. If not they cannot b honoured free of charge.

For further information, or a free sample copy of this or any other Elsevier Science Publishers journal, readers in th U.S.A. and Canada can contact the following address: Elsevier Science Publishing Co., Inc., Journal Informatio Center, 52 Vanderbilt Avenue, New York, NY 10017, U.S.A., Tel: (212) 867-9040.

Modern Liquid Chromatography of Macromolecules

by **B.G. BELENKII** and **L.Z. VILENCHIK,** Institute of Macromolecular Compounds, Academy of Sciences of the USSR, Leningrad, USSR

JOURNAL OF CHROMATOGRAPHY LIBRARY, 25

Researchers, technologists and students in the fields of physics, chemistry, biology and medicine will all find this book of interest. It considers the chromatography of high-molecular-weight compounds and its main theoretical and methodological features.

Recommendations are made for preparing high-performance chromatographic systems and for selecting the optimum conditions for their operation. Particular attention is paid to the problems of interpreting chromatographic data in order to obtain various molecular-weight and structural characteristics of the macromolecules investigated: AMW, MWD, indices of polymer branching, the compositional homogeneity of copolymers, the functionality of oligomers, etc. The authors also provide examples of various combinations of chromatographic and other methods that can be used to analyse complex polymer systems.

Written mainly for the reader who has some practical experience in chromatography, the book also contains much useful information for the beginner.

CONTENTS: Chapter I. General Theory of Chromatography. II. Main Features of the Chromatography of Macromolecules. III. Interpretation of Data on the Analysis of Polymers by Gel Chromatography. IV. Methodological Problems of Gel-Permeation Chromatography (GPC). V. Use of Gel-Permeation Chromatography for the Analysis of Macromolecules, Investigation of their Interaction and the Characterization of the Porous Structure of Sorbents. VI. High Performance Gel-Filtration Chromatography (HPGTC). VII. Thin-Layer Chromatography of Polymers. VIII. One-Phase Chromatography: Field Fractionation and Hydrodynamic Chromatography.

1984 xviii + 432 pages
US $ 100.00 (USA & Canada);
Dfl. 260.00 (Rest of the World)
ISBN 0-444-42075-4

Elsevier

P.O. Box 211
1000 AE Amsterdam
The Netherlands

P.O. Box 1663
Grand Central Station
New York, NY 10163

ANALYTICA CHIMICA ACTA
VOL. 158 (1984)

ANALYTICA CHIMICA ACTA

International journal devoted to all branches of analytical chemistry

ELSEVIER Amsterdam–Oxford–New York–Tokyo

0003-2670/84/$03.0

Printed in The Netherlands

Analytica Chimica Acta, 158 (1984) 1—13
Elsevier Science Publishers B.V., Amsterdam — Printed in The Netherlands

THE USE OF A ROTATING LEAD-DISK ELECTRODE FOR ELECTROANALYTICAL PURPOSES

STANLEY BRUCKENSTEIN* and ROBERT F. MACK

Chemistry Department, State University of New York at Buffalo, Buffalo, NY 14214 (U.S.A.)

(Received 30th August 1983)

SUMMARY

The behavior of lead as an electrode material for electroanalytical purposes was studied in 1.0 M sulfuric acid. The useful negative range of potential was approximately −0.57 to −1.20 V vs. SCE for conventional voltammetry at a rotating disk electrode. For the sinusoidal hydrodynamic modulation technique, the negative limit was about −1.25 V. Studies of the reduction of cadmium ion, thallium(I) ion, and *p*-nitroaniline showed that the behavior of a rotating lead-disk electrode was comparable to that expected on the basis of theory. Limits of detection are in the micromolar range.

Lead has been used as an electrode material in batteries as well as for other electrochemical processes such as electrowinning, electrosynthesis, and electrodeposition. Because of the many uses of lead and the complexity of the lead-sulfate system, there is a vast amount of information on the electrochemistry of this system. Several comprehensive reviews have been published [1—4]. There is, however, no mention in the literature of lead as an electrode material used purely for electroanalytical purposes.

Most electrochemical determinations at very negative potentials are done with mercury, mercury film, wax-impregnated carbon, or carbon paste electrodes. Pyrolytic graphite and glassy carbon electrodes do not have hydrogen overpotentials as large as these electrodes [5]. Rotating disk mercury film electrodes, at reasonably high electrode rotation speeds, are subject to distortion of the film by centrifugal forces [6] while carbon electrodes have residual currents which raise the detection limits for ordinary trace analysis [5].

An electrode material with a very high hydrogen overpotential which can be used in the form of a solid rotating disk electrode is needed. This study was conducted to determine whether a lead-disk electrode would have any advantages over the carbon or mercury film electrodes which are currently used for studies at very high negative potentials.

Table 1 lists several electrode materials and their hydrogen overpotentials determined in 1.0 M sulfuric acid at a current density of 0.1 A cm^{-2} [7]. Tin, lead, cadmium and mercury all have similar hydrogen overpotentials.

0003-2670/84/$03.00

TABLE 1

Hydrogen overpotentials of several metals [7] (Current density = 0.1 A cm^{-2})

Cathode	Overpotential (V)	Cathode	Overpotential (V)	Cathode	Overpotential (V)
Nickel	0.7	Gold	1.0	Cadmium	1.22
Copper	0.8	Tin	1.2	Mercury	1.3
Silver	0.9	Lead	1.2		

It was decided to study lead instead of tin and cadmium for two reasons. First, the lead electrode has been well characterized because of its use in the lead-acid battery as well as its other electrochemical applications while tin and cadmium are not as widely used as electrode materials. Secondly, lead can also be used over a larger total potential range than tin and cadmium [8].

Because lead has a hydrogen overpotential similar to mercury, it was decided to test the quantitative utility of the rotating lead-disk electrode by determining the diffusion coefficients and detection limits for several species which have been studied previously using mercury electrodes.

Cadmium and thallium compounds are well-suited for polarographic determinations. The electrochemistry of cadmium has been reviewed by Hamson and Latham [9], and the two-electrode reduction of cadmium yields a reversible, well-defined wave in alkaline, acid, and neutral solutions. Also, a comprehensive review of the electrochemistry of thallium has been presented by Bellavance and Miller [10]. The one-electron reduction of thallium-(I) ion is reversible, well-defined and within the potential range of the lead electrode.

p-Nitroaniline is reported to be reduced reversibly by a six-electron process over the entire pH range [11]. Others have confirmed this observation at mercury and carbon electrodes [12—14].

Thus the cadmium, thallium, and *p*-nitroaniline systems were chosen as models to examine the behavior of the rotating lead-disk electrode.

EXPERIMENTAL

Chemicals

Reagent-grade $3CdSO_4 \cdot 8H_2O$ and Tl_2SO_4 (Fisher Scientific Co.) were used. The $3CdSO_4 \cdot 8H_2O$ was used to prepare cadmium solutions of approximate concentration. No quantitative values were determined from the investigation of cadmium. The purity of Tl_2SO_4 was 99.5%. Sulfuric acid (J. T. Baker Chemical Co.) used in supporting electrolyte solutions was of analytical grade. All water was distilled and passed through a Millipore Milli-Q water system immediately before use. *p*-Nitroaniline (Aldrich Chemical Co.) was used as received.

Lead electrodes

Lead-disk electrodes were constructed using m5n5-purity lead ingot (Alfa Division, Ventron Corporation). A 0.25-in. diameter disk was punched from a 0.25—0.40-in. thick slice of the lead ingot. This disk was then attached to a 0.188-in. diameter, 9.5-in. long stainless steel rod. First, one end of the rod was treated with liquid soldering flux (No. 11; Oatey Company, Cleveland, OH). The lead disk was then soldered to the treated end using lead-tin solder. Lead and solder protruding over the edge of the rod were turned down to the diameter of the rod. This electrode assembly was then degreased by suspending it in boiling, soapy water for several minutes. After the electrode had been cooled and rinsed with deionized water, the lower 0.5 in. of the tip was dipped five times into Fluorad FC-721, a non-wetting fluorochemical protective coating (Commercial Chemicals Division, 3M Company). The fluorocarbon coating was then cured for 15 min at 90°C. A teflon sheath (2 in. long and 0.4 in. o.d.) was drilled undersize, heated to 200°C, and press-fitted over the electrode assembly. Excess teflon was faced off the end after it had cooled to room temperature.

The lead electrode surface was very carefully polished flush with the teflon sheath surface using a polishing wheel and microcloth (Buehler, Evanston, IL). Deionized water was used on the microcloth without abrasive. Abrasive would have been imbedded in the soft lead surface.

Four lead electrodes were constructed. One of these was amalgamated as described below.

The lead-disk electrode used in the hydrogen overpotential studies had an area of 0.1762 cm^2, that used in the cadmium and thallium studies had an area of 0.1839 cm^2, and that used to study *p*-nitroanaline had an area of 0.1819 cm^2.

Lead-amalgam disk electrode. Two methods of amalgamating the lead disk were used. The first involved the plating of mercury onto the lead surface from a 1.0 mM mercury(II) nitrate solution in a 0.1 M nitric acid supporting electrolyte. The potential used was —1.0 V which produced a cathodic current of 175 μA when the disk was rotated at 3600 rpm. Lead dissolution occurs at potentials more positive than —0.5 V under these conditions. Various plating times were used to produce the desired layer of mercury.

In the second method, the lead electrode was dipped into mercury for 1—2 min. This method quickly produced a thick layer of mercury on the lead disk. Triple-distilled mercury was used (Bethlehem Apparatus Co.). After an amalgamated electrode had been used for a few hours, enough mercury would diffuse into the lead disk to make it necessary to replenish the mercury. This effect occurred more quickly on electrodes having the thinnest mercury film. For this reason, the second method of mercury deposition seemed preferable since a thicker film is formed more quickly and easily.

After a mercury film had been formed several times at a lead disk, the amalgam surface became recessed below the protective teflon sheath. When this occurred, the sheath was again turned flush with the disk surface.

The surface area of the amalgamated lead-disk electrode was 0.1734 cm^2.

Lead electrode pretreatment. The hydrogen overpotential characteristics of the rotating lead-disk electrode depend upon the history of the electrode surface. The lead-disk electrode was hand-polished with a Buehler microcloth and deionized water before use. Cycling the electrode potential increased the hydrogen overpotential dramatically. The lead electrode was cycled between −0.8 V and the hydrogen evolution region, and the negative potential limit was extended as the hydrogen overpotential increased. In some instances, it took as long as 24 h to obtain a constant hydrogen overpotential. This large hydrogen overpotential could then be greatly reduced by setting the positive potential limit of the potential cycle positive of −0.5 V, the potential required for lead dissolution. Then the hydrogen overpotential on the next cathodic potential sweep could be several hundred millivolt less negative than the hydrogen overpotential observed in the previous potential cycle. The potential shift depended upon the solution in which the electrode was potential-cycled. At this point, the only way to restore the large hydrogen overpotential was to cycle the electrode potential for an extended period of time, being certain to reverse the scan direction negative of the lead dissolution potential. To avoid the need for extensive potential cycling of the lead electrode between experiments, the lead electrode was stored submerged in deionized water.

Gold-disk electrode

The gold-disk electrode used was of the same general physical dimensions as the lead electrodes discussed above. It had an area of 0.1819 cm^2. It was polished by conventional metallurgical techniques, finishing with 0.03-μm alumina. Between experiments it was repolished with 0.03-μm alumina. The electrode was potential-cycled between the hydrogen and oxygen evolution regions until a reproducible current/potential curve was obtained in each solution that was studied.

Procedures

Electrolysis cell, potentiostat, and associated equipment. The three-electrode potentiostat, potential ramp and electrolysis cell used in this study have been described [15] as have the electronics and rotator for the modulation technique [16]. A Princeton Applied Research Model 129A lock-in amplifier was used. All potentials are reported with respect to the saturated calomel electrode.

Modulation technique. Modulated current/potential curves were obtained using the sinusoidal hydrodynamic modulation technique. In this technique, the speed of the rotating disk electrode is modulated in a sinusoidal fashion by combining an a.c. signal of small amplitude with the much larger d.c. signal which drives the electrode rotator. The current/potential response has an a.c. as well as d.c. component. The a.c. component, which contains only currents having a convective diffusion-controlled component, can be separated from the d.c. current component using a lock-in amplifier. A description of

the theory of the modulation technique, and its practice can be found elsewhere [16—19].

Measurement of diffusion coefficients. Plots of limiting current vs. the square root of the electrode rotation speed were obtained at constant rotation speed and constant applied potential on the limiting current region. If the concentration of electroactive species was not varied in the experiment, the limiting current was recorded for selected rotation speeds between approximately 400 to 8100 rpm. If the concentration of electroactive species was varied, a rotation speed of 2500 rpm was used. Data were fitted to a linear least-squares model and in all cases the intercept was zero within the experimental error. All uncertainty values listed are 90% confidence limits.

RESULTS AND DISCUSSION

Current-potential characteristics of the lead-disk electrode

Characteristics reported in the literature. The pH/potential characteristics of the lead electrode in sulfuric acid are well-studied. Ruetschi and Angstadt [20] gave a Pourbaix diagram of the lead-sulfate system as determined from constant potential experiments. This study was an extension of work previously done by Delahay et al. [21]. In 1.0 M sulfuric acid, the electrode surface exists as lead metal from approximately —0.55 V to the cathodic potential limit. The electrode surface is coated with lead sulfate between —0.55 V and 1.35 V, whereas lead dioxide coats the electrode surface from 1.35 V to the anodic limit. Table 2 lists the electrochemically important reactions and the calculated potentials (vs. SCE) at which they occur in 1.0 M sulfuric acid, which were determined by Young et al. [22] using Raman spectroscopy.

Other investigators have since reported the existence of numerous additional lead species present on the lead electrode surface at various potentials. Ruetschi and Angstadt [20] reported that a pH gradient is established in the lead-sulfate layer bacause of the inhibited migration of sulfate through the lead-sulfate layer. Pavlov [23] proved that lead hydroxides are formed at the electrode surface because of the pH gradient which is established in the

TABLE 2

Electrochemically important reactions of lead in 1.0 M sulfuric acid [3] ($[H^+]$ = 1.28 M, $[HSO_4^-]$ = 0.72 M, $[SO_4^{2-}]$ = 0.28 M)

1.	$PbSO_4 + H^+ + 2e^- = Pb + HSO_4^-$
	$E = -0.302 - 0.242 - 0.02958\log([HSO_4^-]/[H^+])$
2.	$PbSO_4 + 2e^- = Pb + SO_4^{2-}$
	$E = -0.356 - 0.242 - 0.02958\log[SO_4^{2-}]$
3.	$PbO_2 + HSO_4^- + 3H^+ + 2e^- = PbSO_4 + 2H_2O$
	$E = 1.628 - 0.242 + 0.02958\log([HSO_4^-][H^+]^3)$
4.	$PbO_2 + SO_4^{2-} + 4H^+ + 2e^- = PbSO_4 + 2H_2O$
	$E = 1.685 - 0.242 + 0.02958\log([SO_4^{2-}][H^+]^4)$

dense lead-sulfate layer. Pavlov et al. [24] later reported that small amounts of $4PbO \cdot PbSO_4$, $3PbO \cdot PbSO_4 \cdot H_2O$, and $PbO \cdot PbSO_4$ also form at a finite rate. Their conclusions were drawn from x-ray data.

Results. A current/potential curve of the rotating lead-disk electrode in 1.0 M H_2SO_4 is presented in Fig. 1. The initial anodic process in the negative to positive potential sweep occurs at —0.55 V and is the dissolution of lead to Pb^{2+} followed by the formation of a lead sulfate surface layer. This layer prevents further lead dissolution and causes the anodic current to return to the residual value. This anodic current peak starting at —0.55 V represents the same process investigated by other researchers [25—28]. Archdale and Harrison [27], using a rotating lead-ring/lead-disk electrode, concluded that lead dissolves as Pb^{2+} at low anodic potentials, while at higher anodic potentials, solid lead sulfate is formed by a solid-state reaction.

Figure 2 is a sinusoidally hydrodynamic modulated (SHM) current/potential curve, and the modulated anodic current peak appears at —0.55 V. In the SHM method, a modulated current response is produced only for processes under (partial) mass-transport control. Oxidation processes are distinguished from reduction processes in SHM current/potential curves using phase angle/potential data. This —0.55-V peak occurs in the potential region that corresponds to the dissolution of lead from the electrode surface. The modulated

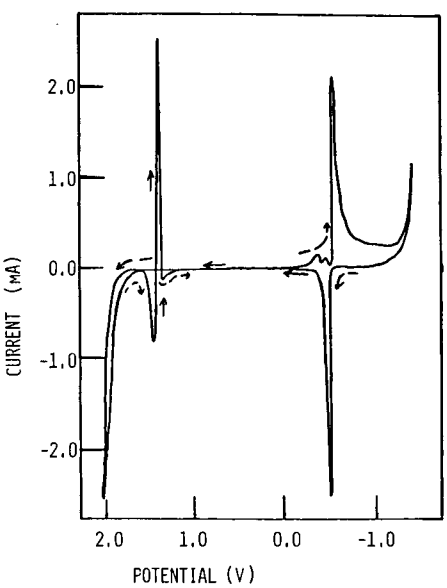

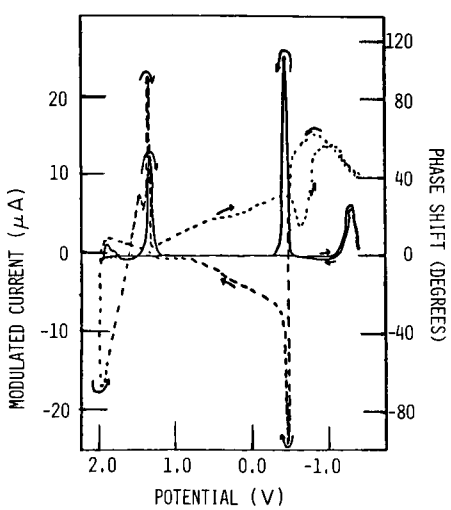

Fig. 1. Current/potential curve of the lead RDE in 1.0 M H_2SO_4. Potential scan rate 5 mV s^{-1}; $\omega^{1/2}$ = 70.82 $rpm^{1/2}$.

Fig. 2. SHM current/potential curve of the lead RDE in 1.0 M H_2SO_4. Potential scan rate 5 mV s^{-1}; $\omega^{1/2}$ = 70.00 $rpm^{1/2}$; amplitude, 1.0 $rpm^{1/2}$; p = 0.1. (—) SHM current/potential curve; (----) phase shift/potential curve.

current also returns quickly to zero indicating that the process has ended very abruptly. These results are consistent with the findings of previous investigators who concluded that lead dissolves as a soluble lead complex until lead sulfate completely covers the lead electrode surface [3]. The dissolution of lead as a lead complex in the absence of significant electrode kinetic complications, followed by filming would produce a SHM anodic current peak as is seen at —0.55 V.

The next anodic current appearing in the sweep to positive potentials occurs at 1.70 V (Fig. 1). If the potential is scanned slightly positive of 1.70 V, gas bubbles form on the electrode surface. Pavlov and Iordanov [29] reported that oxygen evolution begins at about 1.60 V in 1 M sulfuric acid, and it appears that some of the anodic current appearing at 1.70 V is due to oxygen evolution.

On the scan to negative potentials (Fig. 1), an anodic current peak is first noticed at 1.45 V. This current is immediately followed by a much larger cathodic current peak at 1.35 V and by another small anodic current peak at 1.10 V. The SHM current/potential curve (Fig. 2) indicates which, if any, of these current processes result in the dissolution of lead.

A SHM current peak appears on the scan to negative potentials at 1.35 V; its phase angle is 180° out of phase with the SHM anodic current peak at —0.5 V, and therefore, is a SHM cathodic current peak. This current peak is probably the reduction of lead dioxide to lead(II) ions which react to form a lead sulfate surface layer. Because there is no oxidation current in the scan to positive potentials in this region, other than at 1.70 V, the formation of lead dioxide must occur in this region.

In Fig. 3, the sweep to positive potentials was stopped at 1.45 V before the oxygen evolution process could begin. On the reverse potential sweep,

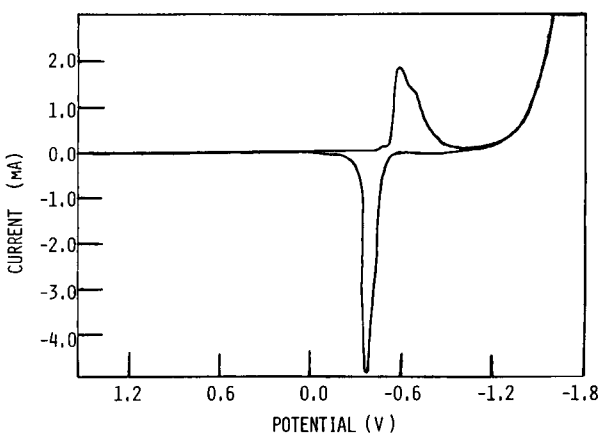

Fig. 3. Current/potential curve of the lead RDE in 1.0 M H_2SO_4. Potential scan rate 5 mV s^{-1}; $\omega^{1/2}$ = 50.35 $rpm^{1/2}$.

the current peaks seen in Fig. 1 between 1.45 and 1.10 V were not observed. Thus, these current peaks appear only after the electrode potential is made more positive than 1.45 V. This possibility was indicated in Fig. 1. Pavlov and Iordanov [29] also reported that the oxidation to lead dioxide is complicated by the evolution of oxygen. No further investigation was made of these processes because they occurred outside the potential range of present interest.

The cathodic current peak appearing in the —0.58 V region on the cathodic potential sweep in Figs. 1 and 3 does not appear in the SHM current/potential curve shown in Fig. 2. Hence this cathodic current peak results from a surface process. Conventional current/potential data were obtained in sweeps to both negative and positive potentials between —0.48 and —1.60 V. On the positive-going potential scan, an anodic current beginning —0.48 V corresponds to the start of the Pb to Pb^{2+} oxidation process. On the cathodic-going potential scan, the large cathodic current peak observed at —0.58 V in Figs. 1 and 3 no longer appears. Because this cathodic current peak appears only after the formation of the lead sulfate surface layer, and the SHM current/potential curve shows this peak to be purely a surface process, this cathodic current peak corresponds to the reduction of the lead sulfate layer to lead. This process occurs at the potentials calculated in Table 2 for reactions 1 and 2.

The large currents at the most negative potentials in Figs. 1—3 are caused by the production of hydrogen.

Current/potential characteristics of the lead-amalgam disk electrode

Archdale and Harrison [30] investigated the lead dissolution and the formation of lead sulfate, using an inverted dropping amalgam electrode. These authors examined the same processes on the rotating lead-ring/lead-disk electrode as previously reported [27]. The dissolution of lead occurred at the same potential on both the lead-disk and lead-amalgam electrodes. At both electrodes the electrochemical processes are the same.

The main objective of this investigation was to study the utility of a lead electrode at negative potentials; therefore the hydrogen overpotential characteristics of the lead-disk electrode had to be determined under ordinary electroanalytical conditions. It also seemed worthwhile to determine the effect of amalgamation on the behavior of lead.

Current/potential curves were obtained at a rotating lead-disk electrode and a lead-amalgam disk electrode in the same 1.0 M sulfuric acid solution. The hydrogen overpotential characteristics of the two electrodes were slightly different, with the lead electrode producing the more desirable result. Current/potential curves of the same electrodes were obtained in 1.0 M sodium sulfate solution. A cathodic wave was seen at —1.20 V and is believed to be due to the reduction of hydrogensulfate ions. This wave was not present when base was added to the solution. An extension of the cathodic

potential range was not achieved through amalgamation of the lead-disk electrode.

Studies of cadmium and thallium

A current/potential curve of a solution containing approximately 1 mM $CdSO_4$ in 1.0 M sulfuric acid electrolyte was obtained at the rotating lead-disk electrode. Figure 4 shows that the reduction wave of cadmium ion begins at about —0.8 V. The limiting current portion of this reduction wave is complicated by the reduction of the supporting electrolyte which begins at about —0.90 V. When the potential scan is reversed at —1.2 V, the current from cadmium ion reduction increases until a potential of —0.8 V is reached, and then the cadmium metal is oxidized from the lead electrode surface. These oxidation processes cause the stripping peak seen at about —0.70 V. The increase in reduction current when the electrode potential is reversed at —1.2 V is due to an increase in the electrode area associated with the plating cadmium. When smaller concentrations or faster potential scan rates were used, this phenomenon was not observed.

A SHM current/potential curve of approximately 1 mM $CdSO_4$ in 1.0 M sulfuric acid electrolyte is shown in Fig. 5. The peak occurring at —0.8 V is

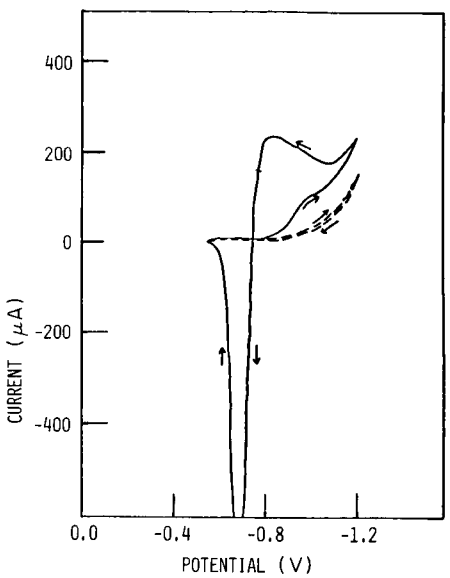

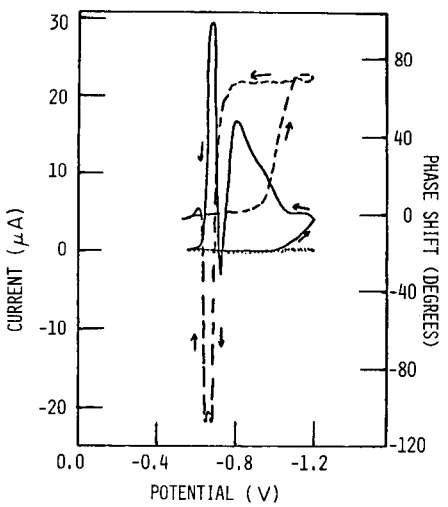

Fig. 4. Current/potential curve of ca. 1 mM $CdSO_4$ at the lead RDE. Potential scan rate 5 mV s^{-1}; $\omega^{1/2}$ = 50.72 $rpm^{1/2}$. (—) 1 mM $CdSO_4$ in 1.0 M H_2SO_4; (---) 1.0 M H_2SO_4.

Fig. 5. SHM current/potential curve of ca. 1 mM $CdSO_4$ at the lead RDE. Potential scan rate, 5 mV s^{-1}; $\omega^{1/2}$ = 50.00 $rpm^{1/2}$; amplitude, 1.0 $rpm^{1/2}$; p = 0.192. (—) SHM current/potential curve; (---) phase shift/potential curve; (•••) residual SHM current/potential curve.

due to the reduction of cadmium ion, while the peak at —0.70 V is due to the stripping of cadmium metal from the lead-disk surface. It can be seen from Fig. 5 that the modulation technique can also be used for anodic stripping voltammetry.

A current/potential curve of 1.0 mM thallium(I) sulfate in a 1.0 M sulfuric acid electrolyte was obtained at the rotating lead-disk electrode. The wave from thallium(I) reduction begins at about —0.7 V, while the anodic stripping of the plated thallium metal is seen in the anodic potential scan. When the potential scan is reversed in the hydrogen evolution region, the reduction current from thallium(I) increases until the stripping potential is reached. This peak can be eliminated by increasing the potential scan rate or reducing the electrode rotation speed, verifying that the peak is due to an increase in electrode area associated with the plated thallium. This peak is not seen with a ten-fold decrease in thallium(I) concentration, supporting the above conclusion.

A SHM current/potential curve of 1.0 mM thallium(I) sulfate in 1.0 M sulfuric acid is shown in Fig. 6. The current response is similar to the response in Fig. 5 for cadmium ion. The current occurring at potentials negative of —0.80 V is due to the reduction of thallium(I) while the current at potentials positive of —0.80 V is caused by oxidation of thallium metal from the lead electrode surface.

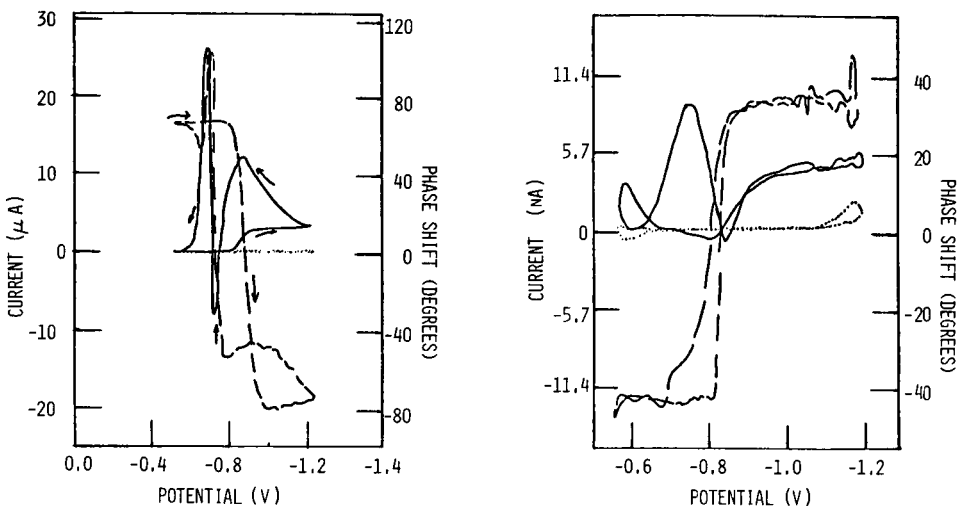

Fig. 6. SHM current/potential curve of 1.08 mM Tl_2SO_4. Potential scan rate, 5 mV s^{-1}; $\omega^{1/2}$ = 50.00 $rpm^{1/2}$; amplitude, 1.0 $rpm^{1/2}$; p = 0.192. (—) SHM current/potential curve; (---) phase shift/potential curve; (• • •) residual SHM current/potential curve.

Fig. 7. SHM current/potential curve of 1.08 μM Tl_2SO_4. Potential scan rate, 3 mV s^{-1}; $\omega^{1/2}$ = 48.30 $rpm^{1/2}$; amplitude, 1.36 $rpm^{1/2}$; p = 0.102 (—) SHM current/potential curve; (---) phase shift/potential curve; (• • •) residual SHM current/potential curve.

The SHM residual current/potential curve in Fig. 6 has no current response from hydrogen evolution over the same potential range where the conventional residual current/potential curve shows a response to hydrogen evolution.

One of the advantages of the modulation technique is the extended potential range in the hydrogen evolution region which is inherent in this method. This result is obtained because electrode kinetics, not mass transport, is rate-determining at the lead electrode for the hydrogen evolution process.

Figure 7 shows the SHM current/potential curves of 1.08 μM thallium(I) sulfate in 1.0 M sulfuric acid. In the conventional current/potential curve, no cathodic current is detected above the residual value. However, a small anodic stripping peak is observed. The reduction wave in the SHM current/potential curve (Fig. 7) is still well-defined at this amplitude of SHM. This result demonstrates that the behavior of the lead-disk electrode is comparable to the behavior observed at rotating disk electrodes fabricated from other materials, when these materials are used in their useful potential range [16].

In order to estimate the lower limit of detection for thallium(I) ion, it was necessary to determine its diffusion coefficient. This was done as described in the Experimental section. First, the diffusion coefficient was determined in a 0.533 mM Tl_2SO_4/1.0 M H_2SO_4 solution on the limiting current region at -1.10 V. Second, it was determined by varying the concentration of thallium(I) ion in the range 0.1—0.5 mM at a rotation speed of 4974 rpm, and measuring the limiting current. The mean value of the diffusion coefficient was calculated to be $1.43 \pm 0.08 \times 10^{-5}$ cm^2 s^{-1}. This value is to be compared with values of 1.65×10^{-5} cm^2 s^{-1} in 1.0 M KNO_3, and a 1.57×10^{-5} cm^2 s^{-1} and 1.50×10^{-5} cm^2 s^{-1} in 1 M KCl [10].

The residual current at the rotating lead-disk electrode in 1.0 M sulfuric acid was found to be 200 nA at -1.10 V. Using the above-determined diffusion coefficient, the detection limit for thallium(I) would be about 2.0×10^{-6} M.

For the conditions used in Figs. 6 and 7, it is possible to predict the modulated current response expected for thallium(I) ion and its phase shift with respect to rotation speed [17]. The Schmidt number was 640 and the p-value was 0.1 [17]. The predicted phase shift from these data was 33.9° and the experimental value reported was 36.4°. The predicted and observed values of the modulated limiting currents agree equally well, i.e., within 2%. These results clearly demonstrate that thallium(I) reduction proceeds reversibly at 1.0×10^{-6} M.

For an 8% SHM in the square root of rotation speed, the predicted detection limit is 2×10^{-7} M thallium(I). This prediction is consistent with the noise levels seen in the modulated current/potential curve of Fig. 7.

Studies of p-*nitroaniline*

The reduction of *p*-nitroaniline at a gold electrode in 1.0 M sulfuric acid begins at about 0.05 V, has a well-defined limiting current region about 0.15 V wide and continues into the hydrogen evolution region which starts at —0.35 V. A plot of the limiting current for *p*-nitroaniline reduction at —0.30 volt against the square root of rotation speed verified that its reduction is convective-diffusion controlled. The slope of the latter plot was $53.6 \pm 2.0\ \mu A\ mM^{-1}\ cm^{-2}\ rpm^{-1/2}$. The calculation of the diffusion coefficient requires a knowledge of the number of electrons involved in the convective-diffusion controlled process. A conventional logarithmic wave analysis of the *p*-nitroaniline reduction process at the gold electrode yielded a slope of 36.40 ± 0.40 mV/decade, suggesting that a two-electron quasi-reversible reaction occurs. On this basis, the calculated diffusion coefficient is $1.68 \times 10^{-5}\ cm^2\ s^{-1}$. Because the present goal was to compare the behavior of the *p*-nitroaniline reduction process at gold and lead rotating disk electrodes, only the magnitude of the current response is at issue. The difference between the present data and the literature data for the number of electrons involved in the reduction process for *p*-nitroaniline was not pursued [11—14].

In 1.0 M sulfuric acid, *p*-nitroaniline was reduced on lead metal over the entire potential range accessible to study, and the cathodic limiting current was flat over a 300-mV range. Hydrogen evolution became significant at —0.85 V.

In the potential region where the rotating lead-disk electrode was coated with lead sulfate, *p*-nitroanaline reduction did not occur. After lead sulfate had been formed on the electrode, the cathodic current accompanying *p*-nitroaniline reduction was complicated by the lead sulfate reduction process which produced a peak at —0.55 V.

The slope of a plot of limiting current at —0.80 V against the square root of rotation speed was $53.7 \pm 1.5\ \mu A\ cm^{-2}\ rpm^{-1/2}$ and had zero intercept. This value of the slope is in excellent agreement with that found with the rotating gold-disk electrode, and clearly the same process is occurring on lead and gold.

The estimated detection limit of *p*-nitroaniline at the rotating lead-disk electrode is about 0.6 μM at 4900 rpm.

This work was supported by the Air Force Office of Scientific Research under AFOSR Grants 78-3621 and 83-0004.

REFERENCES

1 G. W. Vinal, Storage Batteries, Wiley, New York, NY, 1955.
2 H. Bode, Lead-Acid Battery, Wiley-Interscience, New York, NY, 1977.
3 A. T. Kuhn, The Electrochemistry of Lead, Academic Press, New York, NY, 1979.
4 T. F. Sharp, in A. J. Bard (Ed.), Encyclopedia of Electrochemistry of the Elements, Vol. 1, M. Dekker, New York, NY, 1974, Ch. 5.
5 J.-P. Randin, in A. J. Bard (Ed.), Encyclopedia of Electrochemistry of the Elements, Vol. 7, M. Dekker, New York, NY, 1976, Ch. 1.

6 D. C. Johnson and P. R. Gaines, Anal. Chem., 45 (1969) 1670.
7 J. J. Lingane, Electroanalytical Chemistry, Interscience, New York, NY, 1958.
8 R. C. Weast (Ed.), Handbook of Chemistry and Physics, The Chemical and Rubber Co., Cleveland, OH, 1969.
9 N. A. Hamson and R. J. Latham, in A. J. Bard (Ed.), Encyclopedia of Electrochemistry of the Elements, Vol. 1, M. Dekker, New York, NY, 1973, Ch. 4.
10 M. I. Bellavance and B. Miller, in A. J. Bard (Ed.), Encyclopedia of Electrochemistry of the Elements, Vol. 4, M. Dekker, New York, NY, 1975, Ch. 4.
11 O. D. Shreve and E. C. Markham, J. Am. Chem. Soc., 71 (1949) 2993.
12 R. H. Philip, Jr., R. L. Flurry and R. A. Day, Jr., J. Electrochem. Soc., 111 (1964) 328.
13 C. Olson, H. Y. Lee and R. N. Adams, J. Electroanal. Chem., 2 (1961) 396.
14 H. B. Mark, Jr., E. M. Smith and C. N. Reilley, J. Electroanal. Chem., 3 (1962) 98.
15 P. R. Gifford, Ph.D. Thesis, State University of New York at Buffalo, Buffalo, NY, 1980.
16 B. Miller and S. Bruckenstein, Anal. Chem., 46 (1974) 2026.
17 K. Tokuda and S. Bruckenstein, J. Electrochem. Soc., 126 (1979) 431.
18 Y. Kanzaki and S. Bruckenstein, J. Electrochem. Soc., 126 (1979) 437.
19 W. J. Albery, A. R. Hillman and S. Bruckenstein, J. Electroanal. Chem., 100 (1979) 687.
20 P. Ruetschi and R. T. Angstadt, J. Electrochem. Soc., 111 (1964) 1323.
21 P. Delahay, M. Pourbaix and P. Van Rysselberghe, J. Electrochem. Soc., 98 (1951) 57.
22 T. F. Young, L. F. Maranville and H. M. Smith, in W. J. Hamer (Ed.), The Structure of Electrolyte Solutions, Wiley, New York, NY, 1959.
23 D. Pavlov, Ber. Bunseges, Phys. Chem., 71 (1967) 398.
24 D. Pavlov, C. N. Poulieff, E. Klaja and N. Iordanov, J. Electrochem. Soc., 116 (1969) 316.
25 A. N. Fleming and J. A. Harrison, Electrochim. Acta, 21 (1976) 905.
26 G. Archdale and J. A. Harrison, J. Electroanal. Chem., 34 (1972) 21.
27 G. Archdale and J. A. Harrison, J. Electroanal. Chem., 39 (1972) 357.
28 A. N. Fleming, J. A. Harrison and J. Thompson, in E. H. Collins (Ed.), Power Source 5, Academic Press, New York, NY, 1975.
29 D. Pavlov and N. Iordanov, J. Electrochem. Soc., 117 (1970) 1103.
30 G. Archdale and J. A. Harrison, J. Electroanal. Chem., 43 (1973) 321.

Analytica Chimica Acta, 158 (1984) 15—22
Elsevier Science Publishers B.V., Amsterdam — Printed in The Netherlands

CARBON PASTE ELECTRODES MODIFIED WITH CATION-EXCHANGE RESIN IN DIFFERENTIAL PULSE VOLTAMMETRY

J. WANG*, B. GREENE and C. MORGAN
Department of Chemistry, New Mexico State University, Las Cruces, NM 88003 (U.S.A.)
(Received 26th September 1983)

SUMMARY

Chemically modified carbon paste electrodes are prepared by incorporating appropriate quantities of a cation-exchange resin directly into the paste mixture. Ionic analytes can be preconcentrated on these electrodes by an ion-exchange reaction rather than electrolytic plating. Differential pulse voltammetry is used to quantify the accumulated ions. The response is characterized with respect to preconcentration period, bulk concentration, pH, paste composition, reproducibility, and other variables. Copper ion is used as a test system. The procedure exhibits good linearity for 6.25×10^{-5}—3.0×10^{-4} M copper(II) ions and the peak current varies linearly with preconcentration time between 1 and 7 min for the conditions used.

Chemically modified electrodes (c.m.e.) are the focus of considerable current research. Procedures for attaching a large array of molecules to a variety of electrode surfaces have been developed. Chemically modified electrodes have been used mainly for electrocatalytic, photosensitizing, and synthetic applications. This area of electrochemical research offers several unusual analytical possibilities. Various analytical applications of c.m.e. involving selective preconcentration, electrocatalysis, or electrode protection have been reported recently [1—5]. The present paper is concerned with the utilization of c.m.e. for providing alternative approaches for accumulating analytes on electrode surfaces, prior to their voltammetric measurement. Such accumulation can be achieved via a specific reaction between the analyte and a target molecule deliberately introduced on the surface. Various surface-modification procedures can be used for obtaining the specific response. A glassy carbon electrode coated with trioctylphosphine oxide has been used for the determination of uranyl ions after preconcentration [1]. Similarly, a carbon paste electrode containing an ethylenediamine group has been used to determine silver ions [2]. An allylamine-coated platinum electrode has been used to preconcentrate and quantify carbonyl-containing compounds [3].

This paper describes the behavior and use of a carbon paste electrode containing a cation-exchange resin. Various c.m.e. based on ion-containing polymers capable of extracting charged ions from the solution by means of

0003-2670/84/$03.00

electrostatic (ion-exchange) binding have been reported [6—8]. However, other types of c.m.e. containing ion-exchange sites have not been reported previously. Chemically modified carbon paste electrodes have been selected in the present study because they are easy to fabricate by adding the desired quantity of the modifier to the graphite/pasting liquid mixture. To date, various modifiers have been introduced to the paste composition aiming mainly for catalyzing various irreversible redox reductions [9]. In a similar way, ion-exchange resins can be incorporated directly into the paste mixture. Such incorporation results in an alternative approach for the accumulation of ions. For example, if a cation-exchange resin in the hydrogen ion form is used (such as the one employed in the present study) the preconcentration reaction is given by

$$n\overline{RSO_3^-H^+} + M^{n+} \rightleftharpoons \overline{(RSO_3^-)_n M^{n+}} + nH^+ \quad (1)$$

As in ion-exchange equilibria, the efficiency of the preconcentration step, and accordingly the sensitivity of the entire measurement scheme, depend upon the mass distribution ratio, D_m = amount of ion in electrode/amount of ion in solution.

Based on the relative affinities of the resin for ions, the resin-modified electrode would exhibit preference for ions of higher charge, smaller solvated volume, and greater polarizability. The resulting alternative approach for the accumulation of ionic analytes can expand the scope of stripping methods toward the measurement of analytes that cannot be preconcentrated electrolytically. In addition, when coupled with a medium-exchange procedure, a high degree of selectivity toward ionic analytes can be achieved in samples containing excess of nonionic electroactive species. The characteristics of the method are discussed below.

EXPERIMENTAL

Apparatus and reagents

Chemically modified carbon paste electrodes (36% resin by weight) were prepared by thoroughly hand-mixing 1.25 g of graphite powder (Acheson Graphite, Grade 38, Fisher), 1.5 g of silicone grease (Dow Corning), and 2.2 g of the swelled cation-exchange resin beads (Dowex CGC241-sulfonated polystyrene 8% XL). For swelling the beads, 1.8 g of the dry resin was immersed in 10 ml of water for 90 min, after which the excess water was removed. A portion of the paste was packed into the end of a glass tube (3-mm i.d., 5-mm o.d.) and its inner end was connected to a copper wire. Different amounts of the resin were used for evaluating the effect of the paste composition. A fresh carbon paste surface was used daily.

Three 50-ml cells were used. The preconcentration cell contained the sample solution under test; the measurement cell contained the supporting electrolyte solution; the cleaning cell contained 0.2 M hydrochloric acid. The Ag/AgCl (3 M NaCl) reference electrode, and the platinum wire auxiliary

electrode were placed in the measurement cell through holes in its cover. Differential pulse voltammograms were recorded with a Sargent-Welch Model 4001 polarograph. The experimental settings used were 1.0 V min^{-1} scan rate, 50 mV pulse amplitude, and 1 s repetition time.

Deionized water was used to prepare all solutions. Copper ion stock solution, 5×10^{-3} M, prepared by dissolving the metal in nitric acid and diluting as required, was stored in a polyethylene container. The supporting electrolyte was a 0.1 M sodium acetate solution adjusted to pH 6.8 with sodium hydroxide.

Procedure

For the preconcentration step, the modified carbon paste electrode was immersed in a stirred 50-ml sample solution for a given period of time; the preconcentration proceeded at open circuit. The electrode was then removed from the preconcentration cell, briefly rinsed with deionized water, and placed in an electrochemical cell containing a deaerated and quiescent supporting electrolyte solution. The initial potential 0.4 V, was then applied and after 45 s (for the current decay) the voltammogram was recorded by scanning the potential to —0.6 V. After the scan, the potential was returned to its initial value (for 3 s) before transferring the electrode to the cleaning cell for 2 min. A subsequent voltammetric run was used to verify the absence of trapped copper ions on the surface.

RESULTS AND DISCUSSION

The characteristics of the modified carbon paste electrode were evaluated with a strong acid sulfonated resin as the modifier and copper ion as the preconcentrated analyte. Figure 1 shows a differential pulse voltammogram which resulted when the ion-exchange resin containing modified carbon paste electrode, placed in a stirred 4×10^{-6} M copper solution for 10 min, was removed, washed and transferred to an electrolytic blank solution. Open-circuit conditions were used during the preconcentration period. Unlike anodic stripping voltammetry, a cathodic potential scan is used during the measurement step, as the accumulated species is a cation (Eqn. 1). The well-defined peak permits convenient quantitation at the micromolar concentration level. The peak potential for the trapped copper ion (—0.19 V) is similar to that of the dissolved ion (—0.2 V). Differences between the peak potentials of the dissolved and trapped ions have been reported [7]. Renewal of the surface is easily accomplished by immersing the electrode in 0.2 M hydrochloric acid for 2 min; the subsequent voltammetric run shows no copper peak. The effective cleaning and reproducible accumulation is illustrated by the precision obtained during continuous 84-min period of operation. A series of 12 repetitions with 5×10^{-4} M copper yielded a mean peak current of 20.7 μA, with a range of 18.6—21.5 μA and a relative standard deviation of 4%; three response curves are shown in Fig. 2. The precision

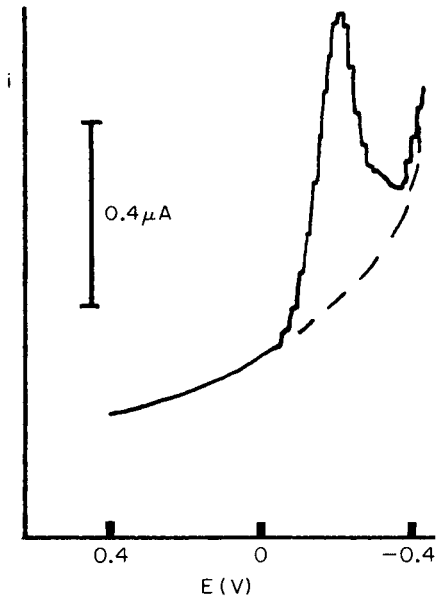

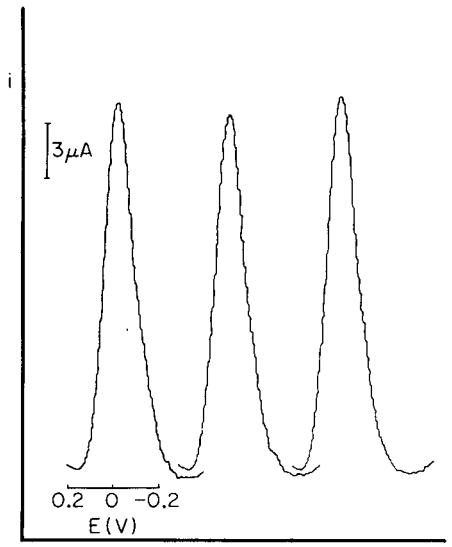

Fig. 1. Differential pulse voltammograms obtained after 10-min preconcentration from a 4×10^{-6} M Cu^{2+} solution, followed by exchange to the blank solution. Stirring rate (during preconcentration), 550 rpm. The dotted line represents the response after preconcentration from the blank solution.

Fig. 2. Differential pulse voltammograms obtained after 2-min preconcentration from a 5×10^{-4} M Cu^{2+} solution, followed by exchange to the blank solution. Stirring rate, 550 rpm. Three successive measurements from a series of twelve.

obtained with the ion-exchange accumulation scheme compares favorably with that reported for other nonelectrolytic preconcentration approaches [3, 10, 11]. These data indicate also the absence of losses of the copper ion during the medium-exchange. When electrolytic preconcentration (i.e., stripping voltammetry) is used, the transfer of the electrode from cell to cell is accompanied by partial reoxidation of the metals when the circuit is interrupted. Because the electrode is cleaned in a different cell, the precision data show that only a negligible fraction of the analyte is involved in the accumulation scheme; this is supported also by the concentration dependence study discussed below. Finally, the above experiments indicate that the electrode preparation results in a stable surface, with minimum leaching of the modifier to the surrounding solution.

The preconcentration of ionic analytes is easily seen from differential pulse voltammograms (Fig. 3) done with a carbon paste electrode which has been immersed in a stirred 2.0×10^{-4} M Cu^{2+} solution for increasing periods of time. The peak height increases with increasing preconcentration period. In contrast to other nonelectrolytic accumulation processes reported re-

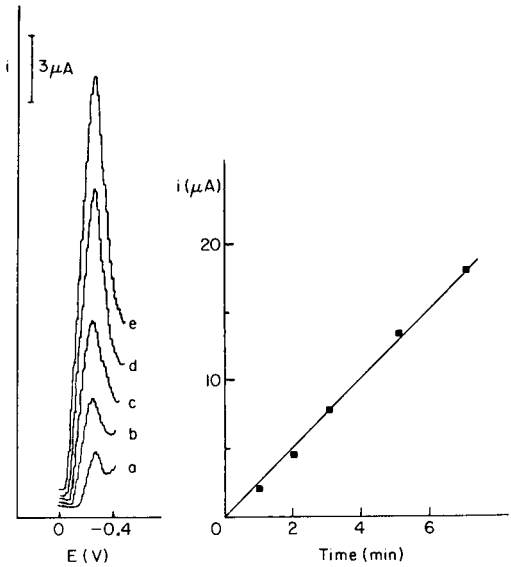

Fig. 3. Effect of preconcentration period on the differential pulse peak current from 2×10^{-4} M Cu^{2+} solution. Preconcentration period: (a) 1, (b) 2, (c) 3, (d) 5, (e) 7 min. Stirring rate, 550 rpm.

cently, the ion-exchange attachment yields a linear dependence between the peak current and the preconcentration period. As in conventional stripping methods, there would be a trade-off between the sensitivity and preconcentration time.

Further information regarding the nature of the accumulation process was obtained by studying the effects of the paste composition and pH. Figure 4 shows the effect of the paste composition on the preconcentration/voltammetric response. Carbon paste electrodes containing 0.5, 1.0, and 2.0 g of the resin (together with 1.25 g of graphite powder and 1.50 g of silicone grease) yielded peak currents of 3.4, 7.6 and 13.3 μA, respectively. Thus, as expected from the increased ion-exchange capacity of the electrode, the amount of copper ion accumulated and the corresponding peak current are proportional to the amount of resin in the paste. The exchange capacity of the electrode may be defined as the total number of equivalents of replaceable hydrogen per unit area of its surface. As indicated from Fig. 3, no saturation of the resin is obtained under the conditions of this study. It is possible that not all the accumulated ions are contributing to the voltammetric response. Only the trapped ions with direct access to the active graphite particles would participate in the redox reaction. Thus, effective mixing of the various components is desirable when preparing the carbon paste electrode. The rate of the redox reaction is probably limited by the slow diffusion from the interior of the ion-exchange bead to the carbon/solution interface.

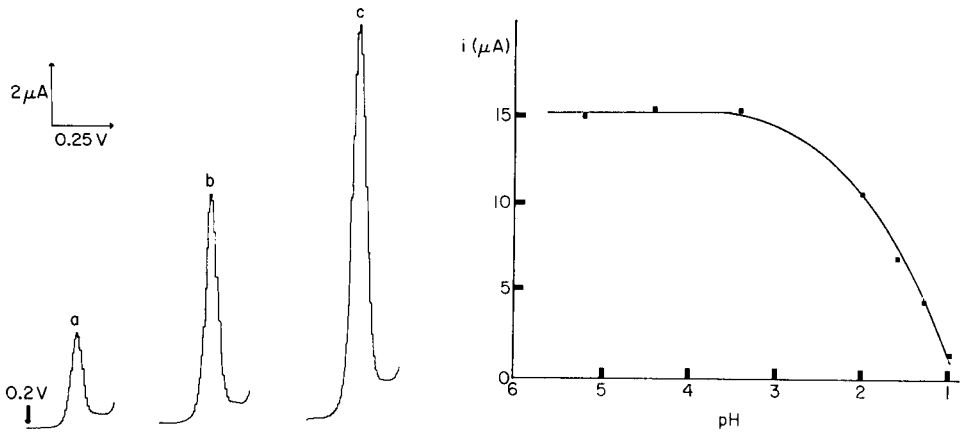

Fig. 4. Effect of carbon paste composition on the differential pulse peak current. Preconcentration for 3 min from a stirred (550 rpm) 2×10^{-4} M Cu^{2+} solution, followed by exchange to the blank solution. Amount of resin in paste: (a) 0.5, (b) 1.0, and (c) 2.0 g.

Fig. 5. Effect of sample pH on the differential pulse peak current. Conditions: 3-min preconcentration from a 2×10^{-4} M Cu^{2+} solution, followed by exchange to the blank solution. Stirring rate, 550 rpm.

Figure 5 shows the dependence of the differential pulse peak current on the pH of the sample solution. The peak current is unchanged at pH 3—5; at pH <3, the peak current gradually decreases until it disappears at pH <1. Electrodes containing different resin (e.g., weak acid) would exhibit different peak current/pH dependence. Variations in stirring rate during the preconcentration step did not alter the peak current. This indicates that other processes, probably the diffusion of the ion into the interior of the ion-exchange bead, control the preconcentration efficiency.

Figure 6 illustrates the preconcentration/medium exchange/differential pulse response to successive standard additions of copper; each addition corresponds to 6.25×10^{-5} M copper. Least-squares treatment of these data yielded the equation $I(\mu A) = (4.14 \pm 0.10)C(10^{-4}\ M) - (0.34 \pm 0.20)\ \mu A$ with the standard error $S_{yx} = 0.22\ \mu A$ and $r = 0.999$. In contrast to other nonelectrolytic preconcentration schemes [3, 11], the peak current is directly proportional to the bulk concentration of the analyte. At higher concentrations and/or longer preconcentration times, deviations from linearity may be obtained because of saturation of the fraction of the accessible resin. Slight variations in current were observed for different batches of the electrode containing the same amount of resin. Thus, the preparation of new calibration plots is recommended each time a new surface is used.

In conclusion, carbon paste electrodes modified with cation-exchange resin allow efficient preconcentration of copper(II) ions before their voltammetric measurement. The procedure is very simple, including the preparation of the electrodes. By using electrodes containing different resins and different

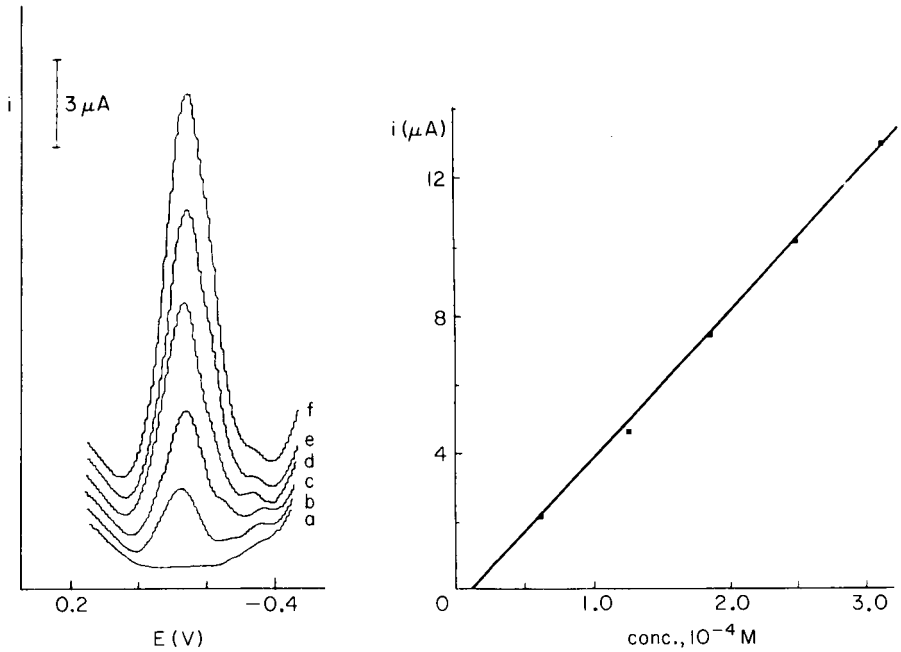

Fig. 6. Differential pulse voltammograms obtained with increasing copper concentrations (6.25×10^{-5} M steps). Preconcentration for 4 min with stirring at 550 rpm.

ratios of the various components it should be possible to select the desired voltammetric response. Future studies will include competitive partitioning experiments to evaluate selectivity in mixtures of ionic analytes. As in conventional ion-exchange equilibria, it is expected that the ratio of the distribution ratios would express the selectivity between various pairs of redox ions. Additional selectivity of the overall methodology is provided by the electroactivity of the analyte. Besides the quantitative significance associated with preconcentration/voltammetric scheme, these studies might allow the direct evaluation of the affinity of various resins for various metal ions.

This work was supported by a grant from the U.S. Department of the Interior through the New Mexico Water Resources Research Institute. C. Morgan acknowledges the financial support of the Crimson Scholar Program at NMSU.

REFERENCES

1 K. H. Lubert, M. Schnurrbusch and A. Thomas, Anal. Chim. Acta, 144 (1982) 123.
2 G. T. Cheek and R. F. Nelson, Anal. Lett., 11 (1978) 393.
3 J. F. Price and R. P. Baldwin, Anal. Chem., 52 (1980) 1940.
4 K. J. Stutts and R. M. Wightman, Anal. Chem., 55 (1983) 1576.
5 G. Sittampalam and G. S. Wilson, Anal. Chem., 55 (1983) 1608.

6 N. Oyama and F. C. Anson, J. Electrochem. Soc., 127 (1980) 247.
7 J. R. Schnelder and R. W. Murray, Anal. Chem., 54 (1982) 1508.
8 I. Rubenstein and A. J. Bard, J. Am. Chem. Soc., 102 (1980) 6641.
9 K. Ravichandran and R. P. Baldwin, J. Electroanal. Chem., 126 (1981) 293; Anal. Chem., 55 (1983) 1586.
10 J. Wang and B. A. Freiha, Anal. Chim. Acta, 148 (1983) 79.
11 H. Y. Cheng, L. Falat and R. L. Li, Anal. Chem., 54 (1982) 1384.

Analytica Chimica Acta, 158 (1984) 23—32
Elsevier Science Publishers B.V., Amsterdam — Printed in The Netherlands

VOLTAMMETRIC OXIDATION OF VINBLASTINE AND RELATED COMPOUNDS

JAMES F. RUSLING*, BARRY J. SCHEER and INAM U. HAQUE[a]
Department of Chemistry, U-60, University of Connecticut, Storrs, CT 06268 (U.S.A.)
(Received 2nd August 1983)

SUMMARY

The indole alkaloids, vinblastine, catharanthine, and vindoline, gave oxidation waves in mixed aqueous/organic media by cyclic, normal-pulse, and differential-pulse voltammetry (d.p.v.). Of the systems investigated, d.p.v. at carbon paste anodes in pH 5.6 acetate buffer in ethanol/water (1:1) is recommended for general analytical work; calibration graphs were linear up to about 1 mM, with limits of detection of 4, 20, and 1.5 μM for vinblastine, catharanthine, and vindoline, respectively. Results obtained by cyclic voltammetry as well as by pulse techniques suggest that electron transfer is preceded by deprotonation and followed by additional chemical reactions. Products of the electrode processes form mechanically unstable films on the electrode surface.

Vinblastine (VB) is a bisindole alkaloid used in the treatment of leukemia and Hodgkins disease [1]. The upper indole half of VB has a structure derived from that of catharanthine (CTH) and the lower dihydroindole half is vindoline (VDL). The determination of these compounds is important in

VB

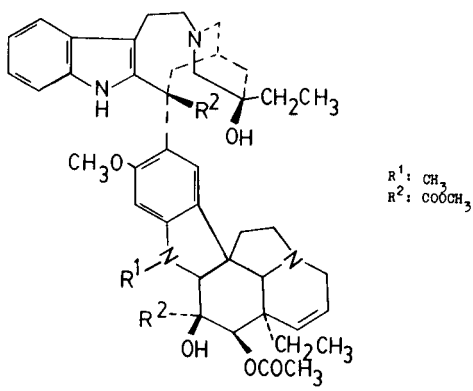

CTH

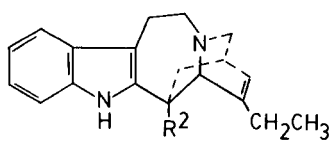

[a]Present address: Department of Chemistry, University of Engineering and Technology, Lahore-31, Pakistan.

0003-2670/84/$03.00

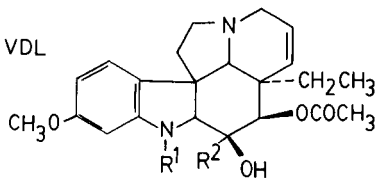

various clinical and biochemical applications. Recent reports describe determinations of VB, CTH, VDL and related alkaloids by radioimmunoassay [2], high-performance liquid chromatography (h.p.l.c.) [3, 4], thin-layer chromatography [5], and ultraviolet spectrophotometry [6]. However, quantitative applications of electrochemical oxidations of VB, CTH, and VDL appear not to have been explored. Tetrahydrocarbazoles with structures related to VB are oxidizable at carbon and platinum electrodes [7—9]. In 1958, Allen and Powell [10] oxidized structurally related iboga alkaloids at a rotating platinum electrode. This paper describes quantitative aspects of normal-pulse and differential-pulse voltammetric (n.p.v. and d.p.v.) oxidations of VB, CTH, and VDL at carbon paste electrodes. Cyclic voltammetry (c.v.) was used to aid in the interpretation of results.

EXPERIMENTAL

Chemicals and solutions

1,2,3,4-Tetrahydrocarbazole (THC; Aldrich Chemical Co.) and vinblastine sulfate (Sigma Chemical Co.) were used as received. Catharanthine hydrochloride, vindoline, 9-methyl-1,2,3,4-tetrahydrocarbazole (9-MeTHC), and *m*-dimethylaminoanisidine (*m*-DMAA) were gifts from J. M. Bobbitt, University of Connecticut. Ferrocene was a gift from S. L. Suib, University of Connecticut. Aniline (Baker Chemical Co.) was purified by distillation under reduced nitrogen pressure. *p*-Chloroaniline (Aldrich Chemical Co.) was purified by recrystallization from benzene. Acetonitrile (ACS reagent grade or spectro-grade) was used as received. All other chemicals were ACS reagent grade. Acetate buffers in ethanol/water (1:1) were prepared from sodium acetate and acetic acid to obtain the desired pH at a total buffer concentration of 0.1 M. Aqueous phosphate buffer, pH 6.4, was prepared from sodium dihydrogenphosphate and disodium hydrogenphosphate at a total buffer concentration of 0.2 M. Stock solutions of electroactive compounds (5—20 mM in the appropriate solvent) were stable at 5°C for at least one month.

Apparatus and procedures

A Princeton Applied Research Corp. (PARC) Model 174A Polarograph, a PARC Model 170 Electrochemistry System, and a Bioanalytical Systems BAS-100 Electrochemistry system were used for voltammetry by procedures described in detail previously [8]. Positive feedback compensation of ohmic drop was used for cyclic voltammograms with scan rates (v) greater than

0.5 V s^{-1}. The three-electrode cells used were a Metrohm cell and a Manoušek-type cell. In the Metrohm cell, a platinum counter electrode and, as reference, either a Ag/Ag^+ (0.001 M) (acetonitrile solutions) or a Ag/AgCl (aqueous media) was used. The Manoušek cell is a small H-cell containing a saturated calomel electrode (SCE) separated from the working electrode compartment by an agar/KCl salt bridge and a medium-porosity glass frit; the cell bottom is a mercury pool of adjustable height which also serves as the counter electrode. Use of this cell with 500-μl sample volumes gave results identical to those obtained with the Metrohm cell. For most experiments, carbon paste working electrodes (A = 0.08 cm^2 or 0.12 cm^2) were used, but glassy carbon (A = 0.07 cm^2) and platinum (A = 0.0012 cm^2) electrodes were used for some purposes. All working electrodes were disks surrounded by an outer layer of insulating material. Electrode construction and surface preparation have been previously described [8, 11]. Electrode surfaces were refinished prior to each voltammetric scan, unless noted otherwise. Assembled cells had resistances of about 500 ohm.

For the dependences of voltammetric behavior on scan rate, concentration, and pH, each value of peak potential and current was the average of at least two individual scans. All potentials are reported vs. SCE. Reproducibility of potential measurements in the Metrohm cells is illustrated by a standard deviation of the peak potential of ferrocene in 0.2 M lithium perchlorate in acetonitrile of ±1.0 mV during one day. In the Manousek cell, a standard deviation for the peak potential for oxidation of hexacyanoferrate(II) was ±1.1 mV over a similar period. Relative standard deviations of current measurements were better than 3% for d.p.v. and about 6% for normal pulse voltammetry (n.p.v.). Analyte solutions were purged with purified nitrogen [8] for 8—10 min prior to the beginning of an experiment.

RESULTS AND DISCUSSION

Analytical voltammetry

Buffered ethanol/water (1:1) solutions, unbuffered acetonitrile/water (9:1) containing 0.2 M lithium perchlorate, and aqueous phosphate buffers were initially investigated as electrolytes for electrochemical oxidation of the indole alkaloids. Although the three alkaloids gave oxidation waves in each electrolyte, vinblastine was insufficiently soluble to be conveniently studied in any except the ethanolic buffer. For this reason and because of inadequate solubilities of common buffer components such as alkali phosphates in ethanol/water, it was concluded that ethanolic acetate buffers would be the most useful of the electrolytes investigated for analytical work. In the pH range 3.6—5.6, a slight dependence of limiting and peak currents for the alkaloids on pH was obtained by n.p.v., d.p.v., and cyclic voltammetry (c.v.) with about 10% larger currents occurring at pH 5.6 than at pH 3.7.

Figures 1—3 show representative voltammograms. Catharanthine is oxidized

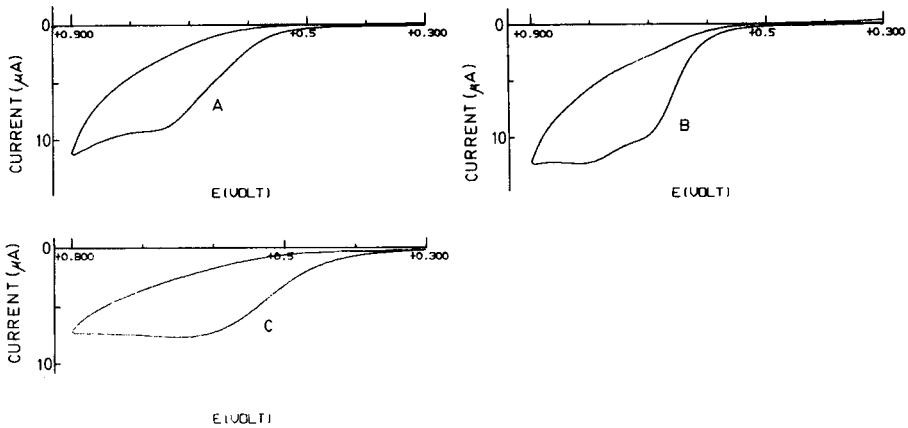

Fig. 1. Cyclic voltammograms at 100 mV s^{-1} on carbon paste in ethanolic acetate buffer, pH 5.6: (A) 0.42 mM vinblastine; (B) 0.42 mM vindoline; (C) 0.63 mM catharanthine.

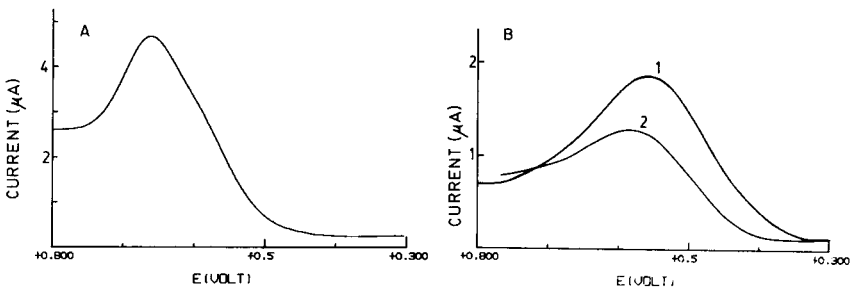

Fig. 2. Oxidation of (A) 0.42 mM vinblastine and (B) 0.63 mM catharanthine by d.p.v. (ΔE = 50 mV, v = 4 mV s^{-1}) on carbon paste in ethanolic acetate buffer, pH 5.6. For (B): (1) initial scan; (2) second scan on same electrode surface after a 5-min wait.

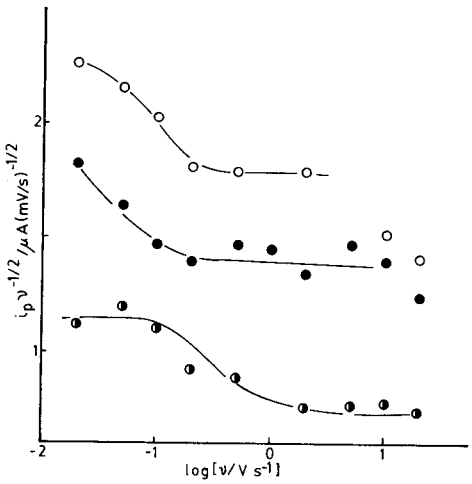

Fig. 3. Influence of cyclic voltammetric scan rate (v) on current function ($i_p v^{-1/2}$) at carbon paste electrodes in ethanolic acetate buffer, pH 5.6. (○) 0.93 mM vinblastine; (●) 0.83 mM vindoline; (◑) 0.83 mM catharanthine. Solid lines represent approximate shapes for partially blocked electrode model (cf. [17]).

at considerable less positive potentials than VB or VDL. Only in the case of catharanthine were well-defined waves obtained by n.p.v.; for the other two compounds, n.p.v. waves were overlapped with secondary waves and estimates of limiting current involved 6—8% uncertainty. However, the improved resolution afforded by d.p.v. led to quantitatively useful peaks for all three alkaloids. Linear calibration graphs were obtained by each of the voltammetric methods. The pulse techniques gave the best limits of detection and linear calibration curves from the micromolar to the millimolar concentration range (Table 1). Standard deviations of the parameters of the calibration graphs and correlation coefficients calculated by linear regression (Table 1) show that better precision was obtained by d.p.v. The shapes of oxidation curves of vinblastine (Figs. 1A and 2A) indicated severe overlap of two peaks. Limits of detection (S/N = 3) by d.p.v. for standard solutions of VB, CTH, and VDL were estimated at 4, 20, and 1.5 μM, respectively.

In n.p.v., the limiting current (i_l), and thus $i_l\,C^{-1}$, is proportional to the apparent number of electrons transferred, n(app). Values of $i_l\,C^{-1}$ for the first oxidation waves of the alkaloids were compared to $i_l\,C^{-1}$ for compounds of known electron transfer number (THC, 9-MeTHC [8], and *p*-chloroaniline [14], all n = 1) in the same electrolyte to estimate n(app). Because of the smaller molecular size of the standards, their diffusion coefficients are larger than those of VB, CTH, and VDL, and the values of n(app) in Table 2 can be considered slight underestimates.

Influence of acidity, concentration, and scan rate (in c.v.) on voltammetric behavior

Half-wave and peak potentials of the first oxidation waves of VB, CTH, and VDL shifted to more negative values (Table 2) as the acidity of the electrolyte solution was decreased (i.e., as pH increased). If it is assumed that

TABLE 1

Characteristics of linear regression of calibration graphs for indole alkaloids in ethanolic acetate buffer, pH 5.6

Compound	Linear range (mM)	N[a]	Slope (μA mM^{-1})	Intercept (μA)	SEE[b] (μA)	Corr. coeff.
Differential pulse voltammetry						
Vindoline	0.0019—1.5	13	26.1 ± 0.6	0.02 ± 0.40	0.86	0.9984
Catharanthine	0.052—1.5	13	13.9 ± 0.2	−0.34 ± 0.22	0.35	0.9991
Vinblastine	0.0065—0.5	6	29.3 ± 0.5	0.32 ± 0.10	0.19	0.9995
Normal pulse voltammetry						
Vindoline	0.015—1.5	12	59.1 ± 5.2	−1.8 ± 4.6	8.2	0.9630
Catharanthine	0.052—1.5	10	45.1 ± 1.4	−1.2 ± 1.0	1.2	0.9986
Vinblastine	0.017—0.86	6	91.2 ± 2.9	1.3 ± 1.2	2.2	0.9980

[a]Number of data points. [b]Standard error of estimate.

TABLE 2

Voltametric characteristics of alkaloids and related compounds[a]

Compound	Method/ medium[a]	n[b]	$\frac{dE_x}{d\log C}$[c] (mV)	$\frac{dE_x}{d\log v}$[d] (mV)	$\frac{dE_x}{dpH}$	$i_p v^{-1/2}$ for 0.02—50 V s^{-1}
Vinblastine	C.v./A		69 (0.1)[e]	33 (0.93)	−61	50% decrease
	N.p.v./A	2.0	55	—	−59	—
	D.p.v./A		16	—	−51	—
Vindoline	C.v./A		30 (0.2)	39 (0.83)	−61	40% decrease
			−27 (10)			
	N.p.v./A	1.3	66	—	−86	—
	D.p.v./A		44	—	−78	—
Catharanthine	C.v./A		86[g] (0.2)[e]	46 (0.81)	−55	40% decrease
	N.p.v./A	1.0	58[g]	—	−41	—
	D.p.v./A		67[g]	—	−40	—
Vindoline	C.v./B	0.9	−32 (0.1)	26 (0.2)	negative	Almost constant
Aniline	C.v./C	1.0	−34 (0.1)	26 (0.45)	negative	20% decrease
THC	C.v./B	1.0	−20 (0.1)	20 (1.0)	negative	Constant
m-DMAA	C.v.[f]/B	1.2	−40 (0.1)	24 (0.23)	negative	20% decrease

[a]Carbon paste electrode unless otherwise noted. A, 0.1 M acetate buffers in ethanol/water (1:1), pH 5.6, except for pH-dependence from 3.6—5.6; B, 0.2 M $LiClO_4$, CH_3CN/H_2O (9:1); C, pH 6.4 phosphate buffer. For c.v., $E_x = E_p$; for n.p.v.: $E_x = E_{1/2}$; for d.p.v., $E_x = E_s$. $v = 2$ mV s^{-1} for n.p.v. and d.p.v. ($\Delta E = 25$ mV). [b]n(app) obtained by comparison of limiting currents in n.p.v. with standards of known n. [c]Scan rate (V s^{-1}) in parentheses. [d]Concentration (mM) in parentheses. [e]Similar result at 10 V s^{-1}. [f]Glassy carbon electrode. [g]$C < 0.6$ mM; at $C > 0.6$ mM, $dE_x/d\log C = 0$.

measured pH provides an approximately valid acidity scale in the aqueous ethanolic buffers, it can be seen that all values of dE_p/dpH obtained by c.v. are close to −59 mV/pH. Indeed, all methods gave shifts in potential with pH reasonably close to −59 mV/pH, the value predicted [12] for a fast deprotonation prior to electron transfer.

Peak potentials for all compounds shifted to more positive values when the scan rate in c.v. was increased (Table 2). Such behavior is consistent with the occurrence of chemical reactions following a reversible electron-transfer step [13]. Follow-up reactions have been demonstrated in the cases of tetrahydrocarbazoles [7—9] and aromatic amines [14], for which data have been included in Table 2 for comparison. Anodic oxidations of both types of compounds probably involve initial formation of a cation radical followed by a second-order dimerization.

The influence of concentration of electroactive compound depended on the compound and the electrolyte solution (Table 2). For oxidative electrodimerizations, potential shifts of −15 to −60 mV/log C are predicted [15, 16], with the exact value depending on the sequence of primary reactions in the oxidation mechanism and the homogeneous or heterogeneous nature of the chemical steps. The anodic dimerization of tetrahydrocarbazole

occurs with a homogeneous dimerization step [8], and values of $-dE_p/d\log C$ and $dE_p/d\log v$ of 20 mV, and a constant current function ($i_p v^{-1/2}$) as v increases are consistent with predicted behavior [15]. Aromatic amines also undergo anodic dimerization, but the reaction is complicated by electropolymerization [14]. As a first approximation, such oxidations could be considered [16] to feature adsorption of all reactants and products at the surface of the electrode. Expected values of $-dE_p/d\log C$ and $dE_p/d\log v$ for surface electrodimerizations at 25°C are 29.6 mV for radical-radical or ion-parent coupling, and 59.2 mV for radical-parent coupling. A decrease in current function as v increases is predicted for radical-radical coupling, but a constant or increasing current function is possible for the other mechanisms [16]. Aniline in aqueous pH 6.4 buffer, and *m*-DMAA and vindoline in aqueous acetonitrile gave shifts of E_p with C and v and dependences of current function on v which were generally consistent with a surface radical-coupling reaction. This interpretation is in agreement with earlier studies of the electrochemical oxidation of aromatic amines in aqueous solutions [14].

Oxidation peaks for the alkaloids in ethanolic acetate buffer showed positive shifts in potential with increasing concentration. This behavior is inconsistent with an uncomplicated electrodimerization mechanism. For vindoline only, when c.v. was done at $v = 10$ V s^{-1}, $dE_p/d\log C$ became negative and its value was consistent with a second-order reaction after electron transfer. Current functions of VB, CTH, VDL all decreased with increasing v (Fig. 3). A possible explanation for the above data, for which additional evidence will be presented below, involves formation of a film on the surface of the electrode which inhibits the electron-transfer process. If this film were formed in an electropolymerization process of order >1, it would occur at a faster rate as the concentration of analyte increased. Thus at higher concentrations, greater coverage of the electrode with the film would be expected, resulting in increased inhibition and a positive shift in potential at higher concentration. The negative shift in E_p with increasing concentration for vindoline at $v = 10$ V s^{-1} can be interpreted in terms of the rate of electropolymerization. If this rate is slow on the time scale of c.v., no film will form, and this is presumably the case for vindoline at $v = 10$ V s^{-1}.

Influence of repeated scans

Repeated voltammetric scans at electrode surfaces which had already been scanned once in solutions of electroactive compounds were used to evaluate the formation of inhibiting films. Assuming that the film forms with preferential growth at specific sites on the surface of the electrode, an initial voltammetric scan would yield an electrode with both blocked and active sites for further electrolysis. Even though the catalytic nature of the electrode surface would change because of film formation during a scan, the model of a partially blocked electrode, as a first approximation, can be used to interpret the data in Table 2. Theoretical treatment for partially blocked electrodes with macroscopic active and inactive sites [17] predicts

both a decrease in c.v. current function and a positive shift in E_p with increasing v, as obtained for the three alkaloids in ethanolic acetate buffer. Furthermore, in comparing a partially blocked with a fully active electrode, the former is expected to yield smaller oxidation waves shifted to slightly more positive potentials. Thus, if formation of a film results in partial coverage of the anode during an initial scan, a second scan of the same electrode should yield smaller currents and possibly a shift in the peak to more positive potentials.

Two types of repeat scan experiments were examined. In the first, the repeat scan was begun immediately after an initial scan. In the second, the repeat scan was initiated after the electrode had been left in open circuit for 5 min after the first scan in the unstirred analyte solution. Electrooxidation of ferrocene and THC, neither of which forms films under the conditions used [8, 18], were studied for comparison. For the reversibly oxidized ferrocene, a second scan by c.v. was nearly identical to the first (Table 3). In the oxidation of THC, electron transfer is fast, but a fast chemical reaction removes the initially-formed cation radical from the vicinity of the electrode [8]. Unlike the case of ferrocene, the reverse scan does not regenerate analyte at the electrode. Thus, after the first scan, a layer of solution depleted of analyte surrounds the electrode, resulting in a second scan with essentially the same peak potential but with smaller currents than the first (Table 3). If enough time is allowed for the depleted

TABLE 3

Comparison of first and second scans of indole alkaloids at carbon paste electrodes[a]

Compound	v (mV s^{-1})	N[b]	i_p ratio[c]	ΔE_p[d] (mV)
Cyclic voltammetry				
THC	10	4	0.94	2
	100	4	1.03	−5
Ferrocene	100	1	0.99	0
Vinblastine	10	1	0.78	8
Catharanthine	10	3	0.86	31
Vindoline	10	1	0.84	2
	100	1	0.96	4
Differential pulse voltammetry				
THC	2	1	0.94	7
Vinblastine	2	1	0.73	13
Catharanthine	2	2	0.70	23
Vindoline	2	1	0.74	5

[a]Electrolytes: ethanolic acetate buffer pH 5.6 for alkaloids; 0.2 M $LiClO_4$ in CH_3CN/water (9:1) for ferrocene and THC. [b]Number of replicate experiments. [c]Ratio of i_p of second scan to that of initial scan. Working electrode allowed to stand for 5 min in open circuit in analyte solution after initial scan. [d]E_p of second scan minus E_p of initial scan.

layer to be regenerated by diffusion of electroactive compound to the electrode, repeat voltammograms of THC are very similar to the initial ones. For compounds which form inhibiting films on electro-oxidation, repeat scans should give smaller currents regardless of the waiting period. However, depletion effects may complicate interpretation of immediate second scans. Peak currents were significantly smaller on second scans for VB, CTH, and VDL (cf. Fig. 2B) when compared to identical experiments with THC, both when second scans were made immediately and after 5 min (Table 3). Similar results were obtained at glassy carbon electrodes. Peaks shifted to significantly more positive potentials for vinblastine and catharanthine on second scans, but negligible shifts were observed for vindoline. These data appear consistent with formation of an inhibiting film on the electrode during anodic voltammetry in ethanolic acetate buffers. The data give a better fit to a model involving a macroscopically nonhomogeneous covering on the electrode [17] than to one for the case of microscopic active and inactive sites [19]. This implies that the sites of film growth on the electrode attain dimensions about the same or greater than the thickness of the diffusion layer [19]. Finally, upon stirring the solution or bubbling with nitrogen for 5 min, second scans of VB, CTH, and VDL became similar to initial scans, indicating that the films on the electrodes were rather fragile and could be removed by convection.

CONCLUSIONS

Although complete elucidation of the electrode reaction mechanisms awaits further investigation, a general picture of the electrode process emerges

$$RH^+ \rightleftharpoons R + H^+ \quad (1)$$

$$R \rightleftharpoons O + e^- \quad \text{(first wave)} \quad (2)$$

$$2O \rightarrow \text{Dimers} \quad (3)$$

$$nO \rightarrow \text{Film} \quad (4)$$

The acid-base equilibrium in Eqn. 1 explains the large shifts in peak potential as solution acidity is changed and is consistent with the expectation that the unprotonated forms of the alkaloids are the most easily oxidized. The n(app) = 1 for vindoline and catharanthine, and the two overlapping waves of vinblastine of total n(app) = 2, as well as the known behavior of model tetrahydrocarbazoles [8] and aromatic amines [14], suggest that O in the above scheme may be a cation radical. This radical would be available for dimerization in Eqn. 3. For vindoline, $dE_p/d\log C = -32$ mV and $n = 1$ in neutral acetonitrile and $dE_p/d\log C = -27$ mV at $v = 10$ V s^{-1} in ethanolic acetate buffer clearly indicate that dimerization or some other second-order process follows an initial reversible electron transfer. Filming of the anode in acetonitrile does not appear to be as serious as in the ethanol/water

system. In the latter system, film formation caused $dE_p/d\log C$ to become positive for VB and CTH, and there is no definitive evidence for dimerization. Film formation may proceed through an initial dimerization and further reaction of the dimer or via another pathway. Electrochemical oxidation of the dimer could cause n(app) to be >1 [16]. The presence or absence of other chemical steps in the oxidation mechanisms cannot be inferred from the available data.

From a quantitative standpoint, these results indicate that, despite filming of the working electrode, pulse voltammetric methods can be used with carbon paste electrodes for determinations of vinblastine and related indole alkaloids in the micromolar concentration range. For direct determinations, d.p.v. yields better limits of detection and more precise calibration graphs than n.p.v. Anodic oxidation would appear to be a particularly attractive method of detecting indole alkaloids after separation by h.p.l.c. because the electrolyte solutions used in this work are similar to solvents recommended for h.p.l.c. separations of indole alkaloids [3, 4]. Film formation would be a minimal problem in an electrochemical detector because of low concentrations of analyte and convective destruction of the films.

This work was supported by U.S. PHS Grant No. 5R01-CA33195 awarded by the National Cancer Institute, Dept. of Health and Human Services. The authors thank Azita Owlia for experimental assistance and the U.S. Educational Foundation/Pakistan for a Fulbright—Hays fellowship awarded (1981—82) to I.U.H.

REFERENCES

1 M. Hesse, Alkaloid Chemistry, Wiley, New York, NY, 1981.
2 V. S. Sethi, S. S. Burton and D. V. Jackson, Cancer Chemother. Pharmacol., 4 (1980) 183.
3 S. Gorog, B. Herenyi and K. Jovanovics, J. Chromatogr., 139 (1977) 203.
4 M. Verzele, L. De Taeye, J. Van Dyck, G. DeDecker and C. De Pauw, J. Chromatogr., 214 (1981) 95.
5 P. Horvath and G. Ivanyi, Acta Pharm. Hung., 52 (1982) 150.
6 L. A. Sapunova, A. V. Gaevskii, G. A. Maslova and E. I. Grodnitskaya, Khim. Farm. Zh., 16 (1982) 708.
7 J. M. Bobbitt and J. P. Willis, Heterocycles, 6 (1977) 899.
8 C. L. Kulkarni, B. J. Scheer and J. F. Rusling, J. Electroanal. Chem., 140 (1982) 57.
9 G. Reymond, J. Vasilevskis and V. Toome, Heterocycles, 19 (1982) 2345.
10 M. J. Allen and V. J. Powell, J. Electrochem. Soc., 105 (1958) 541.
11 J. F. Rusling, Anal. Chem., 55 (1983) 1719.
12 M. Heyrovský and S. Vavřička, J. Electroanal. Chem., 36 (1972) 203.
13 A. J. Bard and L. R. Faulkner, Electrochemical Methods, Wiley, New York, NY, 1980.
14 R. N. Adams, Electrochemistry at Solid Electrodes, M. Dekker, New York, NY, 1969.
15 C. P. Andrieux, L. Nadjo and J. M. Savéant, J. Electroanal. Chem., 26 (1970) 147; 44 (1973) 327.
16 E. Laviron, J. Electroanal. Chem., 34 (1972) 363, 463.
17 T. Gueshi, K. Tokuda and H. Matsuda, J. Electroanal. Chem., 101 (1979) 29.
18 T. Kuwana, D. E. Bublitz and G. Hoh, J. Am. Chem. Soc., 82 (1960) 5811.
19 C. Amatore, J. M. Savéant and D. Tessier, J. Electroanal. Chem., 146 (1983) 37; 147 (1983) 39.

Analytica Chimica Acta, 158 (1984) 33—41
Elsevier Science Publishers B.V., Amsterdam — Printed in The Netherlands

STUDY OF THE TAUTOMERIZATION OF QUINONOID DIHYDROPTERINS BY LIQUID CHROMATOGRAPHY/ELECTROCHEMISTRY

CRAIG E. LUNTE and PETER T. KISSINGER*
Department of Chemistry, Purdue University, West Lafayette, IN 47907 (U.S.A.)
(Received 14th November 1983)

SUMMARY

An investigation of the tautomerization of quinonoid dihydropterins by dual-electrode liquid chromatography/electrochemistry (l.c.e.c.) is presented. The effect of various side-chains in the 6-position of the pterin revealed that wide variations in the rate of tautomerization occur with different pterin species. The effects of two buffers (phosphate and acetate) with low pK_a values were also studied over the pH range 2—8. The rate of tautomerization was much faster for quinonoid dihydrobiopterin in the phosphate buffer than in the acetate buffer whereas the rate of rearrangement of the other quinonoid dihydropterins was little affected by the type of buffer. This report also illustrates the advantages of l.c.e.c. for this type of investigation. Variations in pH are readily studied without changes in experimental conditions. Species that cannot be resolved chromatographically are shown to be resolvable by the electrochemical detector. Stability to rearrangement can be compared to stability to oxidation. Finally, only very little sample is required.

A tetrahydropterin has been shown to be required as a cofactor in the enzymatic hydroxylation of phenylalanine, tyrosine, and tryptophan [1, 2]. In the enzymatic reaction, the tetrahydropterin (A) is oxidized to a dihydropterin (B) which rapidly tautomerizes to the corresponding 7,8-dihydropterin (C). In vivo, the tautomerization to the inactive 7,8-dihydropterin is

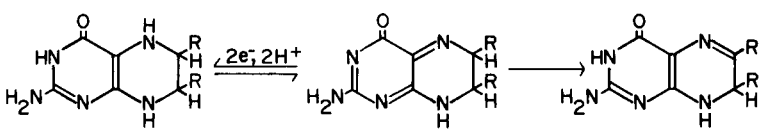

A B C

avoided by reduction of the initial dihydropterin back to the tetrahydropterin by NADH and quinonoid dihydropteridine reductase [3].

It has been assumed that the initial dihydropterin has a quinonoid structure [4, 5] although other structures and redox states have been postulated [6]. No conclusive evidence has yet been presented, but current data strongly suggests the *para* tautomer to be the actual dihydropterin intermediate [7—9]. For clarity, the intermediate will be designated as merely quinonoid dihydropterin in this study.

0003-2670/84/$03.00

The tautomerization of quinonoid dihydropterin has been investigated by a variety of techniques, such as polarography [7], cyclic voltammetry [10], spectroscopy [11, 12] and liquid chromatography with u.v. detection [13]. None of these techniques has proven entirely satisfactory for a general study of quinonoid dihydropterin tautomerization. Electrochemical methods lack resolving power and are complicated by the complex electrochemistry exhibited by pterins. The absorption spectra of the various oxidation states of pterins are badly overlapped, making bulk-phase spectroscopic studies difficult. In addition, studies at various pH values are complicated because the peak maxima shift markedly with pH. The use of liquid chromatography offers an improvement over the bulk-phase spectroscopic techniques owing to the separation it affords. Unfortunately, because of the close similarity in structure, tetrahydropterins are difficult, if not impossible, to resolve from their corresponding quinonoid dihydropterin forms.

Liquid chromatography/electrochemistry (l.c.e.c.) with a dual-electrode detector in a parallel configuration can readily resolve all of the species involved in tetrahydropterin oxidation. Although the chromatographic column cannot resolve the tetrahydropterins from the quinonoid dihydropterins, the dual-electrode detector can achieve this goal because of the difference in the electrochemical behavior of these species. Tetrahydropterins are easily oxidized and can therefore be detected at potentials where quinonoid dihydropterins are not electroactive. Likewise, quinonoid dihydropterins are easily reduced and can be detected at potentials at which tetrahydropterins are not electroactive. Through the judicious choice of detector operating potentials, all of the species of interest can be resolved and detected by dual-electrode l.c.e.c. This methodology has previously been demonstrated for the tautomerization of quinonoid dihydro-6-methylpterin [14]. In this investigation, l.c.e.c. is used to study the rate of tautomerization of several pterins as a function of pH in two buffers of differing pK_a values, one above and one below the pK_a values of the pterins studied.

EXPERIMENTAL

Reagents and apparatus

6-Methyl-5,6,7,8-tetrahydropterin, 6-methyl-7,8-dihydropterin and biopterin were obtained from Calbiochem-Behring (La Jolla, CA), neopterin from Fluka (Basel, Switzerland), and 6-methylpterin from Sigma (St. Louis, MO). The reduced forms of the pterins were prepared as previously described [15]. Octyl sodium sulfate was purchased from Eastman Kodak (Rochester, NY). All other chemicals were reagent grade or better and were used as received.

The liquid chromatographic system consisted of an Altex 110 pump and a Rheodyne 7010 injection valve with a 20-μl sample loop. A Brownlee MPLC RP-18 5-μm column (4.6 mm × 10 cm) was used. Detection was with dual LC-4B amperometric detectors (Bioanalytical Systems, West

Lafayette, IN). These were used in both the series and parallel configurations as will be described. The working electrodes were glassy carbon and the reference electrode was Ag/AgCl. All potentials are reported versus the Ag/AgCl reference.

Chromatography

Reverse-phase ion-pair chromatography was used to separate the various oxidation states of the pterins. The mobile phase was 3 mM octyl sodium sulfate buffered to pH 2.5 with 0.1 M sodium phosphate buffer and containing 15% (v/v) methanol. The mobile phase was prepared from distilled, deionized water and glass-distilled methanol and filtered through a 0.22-μm filter (Millipore, Milford, MA) prior to use. In order to remove dissolved oxygen, the mobile phase was continuously purged with nitrogen and heated to 40°C with refluxing. A flow rate of 2.0 ml min^{-1} was used in all experiments.

Metal ions are known to adsorb on reverse-phase columns and can react with pterins. To circumvent this problem each experiment was followed by several injections of a 1.0 M sodium dithionite solution and flushing of the column with a 0.1 M EDTA in 0.1 M sodium phosphate buffer, pH 6.8, solution as recommended by Haavik and Flatmark [13]. This was followed by reequilibration of the column with the mobile phase.

Oxidation of tetrahydropterins by hexacyanoferrate(III)

Potassium hexacyanoferrate(III) was used to oxidize the tetrahydropterins to dihydropterins. At a mole ratio of 2:1 hexacyanoferrate(III) to tetrahydropterin, oxidation to dihydropterin was complete in a few seconds as previously reported [7]. If excess of hexacyanoferrate(III) was employed, oxidation of the dihydropterin to the fully oxidized pterin was observed. Therefore, a slight excess of the tetrahydropterin was used to insure that oxidation was limited to the dihydropterin state.

To study the rate of tautomerization of the quinonoid dihydropterins, 2.0 ml of a tetrahydropterin solution in 0.1 M buffer was deoxygenated with nitrogen as described by Bratin and Kissinger [16]. A deoxygenated hexacyanoferrate(III) solution, of a concentration such that 20 μl would oxidize the tetrahydropterin solution, was injected forcibly into the tetrahydropterin solution with a syringe. The solutions were mixed by the action of the bubbling nitrogen. After addition of the hexacyanoferrate(III), 15 s was allowed for oxidation to occur and then an aliquot of the reaction mixture was injected onto the chromatographic column. The reaction mixture was kept on the deoxygenating apparatus and at timed intervals additional aliquots were injected.

Chromatographically-assisted hydrodynamic voltammetry

The electrochemical behavior of compounds can be investigated with the assistance of liquid chromatography. In this technique, a series of injections

of a standard solution are made and the detector potential is varied between injections. The current response at each potential is normalized to the current response at the highest potential applied and plotted versus applied potential. In this manner, the familiar hydrodynamic voltammogram of the compound is constructed.

The electrochemical behavior of the quinonoid dihydropterins can also be investigated with l.c.e.c., using the dual-electrode detector in a series configuration. In this configuration, one electrode is positioned upstream of the other such that analyte flows across the two electrodes in sequence. The upstream electrode is used to generate products (quinonoid dihydropterins) which can then be studied at the downstream electrode. For the oxidation of tetrahydropterins, the time interval between generation and detection is such that essentially no tautomerization of the quinonoid dihydropterin produced occurs before detection at the downstream electrode. If a series of injections of a standard solution of a tetrahydropterin is made with the potential of the upstream electrode held on the limiting current plateau for the oxidation of the tetrahydropterin and the potential of the downstream electrode is varied between injections, then the hydrodynamic voltammogram of the quinonoid dihydropterin can be obtained. The anodic current observed at the downstream electrode is due to oxidation of tetrahydropterin which was not oxidized at the upstream electrode. By normalizing the downstream response to the upstream response, any variations in the amount of quinonoid dihydropterin generated upstream are eliminated. Information obtained in this manner is essential in the proper selection of the operating potentials of the electrodes for the investigation of the tautomerization of the quinonoid dihydropterins by dual-electrode l.c.e.c.

RESULTS

Electrochemistry of the pterins

The tetrahydro- and 7,8-dihydro forms of 6-methylpterin, neopterin, and biopterin can all be prepared in solutions sufficiently stable for electrochemical investigations. Figure 1 shows the hydrodynamic voltammogram obtained for these species with the assistance of liquid chromatography. As can be seen, all three tetrahydropterins are easily oxidized while the corresponding 7,8-dihydropterins are much harder to oxidize. The 7,8-dihydropterins can also be reduced; however, their reduction potentials are such that reductions cannot easily be achieved in aqueous solution because of reduction of the solvent. Only the reduction of 6-methyl-7,8-dihydropterin could be observed by l.c.e.c. and this reduction was at the limit of achievable potentials. In contrast, the initial product of the oxidation of tetrahydropterins is easily reduced. Indeed, the quinonoid dihydropterins all form reversible couples with their corresponding tetrahydropterin states. This is shown in Fig. 2 for the pterins studied.

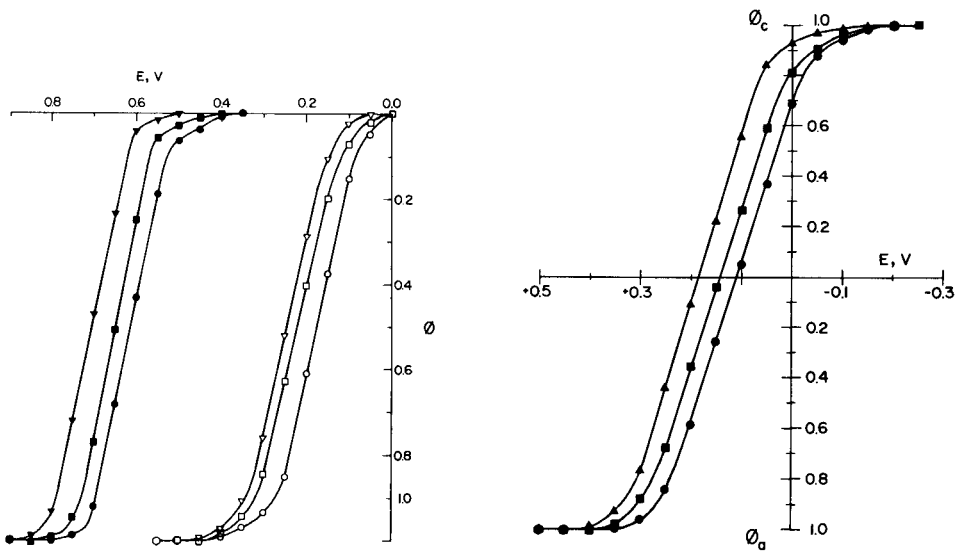

Fig. 1. Hydrodynamic voltammograms for the oxidation of tetrahydro- and dihydropterins: (•) biopterin; (▪) neopterin; (▾) 6-methylpterin. Open symbols are the tetrahydropterins and filled symbols are the dihydropterins. Ø is the normalized current.

Fig. 2. Hydrodynamic voltammograms for the product of oxidation of tetrahydropterins: (•) tetrahydrobiopterin; (▪) tetrahydroneopterin; (▲) tetrahydro-6-methylpterin.

For l.c.e.c., the tetrahydropterins can be detected at +500 mV (limiting current plateau) whereas a potential of +900 mV is required for the detection of the 7,8-dihydropterins. The quinonoid dihydropterins can be detected at −300 mV (limiting current plateau). By using the dual-electrode detector in the parallel configuration in which the electrodes are adjacent to each other and aligned normal to the direction of flow, all three species can be resolved and detected. One electrode is operated at +900 mV to detect the tetrahydropterins and the 7,8-dihydropterins and the other electrode is operated at −300 mV to detect the quinonoid dihydropterins. Therefore, even if the tetrahydropterins and the quinonoid dihydropterins cannot be resolved chromatographically, they are resolved by the dual-electrode electrochemical detector.

Tautomerization of quinonoid dihydropterins

Archer and Scrimgeour [12] have studied in detail the effect of the buffer on the tautomerization of quinonoid dihydro-6,7-dimethylpterin. They found that at pH values above 5.5, the tautomerization is catalyzed by both the acidic and basic forms of the buffer. From isotopic labeling experiments, they also determined that cleavage of the C—H bond at the 6-position was the rate-limiting step. In the experiments reported here, the utility of dual-electrode l.c.e.c. in the study of these rearrangement reactions will be

demonstrated through an investigation of the effect of the substituent at position 6 on the rate of tautomerization. The effect of two common buffers with pK_a values below 5, namely acetate and phosphate, will also be briefly studied.

Figure 3 shows typical chromatograms obtained upon oxidizing tetrahydrobiopterin, tetrahydroneopterin and tetrahydro-6-methylpterin with hexacyanoferrate(III). All show initial production of an easily reducible species that disappears with time. The appearance of an oxidizable species coincides with the disappearance of the reducible species. The oxidizable species was identified, on the basis of both retention data and electrochemical characterization, as the 7,8-dihydro form of the initial tetrahydropterin. By comparing the electrochemical behavior of the reducible species with the behavior of quinonoid dihydropterins produced in the series dual-electrode experiment, these species were identified as the corresponding quinonoid dihydropterins.

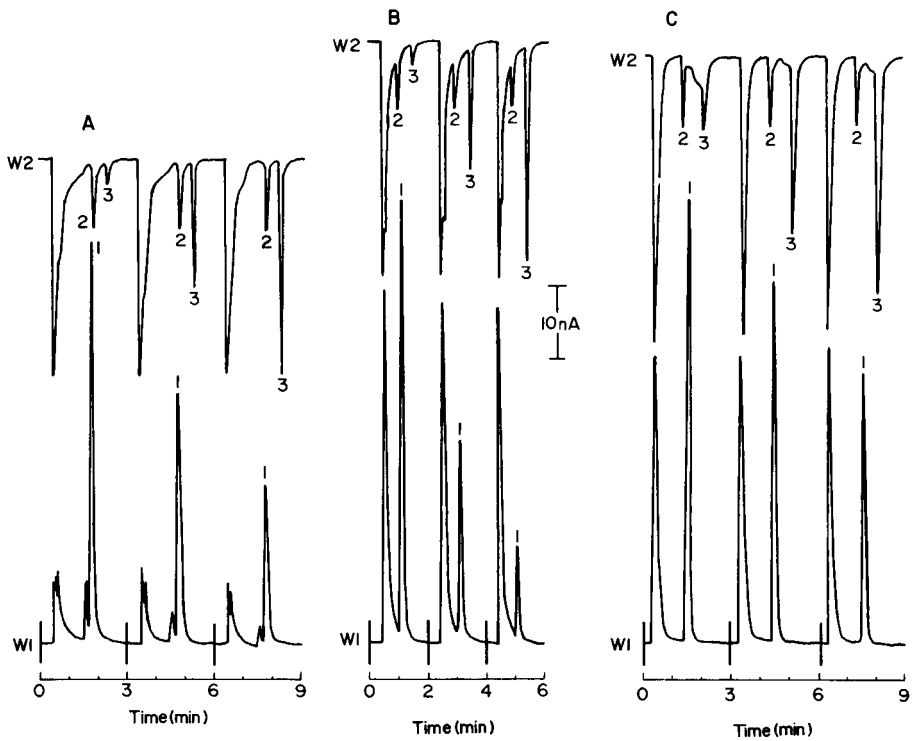

Fig. 3. Chromatograms obtained after oxidation of the tetrahydro compounds by hexacyanoferrate(III): (A) tetrahydrobiopterin; (B) tetrahydroneopterin; (C) tetrahydro-6-methylpterin. Chromatographic conditions: 3 mM octyl sodium sulfate in 0.1 M sodium phosphate buffer, pH 2.5, 15% methanol. Electrode potentials: W1 = −300 mV, W2 = +900 mV. Peak identities: (1) quinonoid dihydro compound; (2) tetrahydro compound; (3) 7,8-dihydro compound.

The pK_a values for the N-5 position of 6-methylpterin and biopterin have been reported to be 2.6 [17] and 2.43 [18], respectively. Of the 7,8-dihydropterins, only the pK_a of 6-methyl-7,8-dihydropterin has been reported; this is 4.17 [17]. However, based on the pK_a values reported for several other pterins [17—20], it is likely that the pK_a values for all of the 7,8-dihydropterins used in this study are near 4.2 ± 0.4. As suggested by Archer and Scrimgeour [12], the pK_a values of the quinonoid dihydropterins should be similar to the pK_a values of their corresponding 7,8-dihydropterin. Therefore, the pK_a values for the pterins all fall between the pK_a values of the two buffers used (acetate pK_a = 4.76 and phosphate pK_a = 2.13).

Figure 4A shows the pH dependence of the observed rate constant for the tautomerization of the quinonoid dihydropterins in acetate buffer. All three pterins show a maximum in their reaction rate at approximately pH 5. This is in agreement with the behavior previously reported for quinonoid dihydro-6,7-dimethylpterin [12]. In this buffer, quinonoid dihydrobiopterin and quinonoid dihydro-6-methylpterin have similar reaction rates, while quinonoid dihydroneopterin tautomerizes considerably faster. The rate of tautomerization of quinonoid dihydroneopterin is very close to the rate reported for quinonoid dihydro-6,7-dimethylpterin in this buffer [12].

These pterins were found to behave differently in phosphate buffer. From Fig. 4B, it can be seen that the maximum rate of tautomerization has shifted to above pH 5. The reaction rates of quinonoid dihydroneopterin

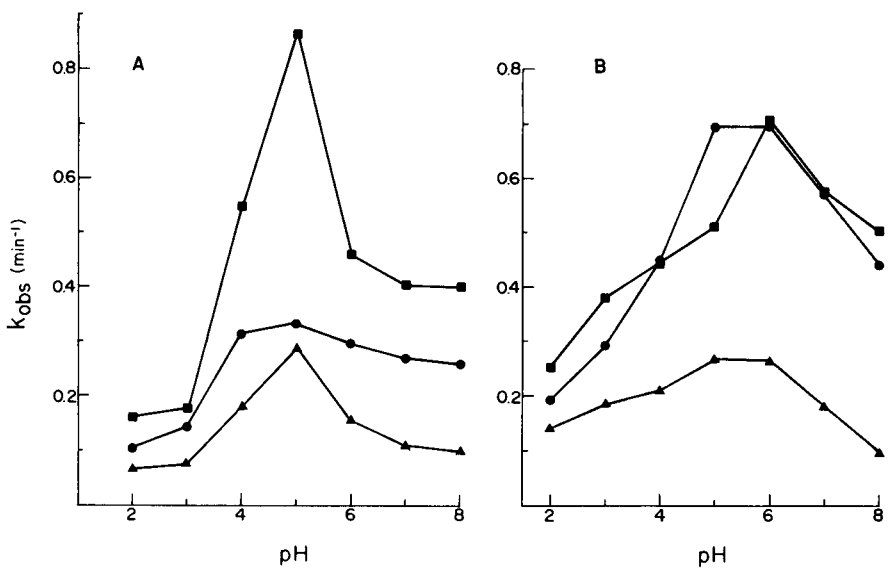

Fig. 4. Variation of observed rate constant (k_{obs}) for the tautomerization of quinonoid dihydropterins with pH: (A) acetate buffer; (B) phosphate buffer. (•) Quinonoid dihydrobiopterin; (▪) quinonoid dihydroneopterin; (▲) quinonoid dihydro-6-methylpterin.

and quinonoid dihydro-6-methylpterin show little change in magnitude arising from the different buffer. Quinonoid dihydrobiopterin, however, exhibits a much higher rate of tautomerization in the phosphate buffer. In this buffer, quinonoid dihydrobiopterin and quinonoid dihydroneopterin have similar rates of tautomerization whereas quinonoid dihydro-6-methylpterin rearranges at a much slower rate.

DISCUSSION

In reactions involving the oxidation of tetrahydropterins, it has been demonstrated that the choice of buffer is important in determining the rate of tautomerization of the resulting quinonoid dihydropterin to the 7,8-dihydropterin [12]. The rate of tautomerization is significant because the natural system for the regeneration of the tetrahydropterin is specific for the quinonoid form of the dihydropterin and, if tautomerization is too rapid, an auxiliary enzyme, dihydrofolate reductase, is required [21]. This work demonstrates that the substituent at the 6-position is also an important consideration.

The ease of oxidation of the tetrahydropterins follows the sequence tetrahydrobiopterin < tetrahydroneopterin < tetrahydro-6-methylpterin. In this same buffer above pH 4, the rate of tautomerization of the quinonoid dihydropterins follows the reverse order. It is likely that the cause of stabilization of the tetrahydro state also stabilizes the quinonoid dihydro form.

Buffers of relatively low pK_a were also shown to affect the tautomerization of the quinonoid dihydropterins. While the effect on the tautomerization of quinonoid dihydroneopterin and quinonoid dihydro-6-methylpterin was small, the effect on the rate of tautomerization of quinonoid dihydrobiopterin was dramatic. This is in agreement with earlier observations of tetrahydrobiopterin oxidation in phosphate buffer [21]. When the tetrahydropterins are used as enzyme cofactors, where tautomerization to inactive 7,8-dihydropterins is undesirable, both the buffer and the pterin should be chosen carefully.

This study also shows the utility of dual-electrode l.c.e.c. in the investigation of the oxidation of tetrahydropterins. Electrochemical detection offers several advantages in these studies. The electrochemical properties of both intermediates and end products can readily be determined by l.c.e.c. Components that cannot be resolved chromatographically, i.e., tetrahydropterins and quinonoid dihydropterins, can often be resolved by the electrochemical detector. Finally only very little sample is necessary to complete an investigation by l.c.e.c.

REFERENCES

1 S. Kaufman, Biochim. Biophys. Acta, 27 (1958) 428.
2 S. Kaufman and D. B. Fisher, in O. Hayaishi, (Ed.), Molecular Mechanisms of Oxygen Activation, Academic Press, New York, NY, 1974, p. 285.

3 K. H. Nielsen, V. Simosen and K. E. Lind, Eur. J. Biochem., 9 (1969) 497.
4 P. Hemmerich, in W. Pfleiderer and E. C. Taylor (Eds.), Pteridine Chemistry, Pergamon Press, London, 1964, p. 323.
5 S. Kaufman, J. Biol. Chem., 239 (1964) 332.
6 A. Bobst, Proc. Natl. Acad. Sci. U.S.A., 68 (1971) 541.
7 M. C. Archer, D. J. Vonderschmitt and K. G. Scrimgeour, Can J. Biochem., 50 (1972) 1174.
8 R. A. Lazarus, C. W. DeBrosse and S. J. Benkovic, J. Am. Chem. Soc., 104 (1982) 6871.
9 D. Ege-Serpkenci, R. Raghavan and G. Dryhurst, Bioelectrochem. Bioenerg. 10 (1983) 357.
10 S. Kwee and H. Lund, Biochim. Biophys. Acta, 297 (1973) 285.
11 L. G. Karber and G. Dryhurst, J. Electroanal. Chem., 136 (1982) 271.
12 M. C. Archer and K. G. Scrimgeour, Can. J. Biochem., 48 (1970) 278.
13 J. Haavik and T. Flatmark, J. Chromatogr., 257 (1983) 361.
14 C. E. Lunte and P. T. Kissinger, Anal. Chem., in press.
15 C. E. Lunte and P. T. Kissinger, Anal. Chem., 55 (1983) 1458.
16 K. Bratin and P. T. Kissinger, J. Liq. Chromatogr., 4(2) (1981) 321.
17 W. Pfleiderer and H. Zondler, Chem. Ber., 99 (1966) 3008.
18 M. Viscontini and E. Möhlmann, Helv. Chim. Acta, 42 (1959) 1679.
19 W. Pfleiderer, Chem. Ber., 95 (1962) 2195.
20 J. M. Whiteley and F. M. Huennekens, Biochemistry, 6 (1967) 2620.
21 S. Kaufman, J. Biol. Chem., 242 (1967) 3934.

Analytica Chimica Acta, 158 (1984) 43—55
Elsevier Science Publishers B.V., Amsterdam — Printed in The Netherlands

QUANTITATION OF METAL COMPLEXES BY REVERSE-PULSE AMPEROMETRY AND MOLECULAR-EXCLUSION CHROMATOGRAPHY

MARY L. ADAMIC and DUANE E. BARTAK*
Department of Chemistry, University of North Dakota, Grand Forks, ND 58202 (U.S.A.)
(Received 19th August 1983)

SUMMARY

An electrochemical flow cell in conjunction with modified molecular-exclusion chromatographic techniques is used to identify and quantify a series of copper complexes. A reverse-pulse amperometric mode is used to quantify the complexes and to minimize oxygen interference. The chromatographic eluent is modified by "buffering" with copper(II) to prevent dissociation of labile complexes. A Sephadex G-25 column is shown to resolve a mixture of copper complexes of polyaminocarboxylic acids. A detection limit of 0.65 μg was obtained for the Cu-EDTA complex. Copper(II)-citrate complexes were well resolved on the Sephadex column as a dimeric complex with a detection limit of 1.0 μg. Fulvic acid complexes of copper were quantified with the above techniques upon elution from a Sephadex G-15 column. A detection limit of 5 μg was found for a copper-fulvic acid complex. EDTA can be quantified in the presence of fulvic acid by these techniques.

Quantifying metal-binding or complexing agents in aqueous environments is an important problem. The binding agents will affect the chemical speciation of trace metals, which ultimately determines the reactivity, transport, and biological availability of the metal. Two important factors which should be known are the nature of the binding agent (i.e., stability constants of pertinent complexes) and the binding agent concentration. For example, reports have indicated that complexation of copper, cadmium, and lead with EDTA at typical concentrations found in aquatic environments is probably more important than the complexation of these metals with humic substances [1, 2]. In addition, it has been shown that the extent of the biodegradation of EDTA in natural aquatic systems is apparently quite small [1].

Several workers have reported on methods to determine EDTA and related chelating agents. Techniques which have been utilized include chromatographic (e.g., gas-liquid) [3], spectrophotometric (e.g., zinc-zincon) [4], and electrochemical methods. Several electrochemical methods, which are based on addition of a specific metal ion to the analyte, utilize the direct reduction of the resultant metal chelate. Metals examined include Bi(III) [5, 6], In(III) [7], and Cd(II) [8]. Recently, oxidation of mercury in the presence of EDTA and related chelating agents has been used to quantify

0003-2670/84/$03.00

EDTA and related compounds [2]. However, some of the electrochemical techniques suffer from a lack of adequate resolution for mixtures of ligands which have similar stability constants. The problem of overlapping waves for mixtures of electrochemically active species has resulted in the development of various forms of liquid chromatography (including h.p.l.c.) coupled with electrochemical detection (l.c.e.c.) [9—13]. Most of the work has been directed toward oxidative electrochemistry on organic compounds. However, l.c.e.c. has been used recently for trace metal determinations by complexation with chelating agents such as dithiocarbamates [14, 15].

The metal-binding chemistry of fulvic acid (or the water-soluble portion of humic material) has recently been the subject of an excellent review by Saar and Weber [16], who pointed out that determinations of these materials can be complicated by shifts in chemical equilibria during measurement and adsorption of the organic material on membranes and electrodes. The problem of shifting equilibria has been most common with separation techniques. However, Mantoura and Riley [17] used a modified molecular-exclusion chromatographic technique in which the eluent contained an excess of metal ions to maintain equilibrium between metal complex forms and "free" metal during separation. Although they determined stability constants and binding stoichiometries for copper, nickel, and zinc complexes of fulvic acid, they did not determine the applicability of the technique to the measurement of fulvic acid.

This report describes the application of modified molecular-exclusion chromatography coupled with electrochemical techniques for quantifying a series of ligands including EDTA, citric acid, and fulvic acid. In addition, EDTA is quantified in the presence of water-derived fulvic acid. An electrochemical flow cell is utilized as a metal complex detector on the eluent from the column. The utility of an electrochemical cell with reticulated vitreous carbon as a detector for copper(II)-polyaminocarboxylic acid complexes has been demonstrated [18]. In addition to measurement of the metal complexes, the electrochemical detector is capable of monitoring the unreacted metal ions in the eluent, which provides a measure for the metal ions removed from the eluent. Because of the interferences of oxygen in the measurement of reducible metals in the flow system, reverse-pulse amperometry at a static mercury electrode is used to quantify the metal complexes and the amount of metal remaining in the eluent [19].

EXPERIMENTAL

Cells and instrumentation

A static dropping mercury electrode (Model 303, Princeton Applied Research) was used to obtain the pulse polarograms. Amperometric detection for the chromatographic experiments was accomplished with a flow-through polarographic detector (Model 310, PAR) in the dropping mercury electrode (d.m.e.) mode. The geometrical drop areas for the d.m.e. were found to be:

small = 9.3×10^{-3} cm^2; medium = 1.7×10^{-2} cm^2; large = 2.6×10^{-2} cm^2. The glass capillary was siliconized at least monthly with a 5% solution of dichlorodimethylsilane in tetrachloromethane. The reference electrode was a Ag/AgCl electrode with saturated KCl and AgCl as the filling solution, which was isolated from the rest of the cell with a porous glass salt bridge. The porous glass separator in the reference electrode bridge was changed monthly. A platinum electrode was used as the counter electrode. Potential control and current-to-voltage conversion were made with a PAR Model 174A Polarographic Analyzer. The instrument was operated in the pulse mode for both reverse-pulse polarography and reverse-pulse amperometry, utilizing previously published procedures [19]. Polarograms were recorded on a Soltec Model BW-133B x-y recorder. Chromatograms were recorded on a Houston Omniscribe strip-chart recorder.

Chromatography

Model systems. The chromatographic system consisted of a Milton Roy Model minipump with pulse dampeners and a Rheodyne 7125 sample injector with a 50-μl sample injection loop. The columns were made from glass tubing (134 cm × 0.7 cm) with Omnifit chemically inert, high-pressure fittings. Stainless steel tubing (0.3 mm i.d.) was used between injector, column, and detector (PAR 310). The column was packed with Sephadex G-25 (Pharmacia, superfine, 10—40 μm) by a slurry packing method. The Sephadex gel was allowed to swell in the distilled, deionized water at 80°C for at least an hour. Treatment of the gel with sodium tetrahydroborate (0.4 g/100 ml) and sodium hydroxide (0.2 g/100 ml) during swelling was used in an attempt to hydrogenate mildly the adsorptive sites on the column. However, because there appeared to be no significant difference in retention volumes of polyaminocarboxylic acids on a sodium borohydride-treated vs. untreated column, this procedure was not consistently used. After cooling, the gel was rinsed at least three times with 0.05 M tris(hydroxymethyl)-aminomethane (Tris)acetate buffer, pH 7.4. Excess of buffer and Sephadex fines were decanted and the slurry was poured into the column. A vacuum water pump was attached to the bottom of the column to aid in the packing process. The packed column was topped with an adjustable teflon adaptor with a plunger so as to minimize void volumes at the top of the column caused by compression of the gels. The pressure was maintained below 100 psi to avoid collapse of the gels; flows up to 1.6 ml min^{-1} could be maintained at these pressures [20]. The Tris acetate buffer was pumped from a large reservoir in which it was continuously purged with nitrogen, which had been purified by passing it over BTS R3-11 copper catalyst. In addition, a blanket of nitrogen was also kept over the contents of the electrochemical cell during each experiment.

Fulvic acid systems. The chromatographic system consisted of an Altex Model 110A h.p.l.c. pump with pulse dampeners and a Rheodyne 7125 sample injector with various sample-injection loops. The columns were

stainless steel (120 cm × 0.8 cm) with h.p.l.c. fittings. Stainless steel tubing (0.3 mm i.d.) was used between injector, column, and detector (PAR 310). The column was packed with Sephadex G-15 (Pharmacia) gel by a slurry packing method. The Sephadex gel was prepared as above and eluted with 0.01 M Tris acetate buffer, pH 7.4.

Chemicals

All chemicals were of analytical-reagent grade. The mercury used in the d.m.e. was triply distilled. All water used was distilled and passed through a Millipore-Q system. The eluent buffer used for most experiments contained 0.050 M Tris adjusted to pH 7.4 with acetic acid, 0.1 M $NaNO_3$, 1.57×10^{-4} M (10 mg l^{-1}) copper, and was prepared from preboiled water, which was cooled under nitrogen immediately before preparation. In addition, in several of the initial polyaminocarboxylic acid experiments, 0.1 g l^{-1} sodium azide was added to prevent bacterial growth on the column [21]; however, since the azide ion is an effective complexing agent, this procedure was discontinued. The column packing (gel) was subsequently changed on a monthly basis. Bacterial growth did not appear to be a problem in the columns through which eluent had been pumped on a daily basis.

A water-derived fulvic acid sample was isolated and purified as reported by Weber and Wilson [22]. Water was collected in 5.3 gallon polyethylene (Nalgene) carboys from the English Coulee (Grand Forks, ND) and transported to the laboratory. The English Coulee is a slow moving waterway that appeared light-brown in color. The water was filtered through glass wool before it passed through two (45-cm × 4.5-cm) columns packed with Amberlite IRA-458 anion-exchange resin in the hydroxide form. A total of about 100—125 gallons of prefiltered water was passed through the two columns from the bottom. The water was propelled by a Bio-fiber peristaltic pump module (Bio-Rad Laboratories) at a maximum rate of 5 gal. min^{-1}.

The fulvic and humic acids were eluted by pumping 2 M sodium chloride through the columns until no further color was eluted. The resin was regenerated by pumping about 1.5 l of aqueous 1% (w/v) sodium hydroxide, and washed with water until free of chloride ion. The sodium chloride solution of the humic and fulvic acids was acidified to pH 1, whereupon the humic acids precipitated. The soluble fulvic acid was predominantly in the molecular (unionized) form and was adsorbed on the Amberlite XAD-2 (Baker Chemical) resin. The acidified solution was slowly passed through a (45-cm × 4.5-cm) XAD-2 column at about 3 ml min^{-1}. Most of the insoluble humic acids remained at the top of the column, while the fulvic acid was adsorbed on the column. The column was then eluted with an aqueous 1% (w/v) sodium hydroxide solution, forming the sodium salt of fulvic acid. No eluent was collected until its pH was 8 or above. Eluent which had a pH less than 8 was treated again on the column. The fraction of the eluate above pH 8 was passed through a Rexyn 101(H) (Fisher Science Co.) cation-exchange resin (hydrogen ion form) to insure the removal of all the sodium ion.

The eluate from the cation-exchange column was filtered through a 0.45-μm Millipore filter, and evaporated to 250 ml on a rotary evaporator. The remaining eluate was freeze-dried to a brown powder. The yield was 0.25 g/100 gallons of water. This is very low when compared to Weber's yields, because of the apparent low concentration of fulvic acid in the English Coulee as indicated by the light-brown color of the Coulee water.

RESULTS AND DISCUSSION

Reverse-pulse amperometry and reverse-pulse polarography

In several of the earlier experiments, the electrochemical flow cell was used as an amperometric detector with a constant potential applied to the working electrode so as to effectively maintain the boundary condition of zero concentration of the electroactive species at the electrode surface [18]. However, as noted previously, the cell is sensitive to oxygen so that both the mobile phase and sample solutions must be deoxygenated carefully. Maitoza and Johnson [19] have recently suggested that electrochemical detection of metal ions in a flow system without the interference of dissolved oxygen is possible by reverse-pulse amperometry (r.p.a.). The r.p.a. technique with a mercury electrode consists essentially of a deposition step (2—5 s) followed by a stripping step (57 ms) during which the anodic current is measured during the last 17 ms of the step.

Reverse-pulse polarography (r.p.p.) has been recently revived and applied to the determination and mechanistic studies of organic compounds by Osteryoung and coworkers [23]. Here, r.p.p. was used to elucidate the electrochemistry of copper-complexing agent systems. In order to select deposition and stripping potentials for r.p.a., the r.p.p. technique was applied to a series of solutions containing copper and complexing agents. Figure 1 illustrates the r.p.p. behavior of the copper-EDTA system. An initial potential (E_i) of —0.75 V was selected to insure reduction of uncomplexed as well as complexed copper(II). These samples were well deaerated so as to facilitate interpretation of the polarograms. Polarogram B for uncomplexed copper in Tris acetate buffer at pH 7.4 shows a single oxidation or stripping wave with $E_{1/2}$ = —0.12 V. For a 2:1 ratio of copper(II):EDTA solution, oxidation waves appear at —0.29 V and —0.12 V (polarogram C). The wave at —0.29 V represents the oxidation of copper in the presence of EDTA

$$Cu(Hg) \rightleftharpoons Cu^{2+} + Hg + 2e^-; Cu^{2+} + H_2Y^{2-} \rightleftharpoons CuY^{2-} + 2H^+$$

The $E_{1/2}$ values and wave shapes obtained with this 2:1 ratio indicate essentially a "buffer capacity problem" in that EDTA is depleted at the electrode surface. The 1:1 Cu(II):EDTA polarogram (polarogram D) indicates an irreversible wave (slope of log plot = 95 mV) at $E_{1/2}$ = —0.27 V with a second wave at $E_{1/2}$ = +0.04 V. The latter wave is due to uncomplexed EDTA at the electrode surface resulting in a mercury anodization wave

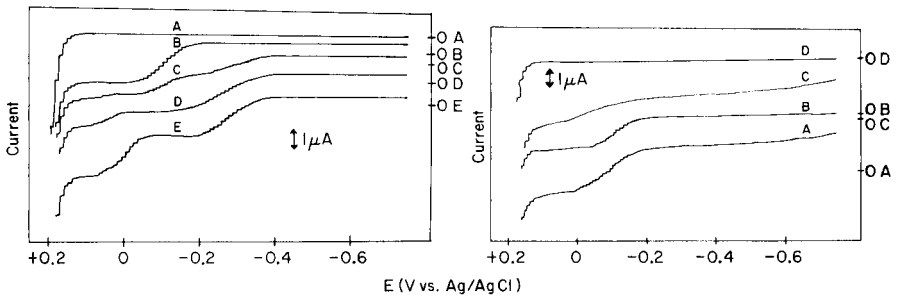

Fig. 1. Reverse-pulse polarograms for copper(II) in the absence and the presence of EDTA. Conditions: pulse amplitude increasing at a rate of 10 mV/drop; drop time 1 s; pulse width 57 ms. (A) 0.10 M $NaNO_3$ and 0.05 M Tris buffer at pH 7.4; (B) 1.6×10^{-4} M (10 mg l^{-1}) copper(II) in same buffer; (C) 1.6×10^{-4} M copper(II) and 8×10^{-5} M EDTA in same buffer; (D) 1.6×10^{-4} M copper(II) and 1.6×10^{-4} M EDTA in same buffer; (E) 1.6×10^{-4} M copper(II) and 3.2×10^{-4} M EDTA in same buffer.

Fig. 2. Reverse-pulse polarograms for copper(II) in the presence and absence of oxygen. Conditions as in Fig. 1. (A) Buffer containing 1.6×10^{-4} M copper(II) saturated with oxygen; (B) deaereated buffer containing 1.6×10^{-4} M copper(II); (C) buffer saturated with oxygen; (D) deaereated buffer containing 0.10 M $NaNO_3$ and 0.05 M Tris at pH 7.4.

$$Hg \rightleftharpoons Hg^{2+} + 2e^-; \quad Hg^{2+} + H_2Y^{2-} \rightleftharpoons HgY^{2-} + 2H^+$$

This wave shifts in the negative direction with increasing concentration of EDTA as expected. The r.p.p. experiments suggest an initial potential range of —0.75 V to —0.55 V for the r.p.a. technique; however, the choice of the final potential must take into account the mercury oxidation wave in the presence of excess of EDTA at the electrode surface.

The significant advantage of r.p.a. vs. conventional amperometry is the elimination of oxygen interference. This is illustrated in Fig. 2; polarogram D represents only deaerated buffer while polarogram B was obtained on a 10 mg l^{-1} copper solution in deaerated buffer. Polarogram C resulted from buffer at pH 7.4 saturated with oxygen; the irreversibly-shaped wave (log plot slope = 91 mV) is consistent for the apparent oxidation to H_2O_2 (pK_a = 11.7). Comparison of the polarograms in Fig. 2 indicates that a final potential of 0.0 V to 0.1 V should optimize the elimination of residual oxygen interference after deaeration. This should not be done if excess of a ligand such as EDTA is present. However, the eluent used in the chromatographic separation of the polyaminocarboxylic acids and other ligands in this study was "buffered" with regard to copper(II) (i.e., excess of Cu(II) relative to ligand) (see below).

An electrochemical flow cell, with the static dropping mercury electrode (s.m.d.e.) in the PAR Model 310, was used in a constant amperometric mode to check the response of the detector used in the chromatographic system (see below). A series of copper(II) solutions was introduced directly into the flow cell with the sample injector using the Tris buffer. Calibration curves

indicated that the response of the detector in terms of peak height (i.e., current, μA) was linear with amount injected. The least-squares equation for eight samples of copper between 10 and 45 mg l^{-1} was $i(\mu A) = (1.046 \pm 0.013)\ C_{Cu(II)}$ (mg l^{-1}) + (3.338 ± 0.364) (μA) with $S_{yx} = 0.394$. A detection limit for the detector in a current-sampled, constant-potential amperometric mode was calculated from the slope (m) and standard deviation (s) of the calibration graph. A detection limit = ts/m was calculated using a t-test at the 95% confidence level [24]; a value of 0.9 mg l^{-1} was obtained from the above data. The r.p.a. technique was tested for the detection limit using six samples. The least-squares equation was $i(\mu A) = (2.054 \pm 0.103)\ C_{Cu(II)}$ (mg l^{-1}) + (0.027 ± 0.072) μA with $S_{yx} = 0.052$. The detection limit for the r.p.a. technique was found to be 0.06 mg l^{-1}.

Molecular-exclusion chromatographic separation of metal complexes

Polyaminocarboxylic acids. Hummel and Dreyer [25] have suggested that molecular exclusion (gel filtration) could be used to separate and measure substances which are binding agents in biological systems. They measured the binding ability of a protein for a substance of lower molecular weight by passing the protein through a suitable column with an eluent which contained the binding substance. More recently, Miyajima et al. [26] have shown that the modified molecular-exclusion chromatographic technique can be used to separate metal phosphate complexes and to determine their stability constants. The approach was to "buffer" the eluent with metal ions so as to prevent dissociation of labile complexes as they migrate down the column. In addition, the metal complex and the free ligand should have approximately the same elution volume in order to avoid dissociation of the complex to the free metal and free ligand [27]. Figure 3 illustrates a typical chromatogram which was obtained from an injection of 50 μl of a 8×10^{-3} M solution of EDTA on a Sephadex G-25 column (see Experimental). The peak representing the copper-EDTA complex with an elution volume of 43.5 ml is followed by a trough with an elution volume of 57.4 ml, representing a band of depleted copper(II) from the eluent. The peak area:trough area ratio of 1.0:0.99 indicates nearly ideal Hummel—Dreyer behavior for this ligand.

The resolution of a typical Sephadex column (G-25, superfine) is illustrated in Fig. 4. A mixture of nitrilotriacetic acid (NTA), EDTA, and diethylenetriaminepentaacetic acid (DTPA) was injected on the Sephadex column. Adequate separations were obtained for these three compounds, so that they could be quantified (Table 1).

The optimum parameters for the determination of polyaminocarboxylic acids were determined on the basis of flow rate of eluent, drop size and drop time of the s.m.d.e., and amount of sample injected. The dependence of detector response on flow rate showed a gradual decrease in peak area with increasing flow rates from 0.3 to 1.0 ml min^{-1}; at flow rates greater than 1.0 ml min^{-1} the peak area remained constant within experimental error.

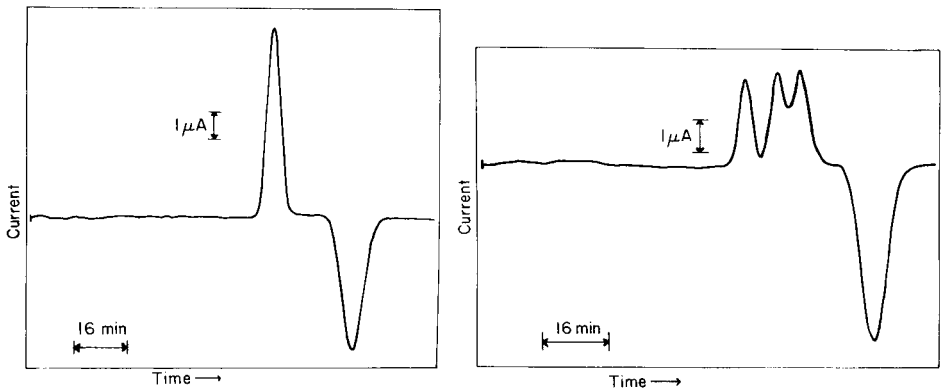

Fig. 3. Chromatogram for 0.40 μmol of EDTA on a superfine Sephadex G-25 column. Conditions: elution with buffer at pH 7.4 containing 10 mg l^{-1} Cu(II), 0.10 M $NaNO_3$ and 0.05 M Tris at 0.6 ml min^{-1}. Detector was the s.d.m.e. flow cell.

Fig. 4. Chromatogram for 0.40 μmol each of a mixture of NTA, EDTA, and DTPA on a superfine Sephadex G-25 column. The order of elution of the copper complexes for these ligands is Cu(DTPA), Cu(EDTA), Cu(NTA); the peaks are followed by a trough representing the metal depletion band. Conditions as in Fig. 3.

This behavior is consistent with mass transport via convection and diffusion at the slow flow rates while convection is the sole mode of transport at faster flow rates. The efficiency of the Sephadex columns was tested with 50-μl samples of EDTA (8×10^{-3} M). The number of theoretical plates increased gradually (ca. 10%) to a value of approximately 1000 plates m^{-1} as the flow

TABLE 1

Chromatographic data for a series of copper complexes of polyaminocarboxylic acids on Sephadex G-25[a]

Ligand	Elution volume of metal complex V_{ec} (ml)	V_{ec}/V_0[b]	Elution volume of metal V_{em} (ml)[c]	V_{em}/V_0[b]	R_s[d]
DTPA	37.7	1.44	57.1	2.18	—
EDTA	43.2	1.65	57.4	2.19	1.15
CDTA	43.9	1.68	57.3	2.19	1.30
NTA	46.8	1.79	57.6	2.20	1.90

[a]All data were obtained on a Sephadex G-25 superfine column (0.7 cm × 135 cm) with an eluent consisting of 10 mg l^{-1} Cu(II), 0.050 M Tris at pH 7.4, 0.1 M $NaNO_3$, at a flow rate of 0.6 ml min^{-1}. [b]The void volume (V_0) of the above column was measured as 26.2 ml using blue dextran, which was measured both spectrophotometrically and electrochemically. [c]The elution volume of the "free" metal is a measure of the location of the trough in each chromatogram. [d]Resolution of each solute with reference to DTPA where $R_s = Z/W$, Z being the distance between two peaks and W the average width of each peak.

rate was increased from 0.30 to 0.65 ml min^{-1}. The efficiency then decreased slowly with increasing flow rate up to 1.2 ml min^{-1}, which produced approximately 900 plates m^{-1}. Thus, an optimum flow rate of 0.65 ml min^{-1}, which had a HETP of 1.2 mm/plate, was selected for most of the subsequent separations. This HETP value compares favorably with rapid molecular-exclusion chromatography using Sephadex which produced HETP values of 0.5—3.3 mm/plate [20].

The detector response for EDTA with Hummel—Dreyer separation was optimized as a function of drop time and drop size of the s.m.d.e. The detector response increased with drop time, as expected because of the longer deposition time for the reduced metal. A response ratio of 1.0:1.5:2.0 was obtained for drop times of 1, 2 and 5 s, respectively. The detector response also increased with drop size as expected. However, because the larger drop size setting on the PAR 303 produced increased baseline noise, a medium-size drop was used normally.

The linearity of the detector response to the amount of EDTA after separation on the Sephadex column was determined using concentrations from 6×10^{-4} M to 4×10^{-3} M with injection volumes of 50 μl. The least-squares equation for five samples of EDTA between 0.03 μmol and 0.2 μmol was: A (area of peak in cm^2 with 600 μC) = (54.07 ± 0.29) (amount of EDTA, μmol) + (-7.95×10^{-3} ± 0.0296) cm^2. The detection limit for EDTA, separated as the copper complex via Hummel—Dreyer chromatography and detected by r.p.a. was calculated as described above to be 0.0022 μmol (0.65 μg).

Citric acid. The citric acid complex of copper was resolved at an unusually small elution volume (V_{ec}/V_0 = 1.56) on the Sephadex G-25 column. Rajan and Martell [28] showed potentiometrically that copper(II) and citric acid (H_4L) react to form a dimeric complex, $Cu_2(HL)_2$, which subsequently loses the hydroxyl protons to form Cu_2L_2. At pH 7.4, citric acid is present as the trinegative anion; therefore the copper complex is probably the M_2L_2 dimer. Calculations based on the experimental conditions (e.g., 1.57×10^{-4} M copper(II), 8×10^{-3} M citric acid) show that the equilibrium concentration of this dimer is significantly larger than the ML-type monomer. Thus, the unusually small volume is consistent with the presence of predominantly a dimeric copper-citrate complex. A detection limit of 1.0 μg was obtained for citric acid using the treatment described above.

Fulvic acids. The above technique was applied to quantify fulvic acid. As previously stated, Mantoura and Riley [17] utilized the modified molecular-exclusion technique with an atomic absorption spectrometer as the detector to determine stability constants of metals with fulvic acid. One of the objectives of the present work was to determine the applicability of the modified technique in conjunction with the more convenient and sensitive flow electrochemical cell. Two fulvic acid samples used were (1) a water-derived fulvic acid sample isolated (see Experimental) from a North Dakota waterway and (2) a soil fulvic acid sample obtained from New Hampshire. The two samples produced quite different chromatographic behavior on the Sephadex G-15

columns, which were eluted with a buffer (of ionic strength 0.02) and 10 mg l^{-1} copper. The water-derived sample produced four peaks or complexes with copper(II) (Fig. 5A). The first large peak represents a copper(II)-fulvic acid complex with a molecular weight greater than 1500 daltons, since it occurs at the column void volume and the exclusion limit of Sephadex G-15 has been reported as 1500 daltons [21]. Three smaller peaks are noted at larger retention volumes. These peaks are the apparent result of lower-molecular-weight copper complexes of fulvic acid and/or adsorption of fulvic acid-metal complexes, which contain functionalities capable of interactions with the column packing. These chromatograms were reproducible on separately prepared Sephadex G-15 columns. Two different water-derived samples, which were obtained and isolated in separate experiments, produced similar chromatograms with the exception of the fourth peak, which had a retention volume that was not reproducible between the two samples.

The above results are somewhat different than those reported by Mantoura and Riley [17]. Their chromatograms showed a single peak, with an area within 1.5% of the trough area; however, the amounts of fulvic acid injected on the columns were considerably higher (2.73 mg vs. 0.05 mg in Fig. 5A). Other factors, including the water source of the fulvic acid, could be important in determining the nature and concentrations of functionalities on the molecules, which affect the adsorption behavior on the dextran-based Sephadex packing. In order to obtain additional information on the multipeak phenomenon of the water-derived samples, a soil-derived fulvic acid sample was tested (Fig. 5B). A single dominant peak for the metal complex is observed at the void volume of the column, again indicating a molecular weight of >1500 daltons for the copper-fulvic acid complex. No additional peaks were noted; however, the peak area is considerably larger than the trough area. This enhanced peak area is probably due to: (1) adsorption of fulvic acid on the d.m.e. of the flow cell resulting in electrode drop vibrations with a concomitant increase in mass transfer and/or (2) functionalities on the fulvic acid-copper(II) complex, which are electroactive. The adsorption of fulvic acid in the presence and absence of metal ions on mercury electrodes

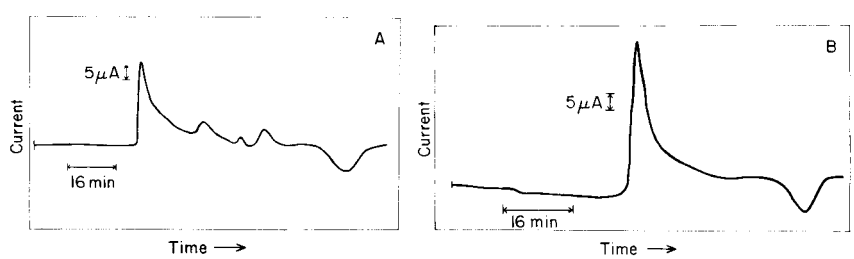

Fig. 5. Modified molecular-exclusion chromatograms for (A) 0.05 mg of water-derived fulvic acid and (B) 0.15 mg of soil fulvic acid on a Sephadex G-15 column. Conditions: elution with Tris buffer at pH 7.4 containing 10 mg l^{-1} Cu(II), 0.01 M $NaNO_3$ and 0.01 M Tris. Flow rate: (A) 0.05 ml min^{-1}; (B) 0.6 ml min^{-1}. Detector was the s.d.m.e. flow cell.

has been documented in the literature and thus increased cell currents could be observed as the eluent containing copper(II) fulvate passed through the flow cell [29]. The electrochemistry of fulvic and humic acids has also been investigated by Cominoli et al. [30]; they showed that although the faradaic currents observed are small, significant changes in capacitive currents can be measured. Fulvic acid was tested for electrochemical behavior in this laboratory by normal and reverse-pulse polarography in the Tris acetate buffer (pH 7.4). No significant redox processes were noted in the potential range 0.0 to —0.75 V, which was employed in the r.p.a. technique. Therefore, the enhanced peak area is probably the result of adsorption of fulvic acid on the d.m.e. Comparison of the combined peak areas (four) vs. the trough area for the water-derived fulvic acid sample indicated similar, but less dramatic behavior (see Fig. 5A).

The linearity of the detector response to the amount of water-derived fulvic acid after separation on the Sephadex column, was determined using amounts from 0.1 mg to 0.3 mg with injection volumes of 50—150 μl. In an attempt to eliminate possible erratic detector response from apparent adsorption of fulvic acid, the areas of chromatogram troughs were measured to construct calibration graphs. The least-squares equation for five samples (0.1—0.3 mg) of water-derived fulvic acid was: A (area of trough in cm^2 with 240 $\mu C\ cm^{-2}$) = (22.1 ± 0.3) (amount of water-derived fulvic acid, mg) + (0.05 ± 0.06) cm^2. The detection limit was evaluated to be 5.5 μg.

In order to demonstrate the feasibility of the method on industrial water samples, a concentrated fulvic acid sample (250 mg l^{-1}) was prepared to simulate a stagnant water system. The sample (100 ml) was spiked with 0.10 mmol of EDTA and a 100-μl aliquot was injected on the Sephadex G-15 column (Fig. 6). Quantitation of the EDTA in the sample by direct calibration showed 95 ± 3% recovery.

Conclusions

The above data suggests that modified molecular-exclusion chromatography combined with electrochemical detection techniques is useful in identifying and quantifying organic binding agents which are capable of metal

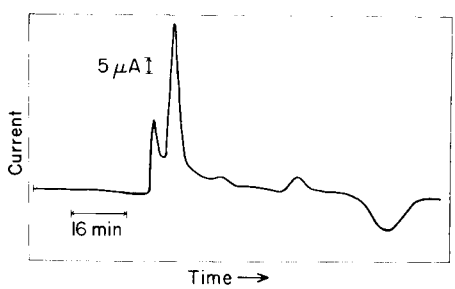

Fig. 6. Modified molecular-exclusion chromatogram for 0.025 mg of water-derived fulvic acid and 0.10 μmol of EDTA on a Sephadex G-15 column. Conditions as in Fig. 5.

complexation. The technique can be used either to quantify the ligand(s) or to separate and identify various metal complexes; the metal buffering technique permits the separation of both inert and labile metal complexes. Although the resolution of various metal complexes was not completely optimized, the modified Sephadex G-25 column was able to resolve a mixture of commonly employed polyaminocarboxylic acids. The optimization of resolution using uniform, small particle-size column packings, such as the 10 μm particle size Spherogel TSK 2000 packings, is currently under study. However, because of the relatively low cost and wide availability of soft gels, these columns could be of more practical value. The described technique is potentially useful in the determination of complexation capacities in water systems. The technique not only provides a measurable "peak", but in addition a trough or metal depletion band is noted in the eluent. The trough therefore can be utilized in measurements of the overall binding ability of an aqueous sample. This could be particularly important for metal complexes that cannot be resolved on a column or that are irreversibly adsorbed onto the column packing.

The authors gratefully acknowledge the support of matching grant B-057-NDAK from the Office of Water Research and Technology and administered by the North Dakota Water Resources Research Institute. We thank Professor James Weber, University of New Hampshire, for the soil-derived fulvic acid sample used.

REFERENCES

1 J. Gardiner, Water Res., 10 (1976) 507.
2 Z. Stojek and J. Osteryoung, Anal. Chem., 53 (1981) 847.
3 J. Gardiner, Analyst (London), 102 (1977) 120.
4 J. E. Thompson and J. R. Duthie, J. Water Pollut. Control Fed., 4 (1968) 306.
5 B. K. Afghan, P. D. Goulden and J. F. Ryan, Anal. Chem., 44 (1972) 354.
6 B. J. Haring and W. V. Delft, Anal. Chim. Acta, 94 (1977) 201.
7 J. P. Haberman, Anal. Chem., 43 (1971) 63.
8 R. J. Stolzberg, Anal. Chim. Acta, 92 (1977) 139.
9 P. T. Kissinger, Anal. Chem., 49 (1977) 447A.
10 L. J. Felice and P. T. Kissinger, Anal. Chem., 48 (1976) 794.
11 P. T. Kissinger, C. Refshauge, R. Dreilling and R. N. Adams, Anal. Lett., 6 (1973) 465.
12 D. G. Swartzfager, Anal. Chem., 48 (1976) 2189.
13 B. Fleet and C. J. Little, J. Chromatogr. Sci., 12 (1974) 747.
14 A. M. Bond and G. G. Wallace, Anal. Chem., 53 (1981) 1209.
15 A. M. Bond and G. G. Wallace, Anal. Chem., 55 (1983) 718.
16 R. A. Saar and J. H. Weber, Environ. Sci. Technol., 16 (1982) 510A.
17 R. F. C. Mantoura and J. P. Riley, Anal. Chim. Acta, 78 (1975) 193.
18 S. A. Cohen and D. E. Bartak, Anal. Lett., 16 (A6) (1983) 429.
19 P. Maitoza and D. C. Johnson, Anal. Chim. Acta, 118 (1980) 233.
20 J. M. Sosa, Anal. Chem., 52 (1980) 910.
21 Gel Filtration: Theory and Practice, Pharmacia Fine Chemicals, Uppsala, Sweden, 1979.
22 J. H. Weber and S. A. Wilson, Water Res., 9 (1975) 1079.

23 J. Osteryoung and E. Kirowa-Eisner, Anal. Chem., 52 (1980) 62; J. Osteryoung, D. Talmar, J. Hermolin and E. Kirowa-Eisner, J. Phys. Chem., 85 (1981) 285.
24 R. K. Skogerboe and C. L. Grant, Spectrosc. Lett., 3 (1970) 215.
25 J. P. Hummel and W. J. Dreyer, Biochim. Biophys. Acta, 63 (1962) 530.
26 T. Miyajima, N. Yoza and S. Ohashi, Anal. Lett., 13 (1980) 1441.
27 N. Yoza, J. Chem. Educ., 54 (1977) 284.
28 K. S. Rajan and A. E. Martell, J. Inorg. Nucl. Chem., 29 (1967) 463.
29 J. Buffle and F. L. Greter, J. Electroanal. Chem., 101 (1979) 231.
30 A. Cominoli, J. Buffle and W. Haerdi, J. Electroanal. Chem., 110 (1980) 259.

Analytica Chimica Acta, 158 (1984) 57—65
Elsevier Science Publishers B.V., Amsterdam — Printed in The Netherlands

DETECTION OF TRACE CONCENTRATIONS OF GASES WITH COATED PIEZOELECTRIC QUARTZ CRYSTALS

HÅKON BEITNES and KNUT SCHRØDER*

University of Trondheim, Department of Chemistry — NLHT, N-7000 Trondheim (Norway)

(Received 4th October 1983)

SUMMARY

Coated piezoelectric crystal sensors for determination of trace constituents in gases are very sensitive. Detection limits down to the sub-ppb range have been reported, using injection techniques. From previous and presented data, this high sensitivity is found to be in disagreement with Sauerbrey's eqn., which allows a maximum sensitivity of about 1 ppm. By considering the adsorption of the gases on the coated surface and the calibration procedures used, the validity of Sauerbrey's eqn. is discussed.

Piezoelectric devices have been used for many years for controlling frequency in communication equipment. Quartz crystals are produced which enable a frequency control of 1 in 10^9 or better. The most familiar uses include the time-controlling unit in electronic clocks and utilization of the temperature dependence of the frequency in temperature measurements.

The resonance frequency of a thin crystal wafer of a material with piezoelectric properties depends on the physical dimensions of this crystal and the electrodes on it. The most commonly used piezoelectric material is quartz because of its water insolubility and long useful temperature range. Temperature dependence can be made very small by using a proper angle of cut of the crystal. The use of quartz crystal oscillators to determine small quantities of deposited matter was first explored by Sauerbrey [1, 2] and Lostis [3]. Because the resonance frequency depends on the quantity of deposited material, piezoelectric transducers used to monitor film thickness are of relatively simple construction and are as sensitive as microbalances. By coating the quartz plates with a non-volatile material which selectively sorbs certain gases, the decrease of the resonance frequency depends on the amount of material sorbed. King [4] utilized this effect in quantitative analysis as well as for detectors in gas chromatography. Since that time coated piezoelectric crystal detectors for trace concentrations of different gases have frequently been studied [5]. In spite of the potential usefulness of this analytical technique, with its high sensitivity, few interferences and low cost, it has not been extensively utilized for real analytical purposes except for humidity determinations. This paper deals with some of the practical and theoretical problems concerning the technique.

0003-2670/84/$03.00

THEORETICAL DEVELOPMENTS

A thin crystal wafer of a material with piezoelectric properties has contacts on its two surfaces and made part of an oscillator circuit. The a.c. field induces thickness-shear oscillations in the crystal. If the surface is sufficiently large, the resonance frequency is inversely proportional to the wafer thickness d and proportional to the propagation velocity of the transverse elastic wave in the direction of thickness, i.e., $f = c/2d$. The surfaces of the wafer are antinodal and the wavelength of the resonance wave l is $2d$. As the wafer thickness is increased, it is found from these equations that the wavelength will increase linearly and the resonance frequency will decrease correspondingly. By differentiating:

$$df/dd = -c/2d^2 = -f/d \text{ or } df/f = -dd/d \quad (1)$$

This equation gives the relative decrease of the resonance frequency with the relative increase in thickness and is frequently used for measuring film thickness and deposition rate [6].

Sauerbrey [2] assumed that the same decrease of the resonance frequency is obtained if the thickness is increased with another material with the same mass, irrespective of the density ρ of the material. Then $d = m/A\rho$ or $dd = dm/A\rho$, where A is the surface area of the quartz wafer. By assuming that the surface area is sufficiently large to neglect the end effect, $df/f = -dd/d = -dm/A\rho d$. This enables the decrease of the resonance frequency, Δf, from its initial value, f_0, to be used for measurement purposes

$$\Delta m = -k\Delta f/(f_0 + \Delta f)^2 \quad (2)$$

where k is a constant. This is a version of Sauerbrey's equation.

If the mass of the deposit is sufficiently small, the decrease in frequency changes linearly with the mass deposited. The validity of the linear part of Eqn. 2 was verified experimentally by Sauerbrey [2, 7]. Thus, at least for a sufficiently thin film, the elastic constants do not contribute to the frequency shift, but only the inert mass. Since 1964, when King [4] introduced the "sorption detector", Sauerbrey's equation has been assumed to be valid for the weight increase of coated electrodes caused by sorption, and much work has been done to utilize this analytically [5]. However, no measurements have been made for absolute verification of the applicability of this equation.

Such experiments can be conducted in two different ways: by equilibrating the coated crystals with the gas containing the constituent to be determined, and by using a flow system with an inert gas, and injecting a fixed volume of the gas to be determined. Most of the previous work has been done with the flow system.

It is of interest to calculate the decrease of the resonance frequency caused by sorption of some gases, using a flow system, and assuming the linear part of Eqn. 2 to be valid. The results are given in Table 1, taking

TABLE 1

Calculated maximum decrease of the resonance frequency (Δf) by injection of 5 ml of ammonia or sulphur dioxide in nitrogen carrier gas, assuming 100% sorption (Resonance frequency f_0 = 9 MHz, wave propagation velocity c = 34.4 MHz mm)

Gas concentration (μl l^{-1})	Δf with NH_3 (Hz)		Δf with SO_2 (Hz)	
	8-mm coating[a]	5-mm coating[b]	8-mm coating[a]	5-mm coating[b]
10	13	33	47	121
1	1	3	5	12
0.1	0	0	0	1
0.01	—	—	—	0

[a]Corresponds to sorption on the entire surface of the crystal wafer. [b]Corresponds to sorption on the electrode component of the crystal wafer.

ammonia and sulphur dioxide as examples. From this Table, the maximum theoretical sensitivity is obtained. However, the sensitivity should be considerably lower because of incomplete sorption, mixing effects with the carrier gas, etc. As a consequence, detection limits will never be lower than concentrations corresponding to shifts of frequencies of about 1 MHz, i.e., in the μl l^{-1} (ppm) range.

Previously [5] much work has been done to find coatings which would increase selectivity and sensitivity by using the injection method. This includes the detection of sulphur dioxide [8] and ammonia [9—11] and explosives [12]; the sensitivities quoted are often in the nl l^{-1} (ppb) range or even better. The most sensitive coating is reported to give linear response down to 0.01 μg l^{-1} ammonia [11]. The decrease in frequency is thus far higher than the value corresponding to Sauerbrey's equation and seems to depend more on the change of properties of the coating used, caused by the deposited material, than on the mass of that material.

The linear part of Eqn. 2 can be expressed as $\Delta f = K\Delta C$, where K is a constant and C is the concentration of the compound to be measured. This equation assumes complete sorption of the gas or sorption corresponding to the linear part of the Langmuir isotherm. In order to plot the change in frequency vs. concentration over a large range, i.e. from 0.01 nl l^{-1} to 100 μl l^{-1} as one graph, log Δf vs. log ΔC is frequently plotted; straight lines are then obtained [11, 12]. According to this equation, the log—log slope should be unity. Previously reported double logarithmic plots have slopes far from that value, e.g., 0.0615 [11] and 0.319 [12].

These unexpected results can be explained by using the familiar Freundlich sorption isotherm. This explanation is doubtful, however, because this isotherm is valid only over a narrow concentration range and at intermediate concentrations. No further explanation of the unexpected slope is available, except that this supports the assumption that the decrease in frequency

seems to depend more on the change of the properties of the coating used than on the mass.

The inaccuracy in the preparation of standard test gases from the $\mu l\ l^{-1}$ to the sub-nl l^{-1} range is obvious, because of adsorption, contamination, etc. One simple way of preparing the test gases is to utilize a syringe dilution method [8], e.g., by successive dilutions of 1 ml of the test gas with an inert gas to a total volume of 10 ml, in order to prepare standards. The initial concentration of the gas is C_0, with the concentration C_i after i dilutions from volume v to V. If a constant fraction (k) of the gas prior to dilution remains in the syringe (e.g., by adsorption on the walls), then

$$C_m = (C_{m-1}v/V) + kC_{m-1} = C_{m-1}(k + v/V) \text{ and } C_m = C_0(k + v/V)^m \quad (3)$$

Combination of this equation with the equation $\Delta f = K\Delta C$ and taking logarithms yields

$$\log \Delta f = \log KC_0 + m \log (k + v/V) \quad (4)$$

Equation 4 shows that systematic errors in the syringe dilution method, e.g., sorption on the syringe wall between dilutions, can explain the unexpected slope of less than one in the log—log calibration plots. This, in turn, also can explain a detection limit that is too small to be possible on the basis of the Sauerbrey equation. However, without experimental evidence, it seems unreasonable that this alone is the explanation.

EXPERIMENTAL

Apparatus

In this study, 9-MHz AT-cut quartz crystals were used. The wafers were circular, of 8-mm diameter and with gold-plated electrodes (5-mm diameter) on both sides (Norwegian Mining Ltd., Oppegaard, Norway). The crystals were mounted in conventional holders as used for radio communication purposes. The design of the detector cell is largely as described by Hlavay and Guilbault [11]. The type of oscillator circuit used was found to be critical for obtaining oscillating crystals, as well as for giving stable frequencies. Different oscillator circuits were tested; the most successful one (Fig. 1) was built in this laboratory and used for the measurements. A conventional power supply was used. In order to improve the stability and reproducibility of the resonance frequency, it was essential to make the distance from the oscillator to the crystal as short as possible and with all the leads in fixed positions. This was done by making the oscillator as a small unit, directly connected to the crystal holder. The frequency output from the oscillator was measured by a Tritron TS-1080 Frequency Counter (Tritron A/S, Trondheim, Norway). The digital output was also converted to an analog signal to allow the use of a recorder (Omniscribe).

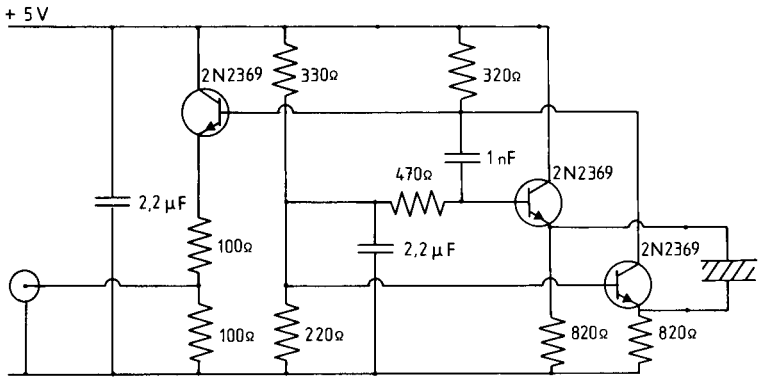

Fig. 1. Electronic diagram of the oscillator circuit.

Reagents

Highly purified nitrogen gas (Norsk Hydro, Norway) was used as carrier and diluting gas. Ammonia gas was taken from a lecture bottle and sulphur dioxide was made from sodium sulphite. L-Glutamic acid hydrochloride, pyridoxine hydrochloride, (both Puriss) and ascorbic acid with silver nitrate were used as coatings in studies of ammonia. Triethanolamine (Merck) was used as a coating in the studies of sulphur dioxide.

Procedures

Coating techniques. L-Glutamic acid hydrochloride was dissolved in ethanol and applied over both surfaces of the crystal with a thin brush, and the ethanol was evaporated. Pyridoxine hydrochloride was dissolved in aqueous ethanol and applied to the crystal as above; the crystal had to be dried for 1 h at 80°C. Ascorbic acid, with different ratios of silver nitrate, was dissolved in ethanol and applied on the crystal as above; the ethanol was evaporated in the presence of carrier gas. Triethanolamine was dissolved in chloroform and applied to the crystal as above; the crystal was dried for 5—7 h at 60°C.

Preparations of diluted sample gases. Most of the experiments were conducted by using the previously reported syringe dilution method [8]. Alternatively, 1-l gas bottles, initially filled with air, were emptied. The gas was pumped out until the remaining gas pressure was about 20 mm Hg. The bottles were filled with the pure test gas (e.g., ammonia) to a pressure of 1 atm. This procedure was repeated. The bottles were next filled with carrier gas (nitrogen), to increase the pressure from 1 to 10 atm. After an equilibration period of about 14 h, the gas was released until the gas pressure was 1 atm., and the bottle was filled with carrier gas as before. From repeated use of this procedure with 1:10 dilution, the required concentration was obtained. The sample was injected into the apparatus, using a syringe previously equilibrated with the sample gas. Alternatively, the diluted gas was used directly, by connecting the gas bottle or the pure carrier gas to the apparatus through a 3-way stopcock.

As another possibility, the latter method was used, but a diluting cell was installed between the 3-way stopcock and the detector cell. This enabled a certain volume of the diluting gas to be added and further dilution to be achieved. The volume was measured with a flowmeter on the outflowing gas.

RESULTS AND DISCUSSION

The deviations from what is expected theoretically were investigated by sorption studies with ammonia and sulphur dioxide on crystals with different coatings and by attempts to monitor the dilution method of standardization of the test gas. When the syringe dilution method was used, log Δf was found to increase almost linearly with the logarithm of the ammonia gas concentration from 10^2 to 10^4 nl l^{-1} ammonia, following the equations (ΔC in nl l^{-1})

$$\log(\Delta f) = 0.05 + 0.4 \log(\Delta C) \quad \text{(pyridoxine coating)}$$

$$\log(\Delta f) = 0.30 + 0.3 \log(\Delta C) \quad \text{(glutamic acid coating)}$$

The slopes, in accordance with previous reports [11], differ from unity, in contrast to what is required if Sauerbrey's equation is valid. Assuming sorption to be complete, the logarithmic form of Sauerbrey's will be (with quantities as in Table 1, 8-mm coating, ΔC in nl l^{-1})

$$\log(\Delta f) = -2.89 + 1.00 \log(\Delta C)$$

Further improvement of the sensitivity by using other coating materials is theoretically impossible if that equation is valid. Karmarkar and Guilbault [9] studied the use of Ucon 75-H-90,000 and Ucon-LB-300X as a coating for ammonia and nitrogen dioxide detection and obtained linearity between 1 nl l^{-1} and 1 μl l^{-1} for both gases and coatings. In contrast to the previously discussed coatings, the logarithmic slope was unity, in accordance with Sauerbrey's equation, but the sensitivity, which exceeded 80 Hz μl^{-1} l (Hz/ppm) cannot be explained by Sauerbrey's equation.

Webber and Guilbault [10] investigated ascorbic acid with silver nitrate as a coating for the detection of ammonia; they used the syringe dilution method. According to the data given in that paper, the frequency change increased linearly with the logarithm of the concentration of ammonia (in nl l^{-1})

$$\Delta f = 70 + 22.5 \log(\Delta C) \quad \text{(ascorbic acid)}$$

$$\Delta f = 100 + 55 \log(\Delta C) \quad \text{(ascorbic acid/silver nitrate)}$$

This logarithmic linearity is again not in accordance with Sauerbrey's equation. Similar investigations were made here, with the result given in Fig. 2. As shown by the indicated 68% confidence limit, the reproducibility is not very good. However, a linear logarithmic plot is not obtained as reported previously [10]. By transforming the curve to a log–log plot, the graph obtained is approximately linear, but the slope is not unity.

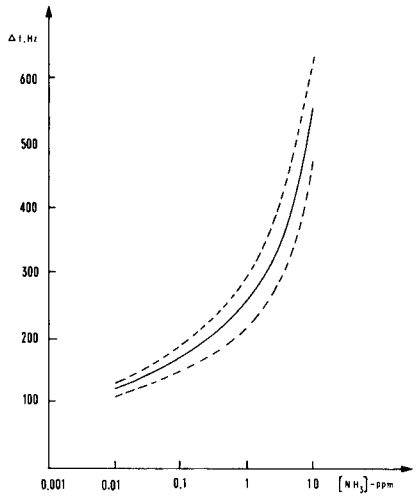

Fig. 2. Plot of ammonia concentration vs. frequency change, using ascorbic acid with silver nitrate as coating material: (---) 68% confidence limit.

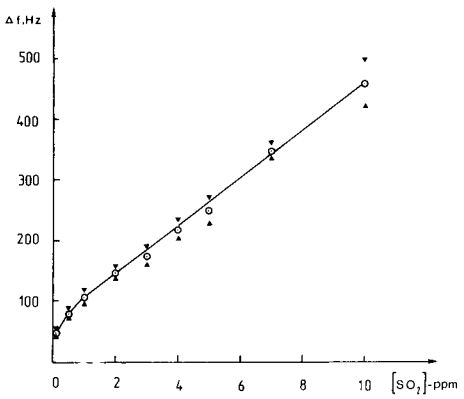

Fig. 3. Plot of sulphur dioxide concentration vs. frequency change, using triethanolamine as coating: triangles indicate the 68% confidence limit.

Detection of sulphur dioxide has previously been reported with different coatings [8]. Assuming 100% sorption, the theoretically most sensitive response, calculated from the data given in Table 1, is given by $\Delta f = 12.1 \Delta C$ (ΔC in μl l^{-1}). The decrease of Δf with different concentrations of sulphur dioxide, using triethanolamine, obtained in the present investigation, is given in Fig. 3. There is a linear response above 1 μl l^{-1} ammonia. These results are about four times more sensitive than those in previous investigations [8]. However, it is of importance to note that, because the actual sorption is considerably lower than 100%, neither the present nor the previously reported results can be explained by the theoretical equation $\Delta f = 12.1 \Delta C$. The slope of the present calibration graph decreases above ca. 1 μl l^{-1}. A similar effect was reported [8] for an Amine 220 coating and was explained by the formation of two different species on the coated surface. This results in a steeper calibration graph at low concentrations, and lowers the detection limit, but it is in further contrast to what is possible with 100% sorption from Sauerbrey's equation.

The syringe dilution method is assumed not to be very accurate for making very diluted standards. Thus, the alternative procedure involving 1-l gas bottles was used for studying ammonia using a coating of ascorbic acid and silver nitrate. The gas was injected into the flow system by using a polyethylene or glass syringe or by a direct injection system connecting the bottle with diluted gas directly to the measuring system via a 3-way stopcock and using a flowmeter to measure the volume of 5 ml. After five successive

dilutions, corresponding to an ammonia concentration of 10 μl l^{-1}, a frequency shift of Δf = 556 Hz was found with the syringe dilution method. When the bottles indicated above were used, considerably lower shifts (114 and 163 Hz, by injection from polyethylene and glass syringes, respectively) were obtained. Although this dilution method is also very inaccurate, the difference between the bottle and syringe dilution methods is significant. But the sensitivity is still above the maximum theoretical value of Δf = 13 Hz obtained from Sauerbrey's equation (Table 1) when bottle dilution is used.

The direct injection method did not give reproducible results, but the Δf values were of the same order of magnitude as the two other methods based on the use of gas bottles.

Tomita and Guilbault [13] used a flask dilution method to obtain the desired concentrations of the sample gas diisopropylmethylphosphonate (DIMP), and a three-component coating. The following calibration equation was obtained

$$\log \Delta f = 1.80 + 0.236 \log \Delta C \quad (\text{in nl } l^{-1})$$

When Sauerbrey's equation is used and 100% sorption is assumed, the corresponding equation is

$$\log \Delta f = -1.88 + 1.00 \log \Delta C \quad (\text{in nl } l^{-1}) \qquad (5)$$

This probably indicates that Sauerbrey's equation is not valid, and that the deviations cannot be explained by errors in the syringe dilution method only.

Recently, Guilbault et al. [14] studied DIMP using other coatings and an evacuation sample dilution method very different from previous methods of dilution. A linear non-logarithmic plot was reported in the range 1—20 nl l^{-1} DIMP, with a slope of 1.4 Δf nl^{-1} l (Hz/ppb) under the most sensitive experimental conditions. This value, however, also does not correspond with Eqn. 5, and supports the limited validity of the theory. The same conclusion was drawn from studies with DIMP and another method of sample dilution [15].

Many other systems have previously been studied, e.g., hydrogen chloride gas with triphenylamine as coating. The reported calibration equations [16] were (ΔC in nl l^{-1})

$$\log \Delta f = 1.00 + 0.24 \log \Delta C$$

$$\log \Delta f = 1.39 + 0.11 \log \Delta C$$

$$\log \Delta f = 1.22 + 0.19 \log \Delta C$$

$$\log \Delta f = 1.21 + 0.21 \log \Delta C$$

which were valid for the concentration ranges 1000—100 000, 100—1000, 10—100 and 1—10 nl l^{-1}, respectively. When trimethylamine was used as a coating for hydrogen chloride, a linear log—log response was reported [16]

in the range 1—100 000 nl l^{-1} with the equation

$$\log \Delta f = 2.26 + 0.0852 \log \Delta C$$

The maximum response based on Sauerbrey's equation, assuming 100% sorption of hydrogen chloride, is

$$\log \Delta f = -2.57 + 1.00 \log \Delta C$$

Detection of a model explosive substance, *o*-nitrotoluene, with a Carbowax 1000 coating has been reported [12]. The following linear log—log calibration equation was valid over the range 7500—3 nl l^{-1}

$$\log \Delta f = 1.06 + 0.319 \log \Delta C$$

The corresponding maximum-response equation is

$$\log \Delta f = -2.00 + 1.00 \log \Delta C$$

It cannot be concluded that Sauerbrey's equation is generally invalid. Recently Ho et al. [17] used a gold-plated detector for traces of mercury and obtained changes of resonance frequencies in agreement with Sauerbrey's equation. To explain the deviations from this fundamental equation, the nature of the deposit as well as the calibration method have to be studied further; this work is in progress.

REFERENCES

1 G. Sauerbrey, Phys. Ver., 8 (1957) 113.
2 G. Sauerbrey, Z. Phys., 155 (1959) 206.
3 M. P. Lostis, J. Phys. Radium, 20 (1959) 25.
4 W. H. King, Jr., Anal. Chem., 36 (1964) 1735.
5 J. Hlavay and G. G. Guilbault, Anal. Chem., 49 (1977) 1890.
6 K. H. Behrndt and R. W. Love, Vacuum, 12 (1962) 1.
7 H. L. Eschbach and E. W. Kruidhof, Vacuum Microbalance Techniques, Vol. 5, Plenum Press, New York, 1966, p. 207.
8 K. H. Karmarkar and G. G. Guilbault, Anal. Chim. Acta, 71 (1974) 419.
9 K. H. Karmarkar and G. G. Guilbault, Anal. Chim. Acta, 75 (1975) 111.
10 L. M. Webber and G. G. Guilbault, Anal. Chem., 48 (1976) 2244.
11 J. Hlavay and G. G. Guilbault, Anal. Chem., 50 (1978) 1044.
12 Y. Tomita, M. H. Ho and G. G. Guilbault, Anal. Chem., 51 (1979) 1475.
13 Y. Tomita and G. G. Guilbault, Anal. Chem., 52 (1980) 1484.
14 G. G. Guilbault, J. Affolter, Y. Tomita and E. S. Kolesar Jr., Anal. Chem., 53 (1981) 2057.
15 E. P. Scheide and G. G. Guilbault, Anal. Chem., 44 (1972) 1764.
16 J. Hlavay and G. G. Guilbault, Anal. Chem., 50 (1978) 965.
17 M. H. Ho, G. G. Guilbault and E. P. Scheide, Anal. Chim. Acta, 130 (1981) 141.

Analytica Chimica Acta, 158 (1984) 67—84
Elsevier Science Publishers B.V., Amsterdam — Printed in The Netherlands

KINETICS IN CONTINUOUS FLOW SAMPLE PROCESSING
Chemical Contributions to Dispersion in Flow-Injection Techniques

C. C. PAINTON and HORACIO A. MOTTOLA*
Department of Chemistry, Oklahoma State University, Stillwater, OK 74078 (U.S.A.)
(Received 22nd August 1983)

SUMMARY

A numerical model based on a basic dispersion equation modified by simultaneous consideration of the chemical effect introduced by a chemical reaction taking place as the sample plug disperses has been tested. Computer analysis and simulation (by use of an alternating direction implicit finite difference approximation) by solving the laminar dispersion equation and the rate expression simultaneously, have been evaluated with experimental studies of a reaction of moderate speed (oxidation of ascorbic acid by dichromate ion). Theoretically generated signal profiles indicated the need for three correction factors representative of the deviation of the experimental system from ideality. The rate coefficient in the chemical kinetic term (if pseudo-first-order is assumed) appears to change in an oscillating manner reflecting the complexity of the overall kinetic process. A straight-line relationship was found between the time at peak maximum and the rate coefficient in computer-simulated curves. Such a correlation provided a way to estimate a value for the rate coefficient of the L-ascorbic acid/dichromate reaction which agreed with the one obtained from batch kinetic determinations. In some of the cases studied, the unbalanced evolution of dispersion forces resulted in chemically induced double-humped peaks.

A recent review has given an overview of dispersion in unsegmented continuous-flow sample processing; it was concluded that surprisingly little attention has been paid to chemical kinetic contributions to signal shape in such systems [1]. This paper reports the testing of a numerical model based on the basic dispersion equation (Eqn. 2 [1]) modified by simultaneous consideration of the chemical effect introduced by an assumed pseudo-first-order chemical reaction taking place as the sample plug is dispersed in the flow stream. The basic concept underlying these investigations is that chemical reactions alter the concentration profile within the plug and its boundaries, which induces diffusion and convection. The resulting mass transfer dynamics in turn affect the collisional frequency that triggers chemical reactions. The combination of these processes in cyclic form is ultimately responsible for the distribution of monitored chemical species that produce the signal detected as the dispersed sample plug passes the detector. Computer analysis and simulation have been accompanied by an experimental study of a moderate-speed reaction previously used to illustrate how chemical reactions can obscure the information provided by the so-

0003-2670/84/$03.00

called "practical dispersion parameter" [2]. The reaction in question is the oxidation of L-ascorbic acid by dichromate ion

$$Cr_2O_7^{2-} + 3C_6H_8O_6 + 8H^+ \rightleftharpoons 2Cr^{3+} + 7H_2O + 3C_6H_6O_6 \quad (1)$$

Intercalation of a dichromate solution into a stream of water of equal pH led to dispersion resulting solely from physical mass transport and as a result of concentration gradients and velocity profiles under laminar flow conditions. Intercalation of similar samples into aqueous streams containing L-ascorbic acid, however, added the chemical effect represented by Eqn. 1. Contributions to dispersion by different reactor geometries and materials cannot be directly included in the model because of their rather empirical nature. They produce serious deviations of experimental observations from the concentration profile predicted by the model but have been, in first approximation, corrected empirically.

EXPERIMENTAL

Apparatus

The spectrophotometric flow system was a custom-assembled unit as described previously [2]. Samples were introduced through a custom-made rotary valve [3]. Because of the construction of this valve, there is an inherent additive volume, V_d, to the volume of the sample loop used. This additive volume is independent of the size of the interchangeable loops, so that the total injected volume is

$$V_s = V_d + \pi a^2 L_s \quad (2)$$

where L_s is the total length of the sample loop tubing of radius a. The additive volume, V_d, was determined from the intercept of a calibration plot obtained by weighing clean mercury. The plot in question corresponded to the actual volume delivered vs. different lengths of sample loops and yielded an intercept corresponding to $V_d = 20.7\ \mu l$.

Because differences in reactor geometry produce deviations which are reflected in the experimentally collected results, a fixed reactor geometry was used for comparison purposes. Detailed measurements for different parts (e.g., connectors) of the sample transport system were as follows. In the sampling portion, the trailing portion of the sample loop was 1.2 cm long, 0.10 cm i.d., the center portion was of various lengths (0.050 cm i.d.) and the leading portion was 1.2 cm long, 0.10 cm i.d. The connection from sampling portion to main reactor path was 0.50 cm long, 0.13 cm i.d. The main reactor tubing was of various lengths (0.050 cm i.d.). The connection to the flow cell was 2.8 cm long, 0.2 cm i.d.; the flow cell inner path was 0.8 cm long, 0.28 cm i.d., the flow cell detecting area was 1.00 cm long, 0.32 cm i.d. Correction factors f_B and f_C discussed later in the text apply to these geometries and reflect the nonideality introduced by connecting portions and the relative length of the main reactor. Corners of concern in

the geometry are the one between the main reactor and the entrance to the flow cell and the one inside the cell itself (see Fig. 1 [2]).

Reagents and solutions

The carrier stream was pumped from a closed dark reservoir at a constant rate. The flow rate was adjusted by varying either the size of the pumping tube or the pump revolutions per unit time. The sample was introduced downstream from the reservoir at a point defining the start of the "reactor". The dispersed or dispersed-reacted sample plug was monitored at the exit of the reactor as it passed through the flow cell. During use of the reaction shown in Eqn. (1), the monitored species was the unreacted dichromate with an absorption maximum at 352 nm. The peristaltic pump was located either before the point of injection or after the point of detection. After detection, the flowing solution was sent to waste.

The carrier stream was a 0.005–0.05 M solution of L-ascorbic acid (used in experiments to evaluate the chemical reaction effect) or aqueous solutions (hydrochloric or perchloric acid) of the same pH as the intercalated plug. All intercalated samples consisted of 0.00050 M potassium dichromate. The flow rate was varied in the range 0.05–6.0 ml min^{-1}. The reactor tube diameters were 0.5, 0.8, 1.0, and 1.3 mm, corresponding to tube volumes of 0.96, 5.03, 7.85, and 13.3 μl cm^{-1}. Straight tube reactors had lengths between 30 and 600 cm and coiled tube reactors were composed of interconnected lengths of 30 cm (straight)—120 cm (coiled)—30 cm (straight) with coil diameters of 3.4, 6.7, 12.2, 15.6, 22.3 mm. The length of the sample loop was varied within the range 7.0–600 cm, corresponding to sample volumes of 33.70—1198 μl. All volumes were determined by calibration with mercury. All tubing was Tygon, microbore, formulation S-54-HL for surgical and hospital use (Norton Plastic and Synthetics Division, Akron, OH).

The chart speed and chart span were selected carefully in order to ensure adequate resolution of details in the recorded signal.

MATHEMATICAL ANALYSIS AND COMPUTER SIMULATIONS

The dispersion equation and its transformation

Dispersion resulting solely from physical mass transport as a result of concentration gradients and velocity profiles is considered here. The dispersion in a laminar flow can be described by

$$(dC/dt) + U_{max}(1 - r^2/a^2)dC/dx = D[(d^2C/dx^2) + (dC/rdr) + (d^2C/dr^2)] \quad (3)$$

where C is the concentration in mol l^{-1}; t is the time in s; U_{max} is the maximum linear velocity on the center axis of the tubing in cm s^{-1}; r is the radial distance from the center axis of the tubing in cm; x is the axial distance from the injection point in cm; D is the molecular diffusion coefficient in cm^2 s^{-1}; and a is the radius of the tubing in cm.

This equation is now transformed into dimensionless form for two reasons.

First, the dispersion of a sample of fluid into a carrier stream flowing in a tubular pipe is a dynamic phenomenon dictated by parameters such as the tube radius (a), flow velocity (u), and molecular diffusion coefficient (D). Thus, it is convenient to have flow parameters which include the overall effect of reactor dimensions and flow mechanics. Secondly, some parameters are normalized to simplify mathematical operations.

The transformed equation is

$$(dC^*/d\tau) + [(1 - y^2)/\tau^{1/2} - (\Omega/2\tau)](dC^*/d\Omega) = (1/\tau N_{pe}^2)(d^2C^*/d\Omega^2) + (1/y)(dC^*/dy) + (d^2C^*/dy^2) \quad (4)$$

as shown in the Appendix.

With intercalation of a dichromate solution into an aqueous solution of L-ascorbic acid, when the chemical reaction contributes to the driving force for dispersion as already noted, Eqn. (3) can be modified as follows

$$(dC/dt) + U_{max}(1 - r^2/a^2)(dC/dx) = D[(d^2C/dx^2) + (1/r)(dC/dr) + (d^2C/dr^2)] - k(C)^n \quad (5)$$

where k is the rate coefficient for the reaction and n corresponds to the order of the chemical reaction in question. This equation states that physical dispersion and the chemical reaction contribute simultaneously to the change of concentration/time profile in the flow system. The problem represented by Eqn. (5) can be regarded as: (a) a situation in dispersion in which some of the dispersing substance reacts as the dispersion proceeds, or (b) a situation in chemical kinetics in which the rate of chemical reaction depends on the rate of supply of one of the reactants by the dispersion. For the experimental conditions studied here, in which the chemical reaction occurs when the sample solution disperses into the carrier solution, or vice versa, from sample/carrier boundaries, it would seem appropriate to accept description (a). Therefore, Eqn. 5 is regarded as two simultaneous equations

$$dC/dt = D[(d^2C/dx^2) + (1/r)(dC/dr) + (d^2C/dr^2)] - U_{max}(1 - r^2/a^2)(dC/dx) \quad (6a)$$

$$dC/dt = -k(C)^n \quad (6b)$$

For a first-order (or a pseudo-first-order) reaction, the concentration resulting from the chemical reaction follows the relationship, $C_{chem} = C_d[\exp(-kt)]$, where C_{chem} represents the concentration resulting from the chemical reaction and the physical dispersion and C_d represents the concentration resulting from physical dispersion alone. This equation can be transformed into a dimensionless form

$$(C_{chem})^* = (C^*)\exp(-\kappa\tau) \quad (7)$$

where $(C_{chem})^*$ represents the normalized concentration remaining from chemical reaction and physical dispersion, C^* represents the normalized

concentration remaining from physical dispersion only, τ is the reduced time, and κ is the reduced rate coefficient ($\kappa = a^2k/D$).

Numerical analysis

The method adopted for numerically solving Eqn. (4) was the alternating direction implicit finite difference approximation [4]. Ananthakrishnan et al. [5] used it to solve for the dispersion occurring at the single sample-carrier boundary resulting from a constant flow injection, and Vanderslice et al. [6] adapted this approach to solve for the dispersion occurring at both boundaries in sample plug injection. These solutions, however, do not allow for the effect of chemical reactions. In the present work, Eqns. 4 and 7 were alternately solved for each time step. Equation 7 is a simple analytical expression and offers no difficulties. The numerical solution of the second-order partial differential equation represented by Eqn. 4 was based on the following rationale. First, for a cylindrical tube of uniform diameter, the dispersion is assumed to be radially symmetrical about the axis. Consequently, a grid point network used in the numerical solution may be arranged using two dimensions as shown in Fig. 1. In the radial direction (y), the grid points are bounded between the center (origin, y_0) and the tube wall. In the longitudinal direction (Ω), the grid points spread out from the entrance of the fluid (Ω_0) to a point sufficiently distant that only a negligible amount of sample is to be found. Second, the dispersion equation is replaced by the following difference equation

$$(C^*_{i,j,2n+1} - C^*_{i,j,2n})/(\Delta\tau) + \{(1-y^2)/\tau^{1/2} - \Omega/2\tau\}\{(C^*_{i+1,j,2n+1} - C^*_{i-1,j,2n+1})/(2\Delta\Omega)\} = (C^*_{i,j+1,2n} - 2C^*_{i,j,2n} + C^*_{i,j-1,2n})/(\Delta y)^2 + \{(C^*_{i,j+1,2n} - C^*_{i,j-1,2n})/(2\Delta y)\}/y + \{(C^*_{i-1,j,2n+1} - 2C^*_{i,j,2n+1} + C^*_{i+1,j,2n+1})/(\Delta\Omega)^2\}/\tau N^2_{pe} \quad (8)$$

Third, the initial and boundary conditions for $\tau = 0$ are set. Fourth, time is advanced by one time step, $\Delta\tau$. Fifth, by proceeding along the Ω direction,

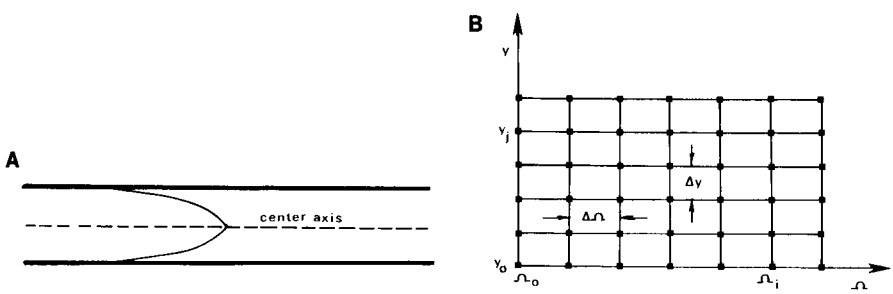

Fig. 1. A, Laminar flow profile in a cylindrical pipe. B, Grid point arrangement in the pipe for numerical calculation of flowing fluid dispersion.

Eqn. 8 is solved on the assumption that the total of grid points in the longitudinal direction is P; this treatment will lead to a set of P simultaneous equations with coefficients that are called the tridiagonal matrix. Sixth, the tridiagonal matrix system is readily solved by a Gaussian elimination method [4]. Seventh, the fifth and sixth steps are applied to the y direction as well. Eighth because an injected sample bolus has two boundaries, steps 1—7 are performed twice, once each for the leading and trailing boundaries. Ninth, the total concentration at a fixed longitudinal positon is integrated over the cross-section. Finally, the sequence of steps 4—9 is repeated until the accumulated time reaches a preset limit.

The stability and the convergence of the solution have been discussed [4, 5]. Mesh sizes that are too large result in divergence and instability of the solution. Mesh sizes that are too small, however, require excessive time and expense. Consequently, the mesh sizes used in the present study were selected via a meticulous trial-and-error process.

Computer algorithm and programming

The computer algorithm used is described by the following series of steps. (1) The mesh sizes for the longitudinal distance, radial distance, and time (i.e., $\Delta\Omega$, Δy, and $\Delta\tau$) were carefully chosen; thus, the total number of grid points in each direction and the total time elapsed was determined. (2) The initial condition was set by assigning computer memory locations to each of the grid points. (3) The leading section and the trailing section of the sample plug dispersion were calculated simultaneously; for the leading section, the sample ($C_0^* = 1$) disperses into the carrier ($C_0^* = 0$) while for the trailing section, the carrier ($C_0^* = 0$) disperses into the sample ($C_0^* = 1$). (4) The time was increased by $1/2\Delta\tau$. (5) Coefficient arrays for the tridiagonal matrix and the solution for grid point concentration were computed for the Ω-implicit equations. (6) The time was increased by $1/2(\Delta\tau)$. (7) Coefficient arrays for the tridiagonal matrix and the solution for the grid point concentrations were computed for the y-implicit equations. (8) The Ω- and y-implicit equations were applied alternately by repeating steps 4—7 for the various time steps. (9) The entire procedure was repeated until the desired value of τ was reached. The grid-point concentration distribution for the sample plug at the end of each $\Delta\tau$ step was calculated by subtracting the distribution of the trailing portion from the distribution of the leading portion. (10) The total concentration within the dimension of the flow cell was then integrated and the resulting concentration/time data were printed out. (11) For the system in which a chemical reaction was occurring in addition to the physical dispersion, Eqn. 7 was used to calculate the final point concentrations at the ends of step 5 and each step 8.

The FORTRAN/WATFIV program incorporating the above algorithm was run on an IBM/370 computer. A listing of the program is available from the authors.

RESULTS AND DISCUSSION

Comparison of the Taylor model with the numerical solution model

This comparison involves only physical dispersion; no chemical kinetic contribution is included. Taylor's model operates under two basic assumptions: (1) the material of mass M is originally concentrated at a point $x = 0$, at time $t = 0$, so that the volume of the sample is negligible in comparison with the volume of the reactor tubing, and (2) $(L/U_{max}) \gg (a^2/3.8^2D)$, where L represents the total length of the reactor tubing. By use of the following two equations

$$C = (1/2)Ma^{-2}\pi^{-3/2}(Kt)^{-1/2}\exp\{-[x - 1/2(U_{max})t]^2/4Kt\} \quad (9)$$

$$K = a^2(U_{max})^2/192D \quad (10)$$

and with input data corresponding to given experimental conditions, the concentration/time profile was calculated and compared with experimentally obtained curves. Figure 2 illustrates such a comparison for values of L/U_{max} typical of flow-injection techniques. Figure 3 serves to locate the region covered in this work in comparison with that of other research groups in flow injection and the area of validity of some models for physical dispersion. The analysis of these figures (and others not illustrated) shows that the second assumption of the Taylor model is not satisfactory; the closer the

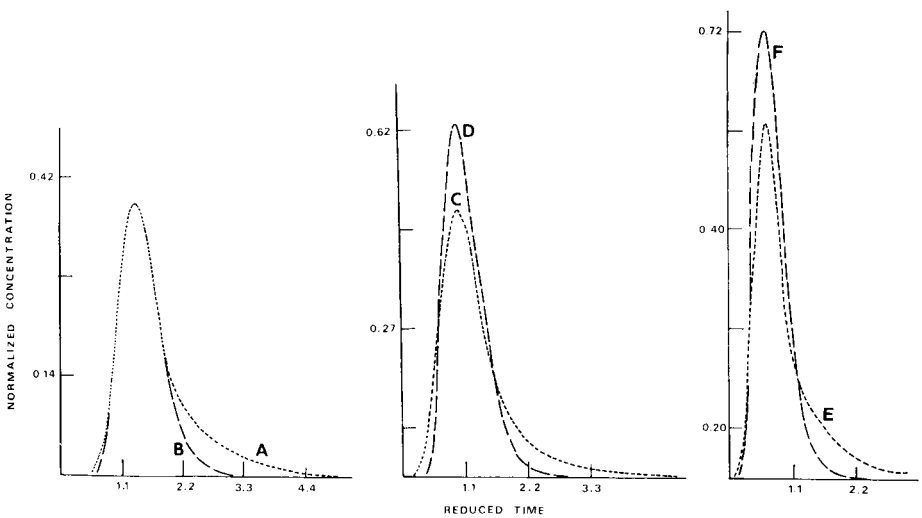

Fig. 2. Comparison of experimental concentration/time profiles (curves A, C, E) with simulated curves obtained from Taylor's model (curves B, D, F). L/U_{max}: curves A and B, 29.8 s; curves C and D, 18.8 s; curves E and F, 11.4 s. Experimental conditions: a (radius) = 0.025 cm; reactor with straight open-tube L = 405 cm (A, B), 255 cm (C, D), 155 cm (E, F); sample volume, V_s = 62 μl; flow rate = 0.80 ml min^{-1}; pH 4.76.

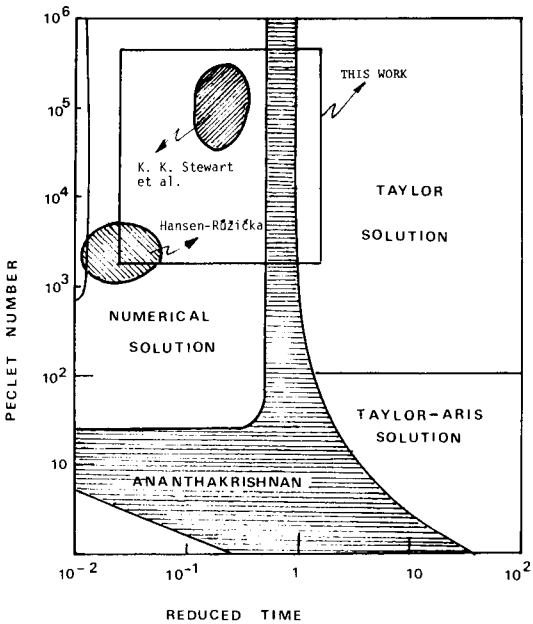

Fig. 3. Graphical representation of the different experimental and solution situations encountered in the consideration of dispersion in unsegmented continuous-flow sample processing as a function of Peclet number and reduced time.

value of L/U_{max} to the value of $(a^2/3.8^2D)$, the larger the discrepancy. Even on a purely physical basis, Taylor's model fails to describe some situations encountered in practice. The first assumption of the model can be validated without much effort, but not the second. To satisfy the second assumption, either very long tubing or a very low flow rate is required. Neither option is practical for flow-injection experiments.

The use of the numerically solved dispersion equation for simulating dispersion curves of the same kind is more satisfactory. Figure 4 demonstrates the agreement between simulated curves generated from the numerical solution of Eqn. 4 and the corresponding experimental ones. Even at low values of L/U_{max}, the agreement was satisfactory. The theoretically generated curves, however, had to be subjected to tail correction because of the nonideality of the experimental conditions. The incorporation of three correction factors, summarized in Table 1, significantly improved the fit. These factors are needed because of nonuniformity of the reactor-connector diameters, the inner path diameters of the injector, and detector flow-cell geometry. Two of the correction factors, f_A and f_B, were calculated by using expressions given by Vanderslice et al. [6] (see Table 1). The third factor is needed because the simulated concentration data were obtained by integrating over the entire cross-section of the monitoring flow cell. In reality, however, the light path does not cover this entire cross-section.

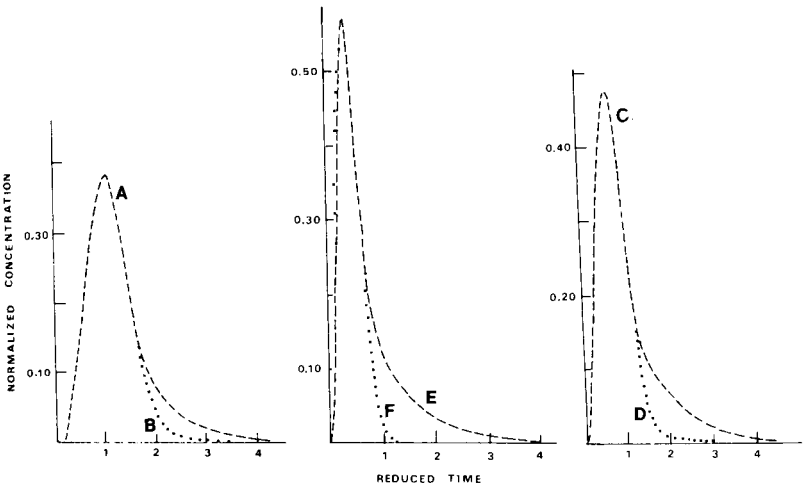

Fig. 4. Comparison of experimental concentration/time profiles (curves A, C, E) with simulated curves obtained from the numerical solution of the dispersion equation (curves B, D, F). L/U_{max} and experimental conditions as in Fig. 2.

Consequently, correction factor f_C must be applied. It was calculated by substituting C^*(experimental) and C^*(theoretical) into the corresponding expression found in Table 1. A value of 2.3 was found appropriate for f_C in the work described here. In the process of calculating theoretical concentration/time curves, f_A was used to divide the time scale in each

TABLE 1

Correction factors for the numerically simulated concentration/time curves[a]

Symbol	What it corrects	Expression for use of the correction factor	Comment
f_A	t_A (travel time)	$t_A = 109a^2D^{0.025}(L/F)^{1.025}/f_A$ $0 < f_A < 1$	Approaches unity as the reactor tube length increases
f_B	Δt_B (time for baseline to baseline)	$\Delta t_B = 35.4a^2f_B(L/F)^{0.64}/D^{0.36}$ $0 < f_B < 1$	Independent of reactor tube length
f_C	C^* (Concentration)	$C^* = (C_{theo})^*/(f_C)$ $f_C > 1$	Independent of reactor tube length

[a]Vanderslice et al. [6] used the same value for f_A and f_B and indicated that such a value is between 0.5 and 1.0 depending on either concentration or detector sensitivity. Such assumption was not valid in our case. It should be noted, however, (Fig. 5) that for reactor lengths larger than 600 cm, the dependence of f_A on reactor length seems to diminish considerably.

numerical time step. When the corrected time scale equals the experimental t_A, f_B is used to multiply the time scale in each numerical step. The factor f_C was used to correct the entire concentration/time profile by dividing each integrated concentration value by f_C.

Correction factor f_A was found to depend on reactor length; such a dependence is illustrated in Fig. 5. In contrast, f_B was found to be constant with tube length in the range studied, as long as the injector, flow cell, and all connections remained the same. This is not surprising because f_B depends on factors (diameters of injector, flow cell, and connectors) that are independent of reactor length. A value of 0.86 was found satisfactory for f_B in the studies reported here. The dependence of f_A on reactor length reflects the dependence of t_A, the travel time [6], on the linear flow velocity. This dependence is diminished as the reactor length increases.

The effect of chemical reactions under nonequilibrium conditions on dispersion (concentration/time profiles)

The difficulties encountered in analyzing a purely physical model of dispersion have just been pointed out. The occurrence of chemical reactions as the sample plug travels from injection to detection point further complicates the picture. The obscuring of the reciprocal of the dilution factor, for instance, has been demonstrated [2]. Figure 6 illustrates the problem. This figure shows computer-simulated profiles for a chemical situation similar to that indicated by Eqn. 1. A distinctive trend is observed:

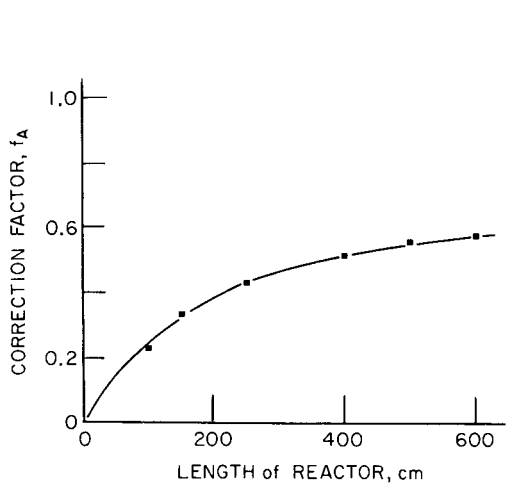

Fig. 5. Variation of the correction factor, f_A, as a function of reactor length.

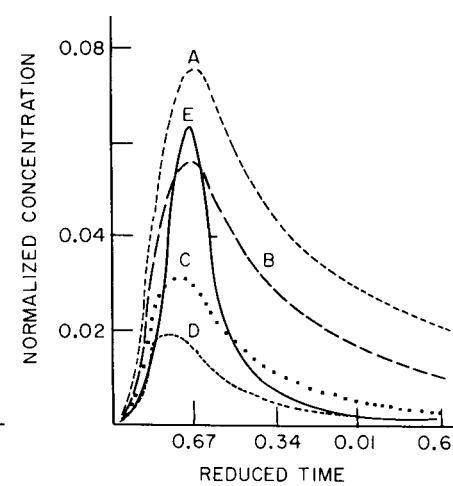

Fig. 6. Comparison of an experimental curve (E) with numerically calculated curves (A—D) at simulated reaction rate coefficients. Experimental conditions: radius 0.025 cm; straight open-tube reactor (L = 405 cm); flow rate 0.80 ml min^{-1}; sample volume 62 μl; pH 4.76. Theoretical curves were calculated with simulated rate coefficients: A, 0.16 s^{-1}; B, 0.20 s^{-1}; C, 0.28 s^{-1}; D, 0.40 s^{-1}.

the larger the rate coefficient, the shorter the time at which the peak maximum appears. This seems to be evidence that while the sample plug is transported, physical dispersion and chemical reaction continuously facilitate each other, and "push" the sample molecules forward. The monitored signal thus must reflect the result of both processes.

Figure 6 shows the numerically simulated curves obtained on the assumption that the rate coefficient is constant throughout the entire body of the sample plug. This assumption, however, is invalid; the kinetics involved within the sample plug are more complex. In Fig. 6 the experimental curve E intersects theoretical curves B—D at different times; this suggests that the rate coefficient "changes" with time. On this rationale, some trial-and-error studies were done to refine the fit of the simulated curve to the experimental one. The experimental curve was then adequately reproduced by varying the rate coefficient throughout the entire calculation process. Figure 7 illustrates the change in rate coefficient as the time elapses. There are

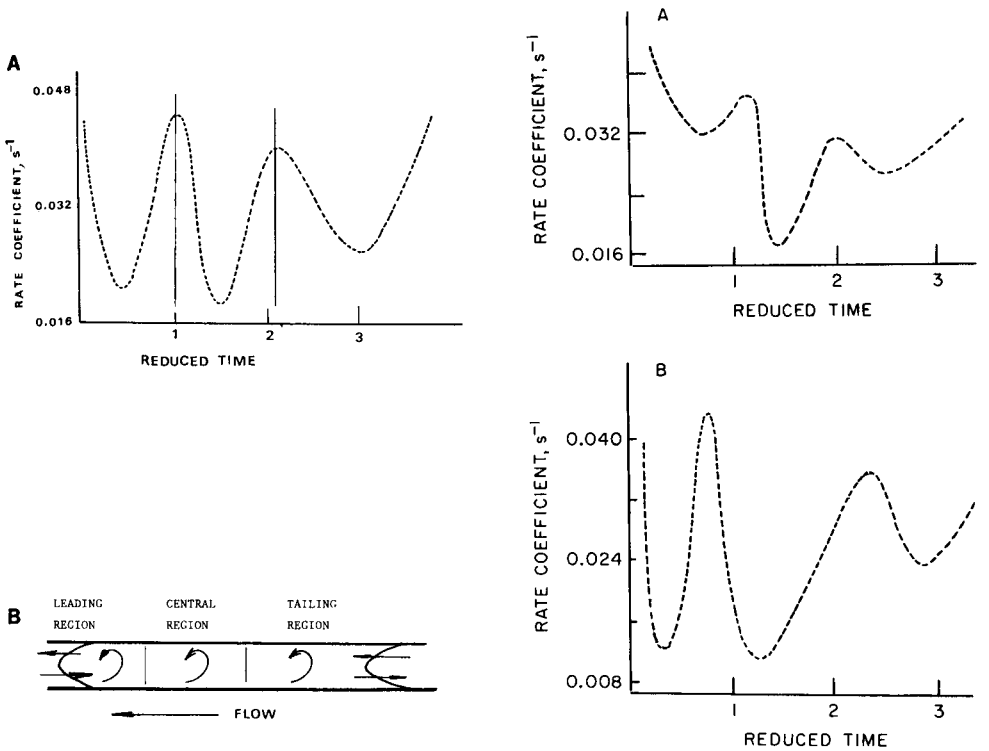

Fig. 7. A, Variation of the rate coefficient with time. B, Corresponding dispersing sample plug.

Fig. 8. Variation of rate coefficient with time as length of reactor is varied: A, reactor length increased about 50% from that of Fig. 7; B, reactor length decreased about 25% from that of Fig. 7.

three cyclic fluctuations that appear throughout the body of the sample plug. This result is reasonable if each fluctuation is assumed to correspond with one of three regions within a sample plug, namely, the leading region, the central region, and the trailing region. Consider a dispersing sample plug which is subdivided into three regions as shown in Fig. 7B. In both the leading and trailing regions, the carrier/sample interfaces induce molecular diffusion, while the velocity profile induces convection. In the central region, where no sample/carrier boundary exists, convection becomes the primary dispersion force. Because the physical dispersions in these three regions of the sample plug differ from one another, the rate coefficients along the length of the plug are expected to vary with a wave pattern. The fact that the reaction rate varies throughout the entire sample plug may mean also that the kinetic order is not constant within the sample plug.

The result in Fig. 8 shows that as the sample plug travels farther (L increased from 405 cm for the curve of Fig. 7 to 605 cm for Fig. 8A), the molecular diffusion at the leading and trailing regions are more developed so that the variation of rate coefficients is less for both regions. An opposite result is observed for a system using shorter reactor tubing (L = 305 cm in Fig. 8B). However, the overall pattern remains the same. First-order kinetics allows a straight-line relationship for the variation of ln C with rate coefficient. It was found that such a relationship also exists between the time at the peak maximum and the rate coefficient. By fitting the data of ln C and time at the peak maximum obtained from the experimental curve into the above two linear relationships, the rate coefficient of the reaction can be estimated. Curves for the ln C and the time at the peak maximum versus rate coefficients, based on the numerical solution of Eqn. 4, are plotted in Figs. 9 and 10. The extracted rate coefficients are listed in Table 2. For comparison, the kinetic data were also extracted with curves simulated from the Taylor model; these values are also included in Table 2. In this table, the rate coefficient obtained from batch experiments was used as a standard to evaluate the accuracy of the predicted rate coefficients obtained from the above theoretical models. Values from the numerical simulation are in good agreement with the value obtained in batch experiments.

Extractions of rate coefficients by using the numerical simulation model were also done at different pH values. Table 3 lists the average per cent error for each pH. As the pH of the system approaches the pK_a value for L-ascorbic acid, 4.05 at 25°C, and 0.1 M ionic strength [7] the observed error decreases; the model would seem to operate better when the HL-species is present.

Double-humped peaks

Double-humped peaks have been observed experimentally [6, 8, 9] and also revealed in Gill and Ananthakrishnan's [10] numerically simulated concentration/time curves. Karlberg et al. [11] and Krug et al. [9] attributed the double-humped peaks to incomplete mixing of the injected sample

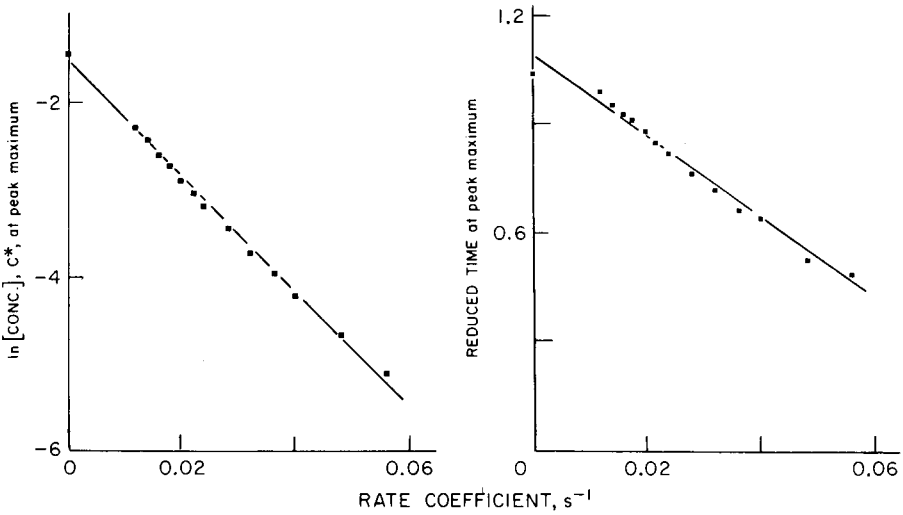

Fig. 9. Variation of ln (peak at maximum) with simulated rate coefficients. (Data extracted from Fig. 6.)

Fig. 10. Variation of reduced time at peak maximum with simulated rate coefficients. (Data extracted from Fig. 6.)

with the surrounding reagent stream. Karlberg et al., however, observed the "double-humped" peaks only for large sample volumes. A split peak may be taken for a double-humped peak, in which the first peak is due to incomplete mixing arising from too large a sample volume while the second one does not relate to the sample size used. Caro [8] explained that the first hump observed in indicator-dilution techniques is due to fast-moving cones of the sample zone while Bate et al. [12] suggested that it may be due to the method of detection. Both suggestions are unclear and lack convincing interpretation. Gill and Ananthakrishnan [10] and Vanderslice et al. [6] reported that a double-humped peak occurs only when the flow condition changes from pure convection to pure diffusion. Mayock et al. [13] pro-

TABLE 2

Evaluation of rate coefficients predicted from theoretical models

Theoretical model	Rate coefficient determined from the batch experiment (s^{-1})	Rate coefficient predicted from ln (C) plot (s^{-1})	Error relative to batch experiment (%)	Rate coefficient predicted from time at peak maximum plot (s^{-1})	Error relative to batch experiment (%)
Numerical simulation model	0.0186 ± 0.0009	0.0186 ± 0.0007	0.00	0.0181 ± 0.0011	2.69
Simulation from Taylor model	0.0186 ± 0.0009	0.0251 ± 0.0005	34.9	0.0251 ± 0.0008	34.9

TABLE 3

Errors for the rate coefficients extracted from numerically simulated curves with respect to the experimental rate coefficients obtained from batch studies at different pH values

pH	3.22	3.64	3.81	4.76	5.25
Error %	9.24	5.09	3.43	1.08	1.16

vided what appears to be the best explanation for the formation of such peaks. Their view is that the first peak is a manifestation of convection dominating in the central region of the tube, while the "gentle" second peak is the evolution of the diffusion shoulder which indicates a strong diffusional influence in the tube wall region. For the same τ value, Reijn et al. [14] observed a double-humped peak with a straight tubing while a coiled-tube and a single-bead-string reactor did not give any such peaks. The enhanced radial mixing in such reactors diminished the axial diffusion and smoothed out the unbalanced influences induced by convection at the central region and by diffusion at the tubing walls. According to Vanderslice et al.'s experimental observations [6], slight pulsation or turbulence in the flow can smooth out the double humps.

In the work reported here, it was observed that under certain experimental conditions, a chemical reaction can induce a double-humped peak which normally would not appear if the monitored species undergoes only physically driven dispersion. Figure 11 illustrates this point. Sample volumes substantially larger than the reactor volume were necessary to observe the effect. This condition, however, is not normally encountered in unsegmented continuous-flow sample processing. Under normal flow injection conditions,

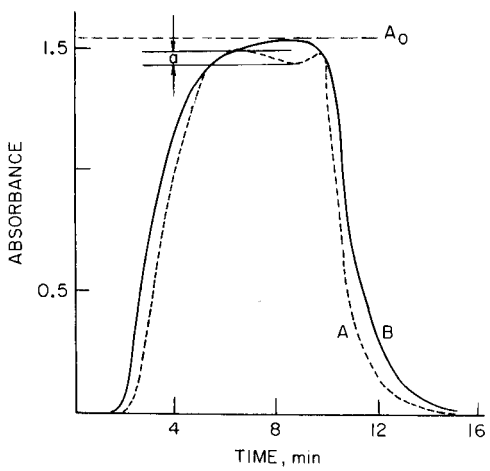

Fig. 11. Curve A: double-humped peak in presence of chemical effect. Curve B: signal profile in absence of chemical reaction. Experimental conditions: radius, 0.025 cm; straight open-tube reactor (L = 95 cm); flow rate 0.14 ml min^{-1}; sample loop length, L_s = 600 cm; pH 5.40; absorbance of original sample, A_0 = 1.56.

TABLE 4

Effect of chemical concentration on the presence of a double-humped peak

Dichromate concentration (mM)	Height of first hump[a] (absorbance)
0.300	0.032
0.400	0.044
0.500	0.060

[a]Corresponding to *a* in Fig. 11. Experimental conditions: sample size 1198 μl; pH 5.40, 5.00 M L-ascorbate, flow rate 0.14 ml min^{-1}; 95-cm straight open-tube reactor.

no double-humped peaks were observed with the chemical system used as model in these studies.

The double-humped peak may arise in this case because the chemical reaction introduces concentration gradients which enhance the diffusional force and cause a transitional change in the dispersion pattern. The greater the transitional change, the more pronounced the hump is; the data of Table 4 would seem to support this because the larger the sample concentration (increased "amount" of chemical reaction) the more pronounced is the hump.

CONCLUSIONS

The results and discussion presented above represent an attempt to explore in more detail the complex kinetic situation occurring inside an inserted plug and at its boundaries in unsegmented continuous-flow sample processing. The case of intercalation (injection) of the sample plug at a distance from the detection area is considered. The observations, which invite further study of the problem to cover other situations, can be summarized as follows.

First, even if dispersion is the result of longitudinal diffusion and convection alone, when compared on equal terms, the "dispersion equation model" (Eqn. 2 [1]) provides a better fit than the widely advocated Taylor model. The dispersion equation model fails, however, to provide good predictions of the falling (tail) part of typical signal profiles. A better fit is obtained with the help of empirical correction factors reflecting geometries, including that of the flow cell.

The effect of chemical reaction can be represented by alternate solutions of the dispersion equation (by alternating direction implicit finite difference approximation) and a simple differential equation reflecting the assumed kinetics of the chemical reaction involved. The rate coefficient in the chemical kinetics term (if pseudo-first-order conditions are assumed to hold) seems to change in an oscillating pattern which reflects the complexity of the overall kinetic process taking place inside the plug and its boundaries.

A straight-line relationship was found to exist between the time at the peak maximum and the assumed rate coefficients in computer-simulated curves. This correlation provides a way to estimate the rate coefficient for the system under study from the value of the reduced time at peak maximum.

Under rather extreme conditions of large sample sizes, the presence of a chemical reaction seems to induce the presence of a double-humped peak that is absent if the monitored species suffer dispersion under the driving force of only physical diffusion and convection.

In summary, this paper is intended to provide additional insight into the problem of dispersion in flow-injection techniques. The complexity of dispersion is undoubted, and further exploration of the approach presented here in other systems with different chemical characteristics is needed.

This work was supported by a grant from the National Science Foundation [CHE-7923956].

APPENDIX

The laminar dispersion equation is

$$D(d^2C/dx^2 + dC/r\,dr + d^2C/dr^2) = dC/dt + U_{max}(1 - r^2/a^2)\,dC/dx \quad \text{(i)}$$

and the transformed parameters are $X = x(D)/a^2(U_{max})$, $\tau = D(t)/a^2$, $\Omega = x(D/t)^{1/2}/a(U_{max}) = X(\tau)^{-1/2}$, $y = r/a$, $C^* = C/C_0$, $N_{pe} = a(U_{max})/D$ (Peclet number). Then the transformations are performed as follows

$$\frac{dC}{dx} = \frac{dC}{d\Omega}\left(\frac{d\Omega}{dx}\right) = \frac{dC}{d\Omega}\frac{d[x(D/t)^{1/2}(aU_{max})^{-1}]}{dx} = \frac{dC}{d\Omega}\frac{(D/t)^{1/2}}{a(U_{max})} \quad (1)$$

$$\frac{d^2C}{dx^2} = \frac{d}{dx}\left(\frac{dC}{dx}\right) = \frac{d}{dx}\left(\frac{dC}{d\Omega}\right)\frac{(D/t)^{1/2}}{a(U_{max})} = \frac{(D/t)^{1/2}}{a(U_{max})}\left\{\frac{d}{dx}\left(\frac{dC}{d\Omega}\right)\frac{d\Omega}{d\Omega}\right\}$$

$$= \frac{(D/t)^{1/2}}{a(U_{max})}\frac{d^2C}{d\Omega^2}\frac{d\Omega}{dx} = \frac{D}{a^2(U_{max})^2 t}\frac{d^2C}{d\Omega^2} = \frac{1}{\tau a^2(N_{pe})^2}\left(\frac{d^2C}{d\Omega^2}\right) \quad (2)$$

$$\frac{dC}{dr} = \frac{dC}{dy}\frac{dy}{dr} = \frac{dC}{dy}\frac{d(r/a)}{dr} = \frac{1}{a}\frac{dC}{dy} \quad (3)$$

$$\frac{1}{r}\frac{dC}{dr} = \frac{1}{r}\left(\frac{1}{a}\frac{dC}{dy}\right) = \frac{1}{a^2 y}\frac{dC}{dy} \quad (4)$$

$$\frac{d^2C}{dr^2} = \frac{d}{dr}\left(\frac{dC}{dr}\right) = \frac{d}{dy}\left(\frac{dC}{dr}\right)\frac{dy}{dr} = \frac{d}{dy}\left(\frac{1}{a}\frac{dC}{dy}\right)\left[\frac{d(r/a)}{dr}\right] = \frac{1}{a^2}\frac{d^2C}{dy^2} \quad (5)$$

$$\frac{dC}{dt} = \left[\frac{dC}{d\Omega}\left(\frac{d\Omega}{dt}\right)\right] + \left[\frac{dC}{d\tau}\left(\frac{d\tau}{dt}\right)\right] = \frac{dC}{d\Omega}\frac{d}{dt}\left[\frac{x(D/t)^{1/2}}{a(U_{max})}\right] + \frac{dC}{d\tau}\frac{d}{dt}\left(\frac{Dt}{a^2}\right)$$

$$= \frac{dC}{d\Omega}\left[-\frac{1}{2}\frac{x(D/t)^{1/2}}{a(U_{max})}\right] + \frac{dC}{d\tau}\left(\frac{D}{a^2}\right)$$

$$= \frac{D}{a^2}\left[\left(-\frac{xD^{1/2}t^{1/2}}{aU_{max}}\frac{a^2}{2Dt}\right)\left(\frac{dC}{d\Omega}\right) + \left(\frac{dC}{d\tau}\right)\right]$$

$$= \left(\frac{D}{a^2}\right)\left[-\frac{1}{2}\frac{\Omega}{\tau}\left(\frac{dC}{d\Omega}\right) + \left(\frac{dC}{d\tau}\right)\right] \quad (6)$$

By substituting Eqns. 2, 4, and 5 into Eqn. (i), the left-hand side of Eqn. (i) becomes

$$D\left[\frac{1}{a^2\tau(N_{pe})^2}\left(\frac{d^2C}{d\Omega^2}\right) + \frac{1}{a^2 y}\frac{dC}{dy} + \frac{1}{a^2}\frac{d^2C}{dy^2}\right]$$

$$= \frac{D}{a^2}\left[\frac{1}{\tau(N_{pe})^2}\frac{d^2C}{d\Omega^2} + \frac{1}{y}\frac{dC}{dy} + \frac{d^2C}{dy^2}\right] \quad (7)$$

Substituting Eqn. 1 and 6 into Eqn. (i) converts the right-hand side of Eqn. (i) to

$$\left(\frac{D}{a^2}\right)\left[-\frac{1}{2}\frac{\Omega}{\tau}\left(\frac{dC}{d\Omega}\right) + \frac{dC}{d\tau}\right] + U_{max}\left(1-\frac{r^2}{a^2}\right)\left(\frac{dC}{d\Omega}\right)\left[\frac{(D/t)^{1/2}}{a(U_{max})}\right]$$

$$= \left(\frac{D}{a^2}\right)\left(1-\frac{r^2}{a^2}\right)\left[\frac{a^2(D/t)^{1/2}}{a(D)}\right]\left(\frac{dC}{d\Omega}\right) + \left(\frac{D}{a^2}\right)\left[-\frac{\Omega}{2\tau}\left(\frac{dC}{d\Omega}\right) + \frac{dC}{d\tau}\right]$$

$$= \left(\frac{D}{a^2}\right)(1-y^2)[a/(Dt)^{1/2}]\left(\frac{dC}{d\Omega}\right) + \left(\frac{D}{a^2}\right)\left[-\frac{\Omega}{2\tau}\left(\frac{dC}{d\Omega}\right) + \frac{dC}{d\tau}\right]$$

$$= \left(\frac{D}{a^2}\right)(1-y^2)(\tau)^{-1/2}\left(\frac{dC}{d\Omega}\right) + \left(\frac{D}{a^2}\right)\left[-\frac{\Omega}{2\tau}\left(\frac{dC}{d\Omega}\right) + \frac{dC}{d\tau}\right]$$

$$= \left(\frac{D}{a^2}\right)\left[\frac{dC}{d\tau} + \left(\frac{1-y^2}{\tau^{1/2}} - \frac{\Omega}{2\tau}\right)\left(\frac{dC}{d\Omega}\right)\right] \quad (8)$$

The (D/a^2) term in both Eqn. 7 and Eqn. 8 can be eliminated by division. Thus, the laminar dispersion equation is transformed to

$$\frac{1}{\tau(N_{pe})^2}\frac{d^2C}{d\Omega^2} + \frac{1}{y}\frac{dC}{dy} + \frac{d^2C}{dy^2} = \frac{dC}{d\tau} + \left[\frac{(1-y^2)}{\tau^{1/2}} - \frac{\Omega}{2\tau}\right]\left(\frac{dC}{d\Omega}\right) \quad (9)$$

Correspondingly,

$$\frac{1}{\tau(N_{pe})^2}\frac{d^2C^*}{d\Omega^2} + \frac{1}{y}\frac{dC^*}{dy} + \frac{d^2C^*}{dy^2} = \frac{dC^*}{d\tau} + \left[\frac{(1-y^2)}{\tau^{1/2}} - \frac{\Omega}{2\tau}\right]\left(\frac{dC^*}{d\Omega}\right) \quad (10)$$

The initial and boundary conditions associated with the equation above are

$$\begin{cases} C^*(0, \Omega, y) = 0 \text{ for } \Omega > 0; \\ C^*(\tau, 0, y) = 1 \text{ for } \tau > 0; \\ C^*(\tau, \infty, y) = 0; \end{cases}$$

and $dC^*/dy(\tau, \Omega, 0) = dC^*/dy(\tau, \Omega, 1) = 0$.

REFERENCES

1 C. C. Painton and H. A. Mottola, Anal. Chim. Acta, 154 (1983) 1.
2 C. C. Painton and H. A. Mottola, Anal. Chem., 53 (1981) 1713.
3 E. H. Hansen and J. Růžička, J. Chem. Educ., 56 (1979) 677.
4 B. Carnahan, H. A. Luther and J. O. Wilkes, Applied Numerical Methods, Wiley, New York, NY 1969, pp. 270–272.
5 V. Ananthakrishnan, W. N. Gill and A. J. Barduhn, A.I.Ch.E. J., 11 (1965) 1063.
6 J. T. Vanderslice, K. K. Stewart, A. G. Rosenfeld and D. J. Higgs, Talanta, 28 (1981) 11.
7 A. Ringbom, Complexation in Analytical Chemistry, Wiley-Interscience, New York, 1963, p. 296.

8 C. G. Caro, J. Physiol., 185 (1966) 501.
9 F. J. Krug, J. Růžička and E. H. Hansen, Analyst (London), 104 (1979) 47.
10 W. N. Gill and V. Ananthakrishnan, A.I.Ch.E. J., 13 (1967) 801.
11 B. Karlberg, P. Johansson and S. Thelander, Anal. Chim. Acta, 104 (1979) 21.
12 H. Bate, S. Rowlands and J. A. Sirs, J. Appl. Physiol., 34 (1973) 866.
13 K. P. Mayock, J. M. Tarbell and J. L. Duda, Sep. Sci. Technol., 15 (1980) 1285.
14 J. M. Reijn, W. E. van der Linden and H. Poppe, Anal. Chim. Acta, 126 (1981) 1.

Analytica Chimica Acta, 158 (1984) 85—91
Elsevier Science Publishers B.V., Amsterdam — Printed in The Netherlands

CATALYTIC-KINETIC DETERMINATION OF SUBSTITUTED THIOUREAS AND THIOACETAMIDE BY AN ABSORPTIOSTAT METHOD WITH BROMOPYROGALLOL RED/HYDROGEN PEROXIDE AS THE INDICATOR REACTION

SIEGBERT PÄNTEL

Institut für Anorganische und Analytische Chemie der Universität, D-7800 Freiburg i.Br. (Federal Republic of Germany)

(Received 4th October 1983)

SUMMARY

In the absorptiostat method described, the concentration of the dyestuff in the bromopyrogallol red/hydrogen peroxide reaction is kept very low and constant by the automatic addition of increments of bromopyrogallol red solution. This is used in aqueous solutions at pH 4.0 to determine the catalysts thiourea, *N*-methylthiourea, *N*-allylthiourea and thioacetamide in the 0.1—1 mmol l^{-1} range with only 0.5-ml samples. The catalytic activities of another nine substituted thioureas are described; they depend on the kind of *N*-substituents as has been shown before for the sodium azide/iodine reaction, but the sequence of activities for different compounds is quite different.

Iodine-containing organic compounds of the general formula R—I catalyze the arsenic(III)/cerium(IV) reaction to different extents [1]; the catalytic activity of iodine in those compounds differs with the kind of organic radical. The same behaviour has been found for substituted thioureas in the sodium azide/iodine reaction [2], but there is a decisive difference between the catalytic activities in the two groups of compounds: the iodine-containing organic compounds retain their catalytic activities completely or almost completely during the reaction time, in agreement with the concept of an ideal catalyst, whereas the sulphur-containing organic compounds in the iodine-azide reaction are deactivated completely or almost completely in a very short time (less than 1 min) [2]. The catalytic activities of those compounds are therefore characterized by the so-called "reactivity number N_R", which gives a measure of the lifetime of the catalyst and the substrate conversion during this time [2]. Of all the substances tested, only cystine proved to be an exception: it showed a "normal" catalytic behaviour; strikingly enough, cystine had a catalytic activity some orders of magnitude smaller than all the other compounds tested.

As has been shown [3], thiourea itself catalyzes the indigo carmine/hydrogen peroxide reaction [4], the catalytic activity remaining constant over a significantly longer period of time. It seemed therefore logical to ex-

0003-2670/84/$03.00

amine the substituted thioureas with this reaction, but it was found that, at the hydrogen peroxide concentration necessary for sufficiently sensitive catalytic activities, these catalysts were oxidized very rapidly. In this paper, it is shown that when the triphenylmethane dyestuff bromopyrogallol red is used instead of indigo carmine, the hydrogen peroxide concentration can be lowered by more than one order of magnitude; consequently, the catalysts are stable for a longer time and the sensitivity of the reaction is higher. The determination of the catalytic activities of substituted thioureas thus becomes possible.

The indicator reaction, A + B---$\xrightarrow{K}$→X + Y, was again followed by using a stat method, an important tool for measurements in the so-called initial state with a rate law of quasi-zero order. In the absorptiostat mode used here, the concentration of a coloured reactant A is kept constant by adding it to the measuring cell at the rate at which it is consumed by the catalyzed oxidation with B in excess. The speed of addition, expressed as $\Delta \tan \alpha = \tan \alpha_K - \tan \alpha_0$ (see Fig. 1a), is a measure of the individual catalytic activity. The oxidation of bromopyrogallol red (λ_{max} = 550 nm) results in a pale-yellow oxidation product (λ_{max} = 390 nm), which does not interfere when a narrow-band optical filter is used. The molar absorptivity of the bromopyrogallol red at 550 nm under the conditions used here (2×10^4 l mol^{-1} cm^{-1}) is about the same as for the indigo carmine used previously.

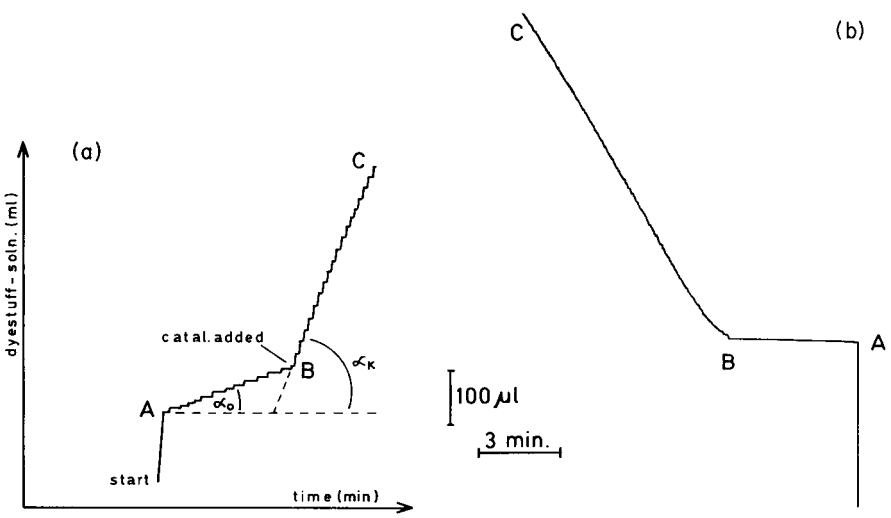

Fig. 1. (a) Schematic addition plot for stat methods (α_0 overdone for better understanding). (b) Original recorder plot for the determination of 5.30 µmol thiourea/15 ml with the bromopyrogallol red/hydrogen peroxide reaction (mirror image on apparatus grounds).

EXPERIMENTAL

Samples, reagents and apparatus

The thioureas used were the same as in the earlier paper [2] to permit comparisons. Bromopyrogallol red was purchased from Riedel de Haen; the aqueous solution must be prepared daily.

The apparatus used consists of a Combi-Titrator 3-D (Metrohm, Herisau, Switzerland) and a Lightelectric Colorimeter Model J (Lange, Berlin, F.R.G.) operated in the "multiflex" mode. In this position, the photometer is internally compensated and adjustable to zero. The multiflex exit is fed to the input of an operational amplifier (Teledyne Philbrick 844-BE) and the amplified mV signal regulates the Combi-Titrator. Figure 2 is a schematic diagram of the apparatus.

The photometer cuvette with 20-mm pathlength used as a reaction vessel is mounted in a thermostatted cuvette holder. The capillary end of the burette (Mikrodosimat, 1-ml burette) is fitted through the plastic cover of the photometer; a 5-mm diameter hole in this cover is used to insert the tip of a 500-μl Eppendorf pipette. The reaction mixture is stirred magnetically (500 rpm). The recorder speed was 1 cm min^{-1} and the working temperature was 25.0 ± 0.2°C. The interference filter used for the photometer had a transmittance maximum of 545 nm with a band-width of 10 nm.

General procedure for the determination of catalysts

In the cuvette are placed 1 ml of hydrogen peroxide solution (unstabilized, 34 mg ml^{-1} H_2O_2), 2 ml of sodium acetate buffer solution (pH 4.0, 0.2 M) and water up to 14.2 ml. The solution is thermostatted for 5 min and the photometer is compensated to 0 and 100% transmittance. Then 300 μl of the aqueous bromopyrogallol red solution (0.10 mM) is added manually from the automatic burette. For this basic concentration (point A in Fig. 1a), which is maintained throughout the measuring time, the resistor R_f (Fig. 2) is adjusted to give a voltage of 60 mV on meter M (working potential). Then the automatic addition of the dyestuff solution from the Mikrodosimat

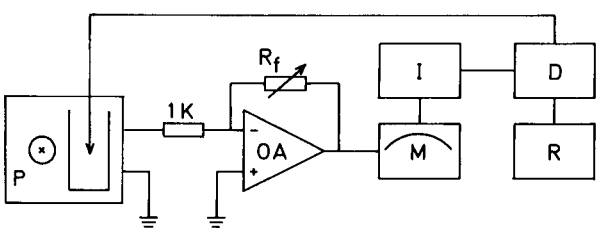

Fig. 2. Schematic diagram of the absorptiostat apparatus: P, photometer; OA, operational amplifier (R_f = 500 kohm); M, mV/pH meter (Metrohm E-510); I, comparator (Metrohm Impulsomat E-473); D, automatic burette (Metrohm Mikrodosigraph E-412); R, strip-chart recorder, mechanically driven from D.

is started and run for 2—3 min to give the addition plot of the uncatalyzed reaction (AB in Fig. 1a). The catalyzed reaction is started at point B by the addition of 0.5 ml of the particular catalyst solution from the Eppendorf pipette; the addition plot is then recorded for a sufficient time (2—15 min; BC in Fig. 1a) for the slope to be measured. A typical addition plot is shown in Fig. 1(b).

A calibration graph is drawn for each compound tested by plotting the $\Delta\tan\alpha = \tan\alpha_K - \tan\alpha_0$ values versus the respective catalyst concentration. The calibration graphs for some thioureas, determined in aqueous solution, are shown in Fig. 3.

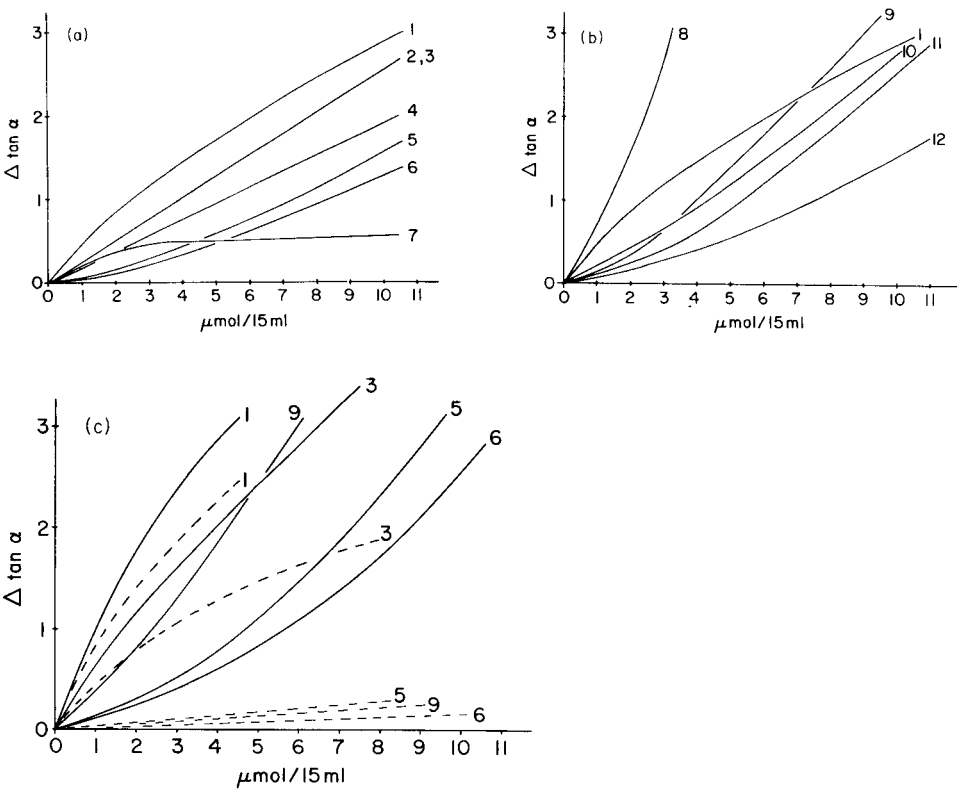

Fig. 3. Calibration graphs for the determination of thioureas with the bromopyrogallol red/hydrogen peroxide reaction. (a) *N*-Substituted thioureas (pH 4.0, 0.1 mM dyestuff solution). (b) *N,N'*-Substituted thioureas (pH 4.0, 0.1 mM dyestuff solution). (c) Selected substituted thioureas at different pH values: (—) pH 4.0; (- - -) pH 5.8; 0.05 mM dyestuff solution. Curves: (1) thiourea; (2) *N*-ethylthiourea; (3) *N*-methylthiourea; (4) *N*-allylthiourea; (5) *N,N*-diethylthiourea; (6) *N,N*-dimethylthiourea; (7) *N*-phenylthiourea; (8) *N,N,N',N'*-tetramethylthiourea; (9) *N,N,N',N'*-tetraethylthiourea; (10) *N,N,N'*-trimethylthiourea; (11) *N,N'*-diethylthiourea; (12) *N,N'*-dimethylthiourea. Thiourea is taken as reference substance in all cases.

RESULTS AND DISCUSSION

Thiourea, *N*-methylthiourea and *N*-allylthiourea were determined in aqueous 0.067 M hydrogen peroxide solution; the results for some single determinations are given in Table 1. The reproducibility of the procedure was tested at a thiourea concentration of 5.30 μmol/15 ml by measuring ten replicate samples. The standard deviation, s, was found to be 0.11 μmol/15 ml; the standard error ($s\ n^{-1/2}$) was calculated as 0.035 μmol/15 ml. The curve for *N*-phenylthiourea quickly became horizontal (Fig. 3a); this is not due to precipitation of the catalyst, and cannot be explained at the present time.

Sulphide, thiosulphate, thioacetamide, diethyldithiocarbamate, cysteine and cystine have only very small catalytic activities in 0.067 M hydrogen peroxide solution. Increase of the hydrogen peroxide concentration by one order of magnitude results in an appreciable increase of the catalytic activities for thioacetamide, cysteine and sulphide, whereas the activities for thiosulphate, diethyldithiocarbamate and cystine remain small. For cysteine and sulphide, the addition plots level off quickly, indicating that the catalyst is deactivated, and evaluation is difficult. Thioacetamide, however, can be determined in this way without difficulties, as can be seen from the results given in Table 1.

The corresponding calibration graphs for the determination in aqueous 0.67 M hydrogen peroxide solution are shown in Fig. 4. It is noteworthy that the catalytic activities decrease in the sequence thiourea > thioacetamide > cysteine > sulphide whilst the sequence is exactly the opposite in the indigo carmine/hydrogen peroxide reaction [3]. There is no obvious theoretical explanation for this behaviour from the present state of knowledge about the mechanisms of these reactions.

TABLE 1

Determination of thiourea, *N*-methylthiourea, *N*-allylthiourea and thioacetamide as catalysts in the bromopyrogallol red/hydrogen peroxide indicator reaction

Thiourea (μmol/15 ml)		*N*-Methylthiourea (μmol/15 ml)		*N*-Allylthiourea (μmol/15 ml)		Thioacetamide (μmol/15 ml)	
Given	Found	Given	Found	Given	Found	Given	Found
1.09	1.20	0.85	0.90	0.75	0.90	1.23	1.30
1.63	1.70	1.71	1.60	1.50	1.50	1.55	1.70
3.27	3.20	2.56	2.50	2.26	2.20	3.09	2.90
4.36	4.30	3.42	3.40	3.76	3.90	3.09	3.30
5.45	5.60	4.27	4.20	4.52	4.60	4.64	4.50
6.54	6.50	5.12	5.30	6.03	5.90	6.19	6.40
7.63	7.70	6.83	6.90	6.78	6.70	7.74	7.90
8.72	8.80	7.68	7.60	7.53	7.60	9.28	9.00
9.81	9.90	8.54	8.70	9.04	8.90	10.83	10.70
10.90	10.70	10.25	10.30	10.54	10.40	12.38	12.40

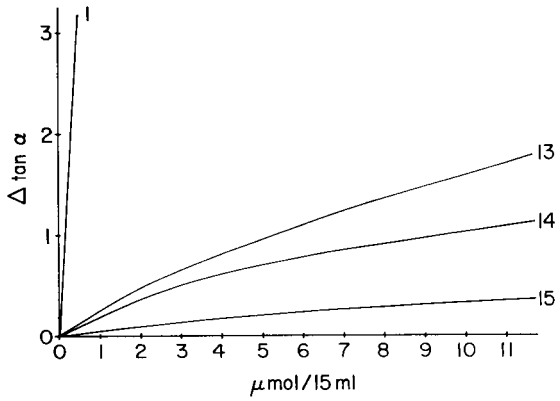

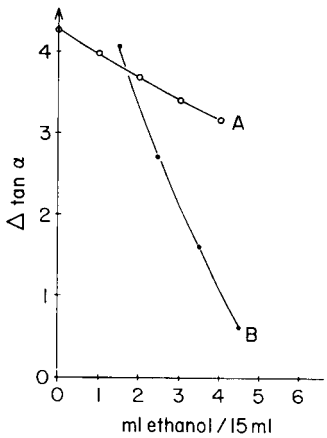

Fig. 4. Calibration graphs for the determination of thioacetamide, cysteine and sulphide compared to thiourea: (1) thiourea; (13) thioacetamide; (14) cysteine; (15) sulphide.

Fig. 5. Influence of ethanol on the catalytic activities of thiourea and tetraethylthiourea: (A) 9.22 μmol of thiourea in 15 ml of final solution; (B) 12.36 μmol of tetraethylthiourea in 15 ml of final solution.

For the iodine/azide reaction, there was a certain order of activities for the thioureas [2], but the order is quite different for the bromopyrogallol red/hydrogen peroxide reaction. The two sequences of activities cannot be compared. The differences may be caused, at least partially, by the different pH values needed for the two indicator reactions. Figure 3(c) shows for some selected examples how much the bromopyrogallol red/hydrogen peroxide reaction depends on the pH. All reaction conditions were the same as in Fig. 3(a) and (b) except the concentration of the dyestuff solution needed to reach higher sensitivity; the reproducibility was lower in this case. At pH 5.8, the catalytic activities were always smaller, to different degrees, whereas for the iodine/azide reaction the use of pH 4.0 cannot be recommended because of the volatility of hydrogen azide.

All substances described above are soluble in aqueous solution. Some other sulphur compounds of interest, such as *N*-(*p*-hydroxyphenyl)-thiourea, *N*-(*p*-nitrophenyl)-thiourea, tetramethylthiuram sulphide, *N*-benzoyl-*N'*-(*p*-hydroxyphenyl)-thiourea, *N*-benzoyl-*N'*-(*p*-nitrophenyl)-thiourea and *N*-benzoyl-*N'*-phenylthiourea are not sufficiently soluble in water. Ethanolic solutions of these substances cannot be applied for this method because the catalytic activities of these substances decrease nearly to zero. The effect of ethanol on the catalytic activity of tetraethylthiourea and thiourea is illustrated in Fig. 5. These two compounds can be determined in 20% ethanolic solution. *N*-benzoyl-thiourea has also an appreciable catalytic activity in this reaction medium, but cannot be evaluated by the tangent method, because it is quickly deactivated by oxidation.

REFERENCES

1 S. Pantel, Anal. Chim. Acta, 141 (1982) 353, and references therein.
2 S. Pantel, Anal. Chim. Acta, 152 (1983) 215, and references therein.
3 H. Weisz, S. Pantel and G. Marquardt, Anal. Chim. Acta, 143 (1982) 177.
4 A. Krause and T. Weimann, Z. Naturforsch., Teil B, 21 (1966) 288.

Analytica Chimica Acta, 158 (1984) 93—111
Elsevier Science Publishers B.V., Amsterdam — Printed in The Netherlands

A GENERALIZED APPROACH FOR THE CALCULATION AND AUTOMATION OF POTENTIOMETRIC TITRATIONS
Part 1. Acid-Base Titrations

J. STUR, M. BOS and W. E. VAN DER LINDEN*

Department of Chemical Technology, Twente University of Technology, Enschede (The Netherlands)

(Received 9th May 1983)

SUMMARY

Fast and accurate calculation procedures for pH and redox potentials are required for optimum control of automatic titrations. The procedure suggested is based on a three-dimensional titration curve $V = f(\text{pH, redox potential})$. All possible interactions between species in the solution, e.g., changes in activity coefficients and influence of redox potential on pH variations, are taken into account. The number of titrant additions can be reduced considerably without loss of precision, by using the fact that the pH of a protolyte or mixture of protolytes at some fraction titrated does not depend strongly on the actual concentration.

Although the number of direct instrumental methods of chemical analysis is continuously increasing, titrations are still important in routine practice in many laboratories. The reason may be that no direct instrumental methods with sufficient selectivity are available, but more probably that better precision is possible with titrations. Titrations done manually tend to be time-consuming and the results often depend on the skill of the technician. Both drawbacks can be largely overcome by automation; various automated titrators are commercially available. Many options are available to control the titration procedure, the addition of the titrant and the evaluation of the data. Table 1 presents a survey of the more important options. Reviews [1, 2] and a monograph [3] on automatic titrations are available. The whole subject can be subdivided into two parts: (i) control of the performance of the actual titration, and (ii) the calculation procedure(s) involved. The more recent literature on both subjects is summarized in Tables 2 and 3, respectively.

Especially for more complicated mixtures, existing automatic titration methods based on calculations with all data points are time-consuming and demand relatively large computing capacities; however, titrant delivery can be relatively simple, e.g., by the use of constant increments. Procedures in which the titration leads to an exact evaluation of the end-point generally force the use of more sophisticated control and delivery systems based on

0003-2670/84/$03.00

TABLE 1

Survey of automatic potentiometric titrations

Control mechanism
(1) Mechanical (2) Electronic (3) Computational (microprocessor)

Titrant addition
(1) Continuous
(a) Constant speed
(b) Decreasing speed
(2) Stepwise
(a) Equal volumes
(b) Decreasing volumes
(i) Mechanical control
(ii) Dynamic control with calculation from an empirical expression or system parameters

Method of obtaining end-point
(1) Addition of titrant is continued beyond the end-point; calculation based on several data points
(2) Addition of titrant stops at end-point; calculation based on one data point

Evaluation of end-point
(1) From inflection point of sigmoidal curve
(a) Biggest potential jump
(b) Steepest part of curve (tangential method)
(c) Intersecting with two midpoints of circles (Tubbs' method)
(d) Maximum of first derivative
(e) Zero of second derivative
(2) From linearized curve
(3) End-point potential
(a) Experimentally (by calibration titration)
(b) Calculated

on-line evaluation of the measurements. Mostly, this evaluation is based on a very simple model for the titration reaction, which does not take into account all the interactions that actually take place in the solution, such as protolytic side-reactions and electrostatic interactions as expressed by the respective activity coefficients of the species.

The object of the investigation presented here was to develop a calculation procedure that is fast enough to be used in an on-line control system for the titrant delivery but will still account for all possible interactions in the solution. As for the titration procedure itself, the number of additions of titrant has to be minimized, maintaining an acceptable level of precision in the determination of the end-point. Furthermore, the end-point found should be identical with the real equivalence point.

THEORY

In order to discuss the calculation procedure in a generalized form, the following symbols are adopted. The letter P is used for any protolyte, A for protolytic compounds that have no redox properties, and X for the set of redox substances; the suffix ox or red denotes the oxidation state if such

TABLE 2

A selected chronological survey of automatic potentiometric titration procedures

Ref.		Equipment computer	Titrant addn.	End-point evaluation	No. of points	Precision (%)
[4]	Empirical eqn. for calcn. of ΔV from preceding titration data points.	Radiometer system	Empirical formula	Inflexion point number.	12	0.6
[5]	Application of micropr. to control titration	INTEL 8001 CYBA-0	Constant rate	Max $\Delta pH/\Delta V$	—	0.3
[6]	Microcomp.-controlled automatic titrator with automatic sample processing.	Mettler system	No information		—	—
[7]	Autom. pot./photom. system, coulom. titrant generation; 3-dimensional plots.	PDP DEC-syst.-10	Constant rate	Overtitration, then calculation	—	
[8]	Versatile microcomp. contr. titrator for pot., photom., coulom., etc. titrations.	ADD 8080	Two different constant rates	Max $\Delta E/\Delta V$	200	0.1
[9]	Microcomp. contr. system for automatic pK determinations.	INTEL 8080	Simplified Christiansen method		50	0.04
[10]	Microproc. contr. automatic differential titr.	INTEL MCS-80	Constant ΔV	Max $\Delta E/\Delta V$	30	0.7
[11]	Microcomp. contr. automatic photometric syst.	INTEL 8080A	Constant	Break point of plot	500	0.6
[12]	Stepwise addition of equal volumes; also suitable for mixtures of polyprotic acids/bases	HP 9835/45	Constant ΔV	First deriv.	25	
[13]	Automatic microcomp. contr. potentiometric titrator for student demonstrations	ALTAIR 8800B	Two different constant rates	$\Delta E/\Delta V$ max.		0.1
[14]	Microcomp. contr. pot. analysis, describes a new computer language CONVERS.	IMSAI 8080	Christiansen method	Second deriv.	50	0.1—1.0
[15]	Learning method, for strong acids and bases.	JOLT system	Determination in learning mode		As manual	
[16]	Full automated computer-controlled system. ΔV approximated on the basis of constant ΔpH.	HP 9835/45	From preceding data	First deriv.	25	—
[17]	Computer contr. titration based on systems theory.	ZILOG 2.80 VARIAN V76	Preceding data, feedback factor	First and second deriv. hyperbolic function	50	0.05
[18]	Robotic sample preparation station. A high-class hardware system.	APPLE II	Constant rate	First deriv.	28	0.6
[19]	A microcomp. contr. system for pharmaceutical use (pK determ.).	IM-6100 m.p.	Constant rate	Second deriv. corrected	100	1.0

specification is necessary, and the suffix s or t refers to the solution titrated (sample) or the titrant, respectively. For example

in the solution $X_s \rightarrow X_{1s} \cdots X_{nxs}$

in the titrant $X_t \rightarrow X_{1t} \cdots X_{nxt}$

where $n$xs is the number of different redox substances in solution, and $n$xt is the number of different redox substances in the titrant; X_s can be present in the ox form, $X_{1sox} \cdots X_{nxsox}$; X_s can be present in the red form: $X_{1sred} \cdots X_{nxsred}$. If $C_{(i)}$ is the analytical concentration of substance i, and

TABLE 3

A selected chronological survey of calculation methods for potentiometric titration curves

Ref.	Topic	Computer language	
[20]	General		End-point of potentiometric titn. at the steepest inflexion of titn. curve.
[21]	Redox, pH		Linearization of titn. curve. The most widely used method for detn. of end-point.
[22]	General		Graphical determination of end-point with the "circle method".
[23]	Redox		Exact numerical calculation of titn. curves with four equations. Definition of inhomogeneous redox systems.
[24]	General		Rigorous least-squares adjustment for calculation of non-linear eqns.
[25]	pH, redox	ALGOL	HALTAFALL program.
[26]	pH, redox	ALGOL	Computer calcn. of titn. curves in multicomponent systems.
[27]	pH, redox		Calcn. of redox titn. curves. Proved: equivalence point ≠ inflexion point.
[28]	pH	ALGOL	Improved linear titn. plots, with activity coefficients.
[29]	General		Numerical methods for data-fitting problems. Detailed review and comparison of methods.
[30]	pH		Learning machine method for calcn. of titn. curves by multiparametric curve-fitting.
[31]		FORTRAN	Non-linear least-squares approach. Simplified LETAGROP = ACBA.
[32]	pH		Calculation of pH titn. curves and end-points. Iterative method with interval halving.
[33]	pH		Unified calcn. of titn. curves (for limited number of components).
[34]	General		Multicomponent analysis computations using Kalman filtering.
[35]	pH, redox		Titration assisted by microcomputers. Electro-activity treated similarly to pH.
[36]	pH		Approximation formula for mixtures of acids and bases. Explicit formula for $[H^+]$ in simple cases.
[37]	General	FORTRAN	Resolution of overlapping electrochem. peaks with Kalman filtering.
[38]	pH	BASIC	TITFIT a comprehensive program, Newton—Gauss—Marquardt method.
[39]	pH		Calcn. using $[H^+]$ as independent and $[B^+]$ as dependent variable using pocket calculators.
[40]	pH	BASIC	Desk-computer program MINIPOT; utilisation of Gauss and Wentworth method.
[41]	pH		The limit of separation of two weak acids.
[42]	pH, redox		Titration in a mixture with resolution of difference u.v.-visible spectra.
[43]	pH	FORTRAN	Data analysis for up to nine components with TITAN program.
[44]	pH		Bjerrum plots for determination of systematic conc. errors.
[45]	pH, redox		Evaluation of digital potentiometric titns. by the Tubbs method.

[X] the actual concentration of species X, then $C(X_{is}) = C(X_{isox}) + C(X_{isred})$ and $C(X_{it}) = C(X_{itox}) + C(X_{itred})$.

For protolyte compounds that have no redox properties $A_s \rightarrow A_{1s} \cdots A_{nas}$ in solution and $A_t \rightarrow A_{1t} \cdots A_{nat}$ in the titrant, where *n*as is the number of protolytes without redox properties in solution, and *n*at is the number of protolytes without redox properties in the titrant.

For the initial analytical (formal) concentration in both solution and titrant, the symbol C ($C_{(i)}$ for the substance i) is used; concentrations in the solution during the titration are denoted by C'

$$C'_{(is)} = C_{(is)}V_0/(V_0 + V); \quad C'_{(it)} = C_{(it)}V/(V_0 + V) \tag{1}$$

Two further symbols will be used for characterization of the substances involved: taking the mostly deprotonated species of a substance as a Brønsted base, $N(i)$ is the maximum number of protons that can be accepted by this species and $g(i)$ is the charge of its totally deprotonated form: in general,

$g(i) \leqslant N(i)$. For example,

EDTA $N = 6; g = 4$
H_3PO_4 $N = 3; g = 3$
NH_3 $N = 1; g = 0$
Fe^{3+} $N = 3; g = 0$ $\{Fe^{3+}(H_2O)_6 + 3H_2O \rightarrow Fe(OH)_3(H_2O)_3 + 3H_3O^+\}$
Me^{2+} $N = 2; g = 0$ $\{Me^{2+} + 4H_2O \rightarrow Me(OH)_2 + 2H_3O^+\}$
K^+ $N = 1; g = 0$

The protonation constants for each species are subscripted with i, the subscript of the substance and j for its serial number. With charges omitted, $K_{i,1} = [HA]/[H][A]$, $K_{i,2} = [H_2A]/[H][HA]$, ... (charges omitted) $K_{i,j} = [H_jA]/[H][H_{j-1}A], \ldots, K_{i,N(i)} = [H_{N(i)}A]/[H][H_{N(i)-1}A]$.

For any protolyte, P, the analytical concentration can be written as

$$C(P) = \sum_{k=0}^{N(P)} [H_kP^{[k-g(P)]+}] \tag{2}$$

where P is X_{isox}, X_{isred}, A_{is} or X_{itox}, X_{itred}, A_{it}. Using the protonation constants, Eqn. (2) can be written as

$$C(P) = [P^{-g(P)}]\ \{1 + \beta_{P,1}[H^+] + \beta_{P,2}[H^+]^2 + \ldots + \beta_{P,N(P)}[H^+]^{N(P)}\} \tag{3}$$

where $\beta_{P,1} = K_{P,1}$; $\beta_{P,2} = K_{P,1}K_{P,2}$; $\ldots$ $\beta_{P,N(P)} = K_{P,1}K_{P,2} \ldots K_{P,N(P)}$ or generally $\beta_{P,k} = \Pi_{j=0}^{k} K_{P,j}$ with $\beta_{P,0} \equiv K_{P,0} = 1$. This yields

$$C_{(P)} = [P^{-g(P)}] \sum_{k=0}^{N(P)} [H^+]\ \prod_{j=0}^{k} K_{P,j} \equiv [P^{-g(P)}]\alpha_{P(H)} \tag{4}$$

where $\alpha_{P(H)}$ is Ringbom's side-reaction coefficient for the interaction of P with protons. So

$$[P^{-g(P)}] = C_{(P)}\alpha_{P(H)}^{-1} \tag{5}$$

$$\text{and } [H_kP] = C_{(P)}\alpha_{P(H)}^{-1}[H^+]^k\ \prod_{j=0}^{k} K_{P,j} \equiv C_{(P)}\alpha_{P(H)}^{-1}[H^+]^k\beta_{P,k} \tag{6}$$

For the redox substances the following quantities are defined $E_{(i)}^0$ is the standard potential of substance i, and $z_{(i)}$ the number of electrons involved in the redox reaction; R, T and F have their usual meanings. The Nernst equation can be used to calculate the redox state of the substance at any stage of the titration. For this calculation, E^0 is chosen so that it applies to the most positively charged form of the oxidized species (i.e., $H_{N(Xiox)}X_{iox}$ with the positive valency of $[N_{(Xiox)} - g_{(Xiox)}]$) whereas for the reduced species, the most negatively charged form X_{ired} with the negative valency of $g_{(Xired)}$ is chosen. The Nernst equation then reads

$$E = E_{(X)}^0 + (RT/z_{(X)}F) \ln\{[H_{N(Xox)}X_{ox}]/[X_{red}]\} \tag{7}$$

with $[H_{N(Xox)}X_{ox}] = C'_{(Xox)}\alpha_{Xox(H)}^{-1}[H^+]^{N(Xox)}\beta_{N(Xox)}$ and $[X_{red}] = C'_{(Xred)} \cdot \alpha_{Xred(H)}^{-1}$. Together with $[H^+] = 1$ (pH = 0), this reduces to

$$E = E^0_{(X)} + (RT/z_{(X)}F)\ln\{\alpha^*_{Xred(H)}\beta_{N(Xox)}/\alpha^*_{Xox(H)}\} + (RT/z_{(X)}F)\ln\{C'_{(Xox)}/C'_{(Xred)}\} \quad (8)$$

Here $\alpha^*_P = (\alpha_{P(H)})_{pH=0}$

The Nernst equation can now be rewritten as

$$E = E^{0*}_{(X)} + (RT/z_{(X)}F)\ln\{C'_{(Xox)}/C'_{(Xred)}\} \quad (9)$$

With $E^{0*}_{(X)} = E^0_{(X)} + (RT/z_{(X)}F)\ln\{\alpha^*_{Xred(H)}\beta_{N(Xox)}/\alpha^*_{Xox(H)}\}$ (10)

If $\Psi_{(X)}$ is defined as

$$\Psi_{(X)} = C'_{(Xox)}/C'_{(Xred)} \quad (11)$$

then $\Psi_{(X)}$ can be calculated from

$$\Psi_{(X)} = \exp\{(E - E^{0*}_{(X)})z_{(X)}F/RT\} \quad (12)$$

and because $C'_{(X)} = C'_{(Xox)} + C'_{(Xred)}$

$$C'_{(Xred)} = C'_{(X)}\{1 + \Psi_{(X)}\}^{-1} \quad (13)$$

$$C'_{(Xox)} = C'_{(X)}\Psi_{(X)}\ \{1 + \Psi_{(X)}\}^{-1} \quad (14)$$

Now two equations can be derived for the two unknown parameters E and pH in the titration mixture. The first equation uses the electron balance as a basis, i.e., the equivalents of reductant produced in the sample equals the equivalents of reductant consumed in the titrant. With Eqn. 13, the equilibrium concentration of the reduced species can be found from the analytical concentrations in the titration mixture, giving

$$\{V_0 + V\}\{\sum_{i=1}^{nxs} C'_{(Xis)}z_{(Xis)}(1 + \Psi_{(Xis)})^{-1}\} - V_0\{\sum_{i=1}^{nxs} C^0_{(Xis)}z_{(Xis)}\} = V\{\sum_{i=1}^{nts} C^0_{(Xit)}z_{(Xit)}\} - \{V_0 + V\}\{\sum_{i=1}^{nts} C'_{(Xit)}z_{(Xit)}(1 + \Psi_{(Xit)})^{-1}\} \quad (15)$$

Here $C^0_{(Xi)}$ represents the analytical concentration of substance X_i originally present in the titrant or sample in reduced form.

With Eqn. 1 this balance can be rewritten as

$$V_0\{\sum_{i=1}^{nxs} C_{(Xis)}z_{(Xis)}\{1 + \Psi_{(Xis)}\}^{-1} - \sum_{i=1}^{nxs} C^0_{(Xis)}z_{(Xis)}\} + V\{\sum_{i=1}^{nxt} C_{(Xit)}z_{(Xit)}\{1 + \Psi_{(Xit)}\}^{-1} - \sum_{i=1}^{nxt} C^0_{(Xit)}z_{(Xit)}\} = 0 \quad (16)$$

or in simplified form

$$F_1 = V_0 P_{1(s)} + V P_{1(t)} = 0 \quad (17)$$

For the second expression, electroneutrality is taken as the starting point

$$\sum_{\substack{\text{all}\\ \text{substances}}} \sum_{k=0}^{N(i)} \{g(i) - k\} [H_k P_i] - [H^+] + [OH^-] = 0 \tag{18}$$

The symbol Q_i is now introduced

$$Q_i = C'_{Pi} \sum_{k=0}^{N(i)} \{g(i) - k\} [H_k P_i] = \sum_{k=0}^{N(i)} \{g(i) - k\} [H^+]^k \beta_{i,k} \alpha_i^{-1}(H) \tag{19}$$

Equations 2, 13 and 14, with the necessary transformations and simplifications, yield

$$V_0 \{[OH^-] - [H^+] + \sum_{i=1}^{nas} C_{(Ais)} Q_{(Ais)} + \sum_{i=1}^{nxs} C_{(Xis)} [Q_{(Xisox)} \Psi_{(Xis)} \{1 + \Psi_{(Xis)}\}^{-1}$$

$$+ Q_{(Xisred)} \{1 + \Psi_{(Xis)}\}^{-1}]\} + V\{[OH^-] - [H^+] + \sum_{i=1}^{nat} C_{(Ait)} Q_{(Ait)}$$

$$+ \sum_{i=1}^{nxt} C_{(Xit)} [Q_{(Xitox)} \Psi_{(Xit)} \{1 + \Psi_{(Xit)}\}^{-1} + Q_{(Xitred)} \{1 + \Psi_{(Xit)}\}^{-1}]\} = 0 \tag{20}$$

or in simplified form

$$F_2 = V_0 P_{2(s)} + V P_{2(t)} = 0 \tag{21}$$

Calculation procedure

For the numerical calculation of F_1 and F_2, the Newton—Raphson method was used. The advantage of this procedure is its fast convergence and the relatively small computer capacity needed. It has some disadvantages, however, for functions that do not show monotonous changes. In that case, large values of the derivatives can be obtained sometimes, which enhances the risk of ending up at a sub-minimum in an irrelevant region of the response plane. By setting appropriate limits of pH and V values and by limiting the allowable maximum and minimum step size, such pitfalls can be avoided. If intermediate results start to oscillate between the limiting pH and V values, one or both limits have to be changed.

Table 4 summarizes the expressions to be calculated. It can be seen that the mathematical expressions of the derivatives to be used in the Jacobian are very similar to the original functions. Hence, this calculation can be easily performed simultaneously with the calculation of the function itself.

In order to reach a precision of 1 in 10^6, generally, 5—6 iterations are necessary, provided that the starting conditions were chosen properly. When no such conditions are available, the arbitrarily chosen values pH = 7, E = 0.5 are used.

TABLE 4

Survey of the equations used for the calculation of the three-dimensional titration curve
(Indices, charges and [ ] are omitted where possible. For explanation of the symbols, see text.)

$D_1 = \frac{\delta F_1}{\delta E} \cdot \frac{\delta F_2}{\delta H} - \frac{\delta F_1}{\delta H}\frac{\delta F_2}{\delta E}$	$\Delta E = \left(-F_1\frac{\delta F_2}{\delta H} + F_2\frac{\delta F_1}{\delta H}\right)/D$	$\Delta H = \left(F_1\frac{\delta F_2}{\delta E} - F_2\frac{\delta F_1}{\delta E}\right)/D$
$F_1 = V_0 P_{1(s)} + V P_{1(t)}$	$\frac{\delta F_1}{\delta E} = V_0\frac{\delta P_{1(s)}}{\delta E} + V\frac{\delta P_{1(t)}}{\delta E}$	$\frac{\delta F_1}{\delta H} = V_0\frac{\delta P_{1(s)}}{\delta H} + V\frac{\delta P_{1(t)}}{\delta H}$
$F_2 = V_0 P_{2(s)} + V P_{2(t)}$	$\frac{\delta F_2}{\delta E} = V_0\frac{\delta P_{2(s)}}{\delta E} + V\frac{\delta P_{2(t)}}{\delta E}$	$\frac{\delta F_2}{\delta H} = V_0\frac{\delta P_{2(s)}}{\delta H} + V\frac{\delta P_{2(t)}}{\delta H}$
$P_1 = \sum_1^{nx} C_{(X)} z S - \sum_1^{nx} C^0_{(X)} z$	$\frac{\delta P_1}{\delta E} = \sum_1^{nx} C_{(X)} z \frac{\delta S}{\delta E}$	$\frac{\delta P_1}{\delta H} = \sum_1^{nx} C_{(X)} z \frac{\delta S}{\delta H}$
$P_2 = \frac{K_W}{H} - H + \sum_1^{na} C_{(A)} Q_{(A)} + \sum_1^{nx} C_{(X)}[(1-S)Q_{(Xox)} + S Q_{(Xred)}]$	$\frac{\delta P_2}{\delta E} = \sum_1^{nx} C_{(X)}(Q_{(Xred)} - Q_{(Xox)})\frac{\delta S}{\delta E}$	$\frac{\delta P_2}{\delta H} = \frac{-K_W}{\delta H^2} - 1 + \sum_1^{na} C_{(A)}\frac{\delta Q_{(A)}}{\delta H} + \sum_1^{nx} C_{(X)}[(1-S)\frac{\delta Q_{(Xox)}}{\delta H} + S\frac{\delta Q_{(Xred)}}{\delta H} + \frac{\delta S}{\delta H}(Q_{(Xred)} - Q_{(Xox)})]$
$S = (1+\phi)^{-1}$	$\frac{\delta S}{\delta E} = -\frac{\delta \phi}{\delta E}(1-\phi)^{-2}$	$\frac{\delta S}{\delta H} = -\frac{\delta \phi}{\delta H}(1-\phi)^{-2}$
$\phi = \frac{M_{(ox)}}{M_{(red)}} \exp\frac{zF}{RT}(E - E^{0*})$	$\frac{\delta \phi}{\delta E} = \frac{zF\, M_{(ox)}}{RT M_{(red)}} \exp\frac{zF}{RT}(E - E^{0*})$	$\frac{\delta \phi}{\delta H} = \left(\frac{\delta M_{(ox)}}{\delta H} M_{(red)} - M_{(ox)}\frac{\delta M_{(red)}}{\delta H}(M_{(red)})^{-2} \exp\frac{zF}{RT}(E - E^{0*})\right)$
$M_{(ox)} = \alpha_{(ox)} H^{-N(ox)}$	$E^{0*} = E^0_k + \frac{RT}{zF}\ln\frac{\alpha^*_{(red)}\beta_{N(ox)}}{\alpha^*_{(ox)}}$	$\frac{\delta M_{(ox)}}{\delta H} = \frac{\delta \alpha_{(ox)}}{\delta H} H^{-N(ox)} - \alpha_{(ox)} N_{(ox)} H^{-(N_{(ox)}+1)}$
$M_{(red)} = \alpha_{(red)} \beta^{-1}_{N(red)}$	$\alpha^* = \sum_{k=0}^{N} \beta_k$	$\frac{\delta M_{(red)}}{\delta H} = \frac{\delta \alpha_{(red)}}{\delta H} \beta^{-1}_{N(red)}$
$Q = L/\alpha$		$\frac{\delta Q}{\delta H} = \left(\frac{\delta L}{\delta H}\alpha - \frac{\delta \alpha}{\delta H} L\right)\alpha^{-2}$

$$L = \sum_{k=0}^{N} (g-k)H^k\beta_k$$

$$\alpha = \sum_{k=0}^{N} H^k\beta_k$$

$$\beta_k = \prod_{j=0}^{k} K_j/\gamma_k (K_0 = 1')$$

$$\gamma_k = \exp\left[-(g-k)^2\, 0.509 \left\{\sqrt{I}\,(1+\sqrt{I})^{-1} + BI\right\}\right]$$

$$I = 1/2\,[10^{-pH}\cdot\gamma_H^{-1} + K_w(10^{-pH}\cdot\gamma_{OH})^{-1}\cdot\Sigma C \sum_{k=0}^{N} (g-k)^2 H^k\beta_k\alpha^{-1}]$$

$$\frac{\delta L}{\delta H} = \sum_{k=0}^{N} k(g-k)H^{k-1}\beta_k$$

$$\frac{\delta \alpha}{\delta H} = \sum_{k=0}^{N} kH^{k-1}\beta_k$$

In Eqns. 3, 4 and 6, stability constants were used based on concentrations. If thermodynamic constants are used, concentrations must be replaced by activities. In that case, activity coefficients for each individual species (γ_{H_kP}) must be calculated. Apart from H_3O^+ and OH^-, the Davies equation was adopted for all species

$$-\log \gamma_{H_kP} = \{g(P) - k\}^2 A \{I^{1/2}(1 + I^{1/2})^{-1} + BI\} \quad (22)$$

where A and B are constants (for aqueous solutions at 25°C, $A = 0.509$ and $B = 0.2$). The ionic strength is calculated from the formula

$$I = 0.5 \left[10^{-pH}\gamma_H^{-1} + K_w(10^{-pH}\gamma_{OH})^{-1} + \sum_{\substack{\text{all} \\ P}} C(P) \sum_{k=0}^{N(P)} \{\{g(P) - k\}^2 \cdot [H^+]^k \beta_k \alpha_{P(H)}^{-1}\}\right] \quad (23)$$

This Davies equation has the advantage of being applicable to solutions with a widely variable ionic strength while no specific information about the substance is required. Therefore, it can be easily incorporated in the program. For H_3O^+ and OH^-, the extended Debye—Hückel equations are used

$$-\log \gamma = 0.5085 I^{1/2}(1 + 0.328\sigma I^{1/2})^{-1} \quad (H^+ : \sigma = 3 \text{ and } OH^- : \sigma = 9) \quad (24)$$

Titration procedure

The concept of optimized titrant delivery is based on the fact that the difference in the shape of titration curves of two systems of similar qualitative composition, but different in concentration, is very small, even in the region of the equivalence point. This allows the use of an "indicator curve" calculated with a concentration of the compound to be determined that is definitely smaller than the guessed concentration for controlling the titrant delivery. The titration can then be done with a small number of arbitrarily chosen steps until the pH of the indicator curve at the end-point is reached. Overtitration is thus avoided. At this stage it is possible to calculate a fairly accurate estimate of the unknown concentration based on the actually measured data pairs of pH and volume of titrant. With this estimate, a new value of the pH of the expected equivalence point can be calculated. Now a maximum change in the pH (ΔpH) per titration step can be found from the required precision of the titration and the titration can be completed by titrant addition steps corresponding to this ΔpH value. After each of these steps, the estimate of the unknown concentration is updated and the titration is finished when the last calculated equivalence point pH is reached.

The final correct concentration can be calculated with the use of all the titration data, but the equivalence volume found in the procedure described above also gives the wanted information with the required accuracy.

In practice, the control of the first stage of the titration is based on an indicator titration curve calculated with a concentration of the component

to be determined equal to one half of the guessed concentration. An example is given in Fig. 1 and Table 5. First the pH_{ind} values on the indicator curve are calculated at titration fractions of 0.5, 0.9, 0.99, 0.999 and 1.0. This indicator curve is based on a concentration $C = C_{guess}/2$. The values are tabulated in the first column of Table 5 and correspond to the points △1, △2, etc. in Fig. 1. Subsequently, the titrant volumes needed to reach these pH_{ind} values are calculated for the guessed concentration (second column, Table 5; points □1, □2, etc. in Fig. 1). The first increment, $\triangle V_1$, is added and the actual pH is measured (point ○2). This pH corresponds to a volume on the guessed curve which in this case is smaller than V_1. In Table 5 this volume is denoted as V_{old} (third column). The second increment $\triangle V_2$ is obtained as the difference between V_{guess} (second column) and V_{old} (third column). After addition of this increment, the actual pH (○3 in Fig. 1) is measured and the corresponding V_{old} is calculated. This procedure is repeated 5 times.

TABLE 5

The first five titration points calculated for the titration of sodium acetate (0.01 M) with NaOH (1.0 M) with the fractions titrated (fr): (1) 0.5; (2) 0.9; (3) 0.99; (4) 0.999; (5) 1.0 for different first guessed concentrations ($C_{(g)}$). V_0 = 100.0 ml, pK = 4.76, pH_{ep} = 3.3891

	pH_{ind}	V_{guess}	V_{old}	$\triangle V$	V_{added}	$pH_{measured}$
Calc. with	$C_{guess}/2$ $V = V_{ep.}$fr	C_{guess} pH_{ind}	C_{guess} $pH_{m\ old}$	V_{guess} $-V_{old}$	$\Sigma \triangle V$	C_{real} V_{added}
	$C_{guess} = 0.008\ M$					
	4.7386	0.3930	0.0	0.3930	0.3930	4.9061
	3.9410	0.6982	0.3165	0.3817	0.7747	4.1957
	3.6268	0.7660	0.6225	0.1434	0.9181	3.7642
	3.5970	0.7715	0.7398	0.0317	0.9498	3.6290
	3.5937	0.7721	0.7650	0.0071	0.9569	3.6023
	$C_{guess} = 0.010\ M$					
	4.7338	0.4911	0.0	0.4911	0.4911	4.7338
	3.8919	0.8834	0.4911	0.3923	0.8834	3.8918
	3.5801	0.9607	0.8834	0.0773	0.9607	3.5801
	3.5403	0.9677	0.9607	0.0070	0.9677	3.5473
	3.5437	0.9683	0.9677	0.0006	0.9683	3.5437
	$C_{guess} = 0.016\ M$					
	4.7235	0.7848	0.0	0.7848	0.7848	4.1717
	3.8506	1.4195	1.2449	0.1746	0.9594	3.5862
	3.4834	1.5464	1.5161	0.0303	0.9897	3.4399
	3.4432	1.5576	1.5585	neg.	0.9897	3.4399
	3.4387	1.5598	1.5585	0.0003	0.9900	3.4384
	$C_{guess} = 0.020\ M$					
	4.7185	0.9800	0.0	0.9800	0.9800	3.4875
	3.8335	1.7770	1.9215	neg.	0.98	3.4875
	3.4384	1.9377	1.9215	0.0162	0.9962	3.4078
	3.3940	1.9518	1.9518	0.0	0.9962	3.4078
	3.3891	1.9534	1.9518	0.0016	0.9978	3.3999

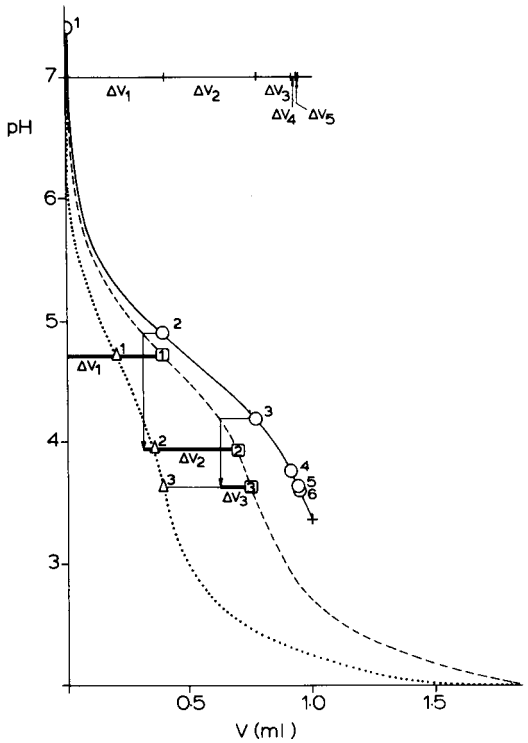

Fig. 1. Titration curves for the system given in Table 5: (——) titration curve; (- - -) first guess curve; (· · ·) indicator curve. (○) Measurement points; (□) indicator values; (△) guessed values; (+) equivalence point. $\triangle V$ is the difference of projected pH values on the guessed curve: $\triangle V = V_{(\text{pH ind})} - V_{(\text{pH measured})}$.

EXPERIMENTAL

Chemicals

Stock solutions of boric, phosphoric and oxalic acid, sodium acetate and potassium hydrogenphthalate were prepared from analytical-grade reagents (Merck). Solutions with known proportions of substances were made by mixing the stock solutions. Sodium acetate was dried at 105°C for 2 h. Phosphoric acid solution was made by diluting the 85% reagent solution and its concentration was checked by titration with sodium hydroxide. Titrant solutions of sodium hydroxide and hydrochloric acid were prepared by diluting Merck ampoules with carbon dioxide-free, double-distilled water and standardized against potassium hydrogenphthalate and also checked against Tris.

Apparatus

Titrations were done in a Metrohm titration vessel thermostated at 22.0 ± 0.05°C (Lauda, Klixon MX-125 thermostat) and equipped with a combined glass/reference electrode (Metrohm EA 121), an inlet tube for nitrogen and a

magnetic stirring bar. The combined glass electrode was calibrated by using at least 5 buffer systems (Merck standard buffer solutions) over a range covering the whole pH domain of the titration.

The titration equipment was constructed from a Heathkit H11 computer with a microprocessor (Digital Equipment Corp. LSI-11A) with 24 kbyte of memory and two H11-2 parallel I/O interfaces. A digital voltmeter (Tekelec Airtronic TE-350-F + s-BCD coded output; 4 digits) was connected to one H11-2 interface. The output of a Knick industrial pH meter (type DIN) was connected to the digital voltmeter. A piston buret (Mettler DV 11) was driven from one TTL signal line from the second H11-2 computer interface on its pulse input terminal. The total volume of the buret was 10.0 ml and its accuracy was 0.001 ml.

Computer program

The programs were written in FORTRAN-10. The operator/program interface is menu-driven and constitutes the main routine of the program. From the choice offered (Table 6), the operator picks the subroutine that performs the requested task (e.g., experimental parameter input). The titration and calculation subroutines offer further options for how the task requested is to be done (Tables 7 and 8). This set offers a very flexible operator/program interaction ranging from full automatic titration and calculation with a minimum of data input for the titration parameters to a very detailed access to specific calculation steps and "manual" control of the titration.

The program is designed in such a way that the values of the different parameters are retained from one experiment to another, so for a new run only the parameters different from the old conditions have to be changed. Most of the options are self-explanatory; only the titration options (Table 7) will be explained in detail as a guide in the choice of the appropriate parameters for a given titration problem.

These titration options offer possibilities to try and compare all the different methods, which are to be used in control of the automatic potentiometric titration. Thus it can be used with fixed volume increments, with fixed pH increments, and with the optimized titrant delivery method.

TABLE 6

Initial choice in program (menu I)

DO YOU WANT: 1. TO INPUT THE CONSTANTS OF SUBSTANCES
2. TO CHANGE THE CONSTANTS OF SUBSTANCES STORED
3. TO LIST THE CONSTANTS
4. TO TITRATE
5. TO MAKE CALCULATIONS
6. TO CHECK AND CHANGE STORED VARIABLES AND CONSTANTS
7. TO TYPE IN TITRATION POINTS
TYPE THE NUMBER OF TASK

TABLE 7

Titration options

```
DO YOU WANT: 1. TO INPUT OR CHANGE PARAMETERS
             2. TO CALCULATE THE PARAMETERS
             3. TO CALIBRATE THE GLASS ELECTRODE
             4. TO PERFORM A FIXED VOLUME TITRATION
             5. TO PERFORM A FIXED DELTA PH TITR.
             6. TO PERFORM AN OPTIMIZED TITRATION
             7. TO PERFORM A SINGLE PH MEASUREMENT
             8. TO OPERATE THE BURET
             9. TO RETURN TO MENU I
TYPE THE NUMBER OF TASK
```

TABLE 8

Calculation options

```
DO YOU WANT TO CALCULATE:
1. THE WHOLE TITRATION CURVE?
2. THE PH FOR A GIVEN VOLUME ADDED?
3. THE VOLUME ADDED FOR A GIVEN PH?
4. THE CONCENTRATION FROM TITRATION DATA?
5. THE PK FROM TITRATION DATA?
6. TO RETURN TO MENU I?
TYPE THE NUMBER OF TASK
```

(1) The parameters VEVP, PHSTART, PHEVP and DELTA(PH) control the titration. In this step they are calculated from the input data of the constants of the substances given and the estimated concentration of the compound to be determined. DELTA(PH) is the maximum change in pH allowed for a titrant addition step and is calculated from the given required precision of the titration. If another equivalence point is wanted in a multi-step titration, it has to be stated here.

(2) PHMETER-ERROR and WAITING TIME are the parameters for the pH measurement and should be given values that match the performance of the pH-meter/glass electrode combination with respect to accuracy and response time. The latter should also allow for the mixing behaviour of the titration vessel. For special purposes the parameters calculated in (1) can be changed in this step.

(3) This step provides the glass electrode calibration. It allows the use of more than two buffers and calculates the calibration constants via least-squares regression.

(4) For pK determinations, the titration is best conducted with the use of fixed titrant additions. The fixed titrant addition per step and the maximum volume of titrant to be delivered should be given as parameters.

(5) In the "extra-fast" titration mode, titrant is delivered in constant pH increments. For the calculation of the appropriate volume to be added

(in contrast to the methods commonly used which are based on an empirical equation), the system parameters for the theoretical titration curve are used. Calculations operate with a ΔV calculated from $V_{(\mathrm{pH\ measured} + \Delta \mathrm{pH})} - V_{(\mathrm{pH\ measured})}$. The estimated concentration is not updated during the titration process.

(6) In the "fast" titration mode, titrant is delivered according to the algorithm described under optimized titrant delivery, with updating of the estimated concentration during titration. There are two options: first, the estimated concentration during the titration can be updated as many times as the user wants; secondly, besides the "standard" fractions described, other combinations of titration fractions can also be used.

(7) and (8) these options offer the possibility of a "manual" titration.

All calculations were done with the use of a small set of subroutines. In all calculating subroutines, the option of using concentrations or activities is offered. The calculation with concentrations, although less exact, avoids numerous iteration processes and is therefore definitely faster. CAVAPD is the main calculating subroutine of the program. It calculates for a given pH value simultaneously all values of P and their derivatives (Eqns. 17 and 21, Table 4) and gives as a result V(act) and V(conc). In the case of activity calculations the subroutine CARIS is used to obtain the ionic strength. This needs the value of V for the calculation of the actual concentrations. The final value is obtained by iteration; the starting value of V is the calculated V(conc). Thus, if the CAVAPD program calculates with activities, it works in a loop, calculating first in a short-cut way the V(conc) and repeating the process for calculation of V(act).

CAPHA calculates the pH for a given titrant volume added (V). For calculation of the function $V = f(\mathrm{pH})$, Eqn. 21 is solved with the Newton—Raphson iteration process. The method is the same as described earlier. In the calculation with activities, one simplifying step is performed, namely in the differential quotient the activity factor is kept constant. For this reason, one or two more iterations may be necessary, but it simplifies the program greatly.

The CADAT subroutine, using a brute force method, calculates from titration data (the starting and terminating number of which can be given) the concentration or pK value. The number of digits calculated can be stated in advance, to regulate the speed of the process. From the same data set, several concentrations and/or pK values can be calculated.

RESULTS AND DISCUSSION

The examples given for acid-base titrations are selected to demonstrate the different capabilities of the above system. The real three-dimensional character of the procedure ($V = f(\mathrm{pH}, E)$) will be more extensively illustrated in a subsequent paper which will deal with redox titrations accompanied with pH changes.

As a first example, the titration of the half-neutralized salt of a relatively strong acid, sodium hydrogenphthalate, is presented. The three samples were titrated with different first-guess concentrations, one close to, and the others lower and higher than, the real value. For better comparison, the same indicator curve was chosen. The results obtained are presented in Table 9.

Titrations of boric acid and sodium acetate are normally impossible without the use of complexing agents, because the sharpness index [3] is below 10. However, the boric acid could be titrated with the present procedure with a sufficient precision in 8—9 steps (Table 10) and so was sodium acetate (Table 11). For comparison, the results produced by another system (the Metrohm automatic titration) are also shown in the Tables.

Although the determination of the separate members of a multicomponent system was not the aim of this work, it can be shown that even in a mixture of weak acids (Table 12) not only the sum of all components but also one

TABLE 9

Titration of potassium hydrogenphthalate with sodium hydroxide
(V_0 = 50.0 ml, Conc. (NaOH) = 0.1 M. Input values: accuracy = 0.1%; first-guess concentration = 0.01 M; conc. for indicator curve = 0.005 M; for phthalic acid, log K_1 = 5.41 and log K_2 = 2.95. For pH measurement: pH stable to 0.001 for at least 3 s. Calculated values: $pH_{(start)}$ = 4.115; $pH_{(ep)}$ = 8.5422; $V_{(ep)}$ = 5.0 ml; $\triangle$pH = 0.458)

Given (M)	Found[a] (M)	$C_{(guess)}$ (M)
0.01	0.010050	0.010
	0.010052	0.015
	0.010048	0.008

[a]Eight points in each case.

TABLE 10

Titration of boric acid with sodium hydroxide
(V_0 = 50.0 ml, Conc. (NaOH) = 0.9940 M. Input values: accuracy = 0.1%; first-guess concentration = 0.01 M; conc. for indicator curve = 0.005 M; for boric acid, log K_1 = 9.23. For pH measurement: pH stable to 0.001 for at least 3 s. Calculated values: $pH_{(start)}$ = 5.5997; $pH_{(ep)}$ = 10.5265; $V_{(ep)}$ = 4.97; $\triangle$pH = 0.0054)

Given (M)	Found (M)	No. of points	First guess (M)	Metrohm titrator (M)
0.01	0.009950	8	0.01	0.01001
	0.009948	9	0.01	
	0.009950	7	0.01	
	0.009906	8	0.01	
	0.009926	8	0.01	
	0.009944	8	0.01	
	0.01005	7	0.001	

TABLE 11

Titration of sodium acetate with hydrochloric acid
(V_0 = 50.0 ml, Conc. (HCl) = 0.10028 M. Input values: accuracy = 0.1%; first-guess concentration = 0.01 M; Conc. for indicator curve = 0.005 M; for acetic acid, log K_1 = 4.76. For pH measurement: pH stable to 0.001 for at least 3 s. Calculated values: $pH_{(start)}$ = 8.3346; $pH_{(ep)}$ = 3.4083; $V_{(ep)}$ = 5.014 ml; $\triangle$pH = 0.0040)

Given (M)	Found (M)	First guess	No. of points	Metrohm titrator (M)
0.01	0.009982	0.01	9	0.00996
	0.009988	0.01	9	
	0.010006	0.01	10	
	0.010016	0.01	10	
	0.010046	0.012	10	
	0.010044	0.080	9	

TABLE 12

Titration of boric acid in a mixture of phosphoric acid (0.001998 M), phthalic acid (0.003018 M), oxalic acid (0.000502 M) and potassium hydroxide (0.003018 M)
(Titrant: sodium hydroxide. V_0 = 50.0 ml, Conc. (NaOH) = 0.09940 M. Input values: accuracy = 0.1%, first-guess concentration = 0.004 M; Conc. for indicator curve = 0.002 M. For phosphoric acid, log K_1 = 12.36, log K_2 = 7.20, log K_3 = 2.12; for phthalic acid, log K_1 = 5.41, log K_2 = 2.95; for oxalic acid, log K_1 = 4.27, log K_2 = 1.25. For pH measurement: pH stable to 0.001 for at least 3 s. Calculated values: $pH_{(start)}$ = 3.0266; $pH_{(ep)}$ = 10.3032; $V_{(ep)}$ = 6.009 ml; $\triangle$pH = 0.0104)

Given (M)	Found (M)	No. of points	$C_{(guess)}$
0.004	0.004039	7	0.004
	0.004045	9	
	0.004025	7	

particular component can be determined, even if there is no sharp potential jump between the components. The sharpness index between the last components is below 1.0 (about 0.25) and the last end-point is also not suitable for common titrations as shown above. In this mixture, boric acid has such a low concentration (0.004 M) that its sharpness index was only 3.38. The results (Table 12) show that all the results are somewhat high. This probably arose from the carbonate concentration of the titrant, which when calculated from the titration data points, accounted exactly for the deviation observed.

With regard to the time needed for the titration, the preliminary calculations for pH(start), pH(ep) and $\triangle$pH need 120 s, and the calculation of indicator pH values takes about 30 s per value. The titration is done with a delivery of 1.0 ml per 30 s; stabilization of pH at the start and near the end-point may take 3 s to 3.0 min, depending on the system, with intermediate waiting times of 3—6 s. Calculation of $\triangle V$ values takes 1—2 s. The calculation time

for concentration can be estimated by means of the expression $TK \times$ data points $\times$ digits calculated; TK = 30 s or 8 s when activity or concentration, respectively, is used for calculation. When the same titration is repeated, the preliminary calculation, which takes about 4.5 min, can be omitted. In that case, a titration with a total titrant consumption of 5.0 ml will take only 5.0 min if the updating calculation is based on concentrations and 8.5 min if the calculation is based on activities.

REFERENCES

1 T. W. Hunter, I. T. Sinnamon and G. H. Hieftje, Anal. Chem., 47 (1975) 497.
2 S. Ebel, Chem. Ing. Tech., 46 (1974) 811.
3 G. Svehla, Automatic Potentiometric Titrations, Pergamon, Oxford, 1978.
4 T. F. Christiansen, J. E. Busch and S. C. Krogh, Anal. Chem., 48 (1976) 1051.
5 D. Betteridge, E. L. Dagless, P. David, D. R. Deans, G. E. Penketh and P. Shawcross, Analyst, 101 (1976) 409.
6 P. V. Früh, L. Meier and H. Rutishauser, Anal. Chim. Acta, 95 (1977) 97.
7 R. W. Hendler, D. Songco and T. R. Clem, Anal. Chem., 49 (1977) 1908, 1914.
8 A. A. B. Wu and H. V. Malmstadt, Anal. Chem., 50 (1976) 2090.
9 D. J. Legget, Anal. Chem., 50 (1978) 718.
10 N. Busch, P. Freyer and H. Szamelt, Anal. Chem., 50 (1978) 2166.
11 L. Andersson, A. Granéli and M. Strandberg, Anal. Chim. Acta, 103 (1978) 489.
12 L. Pehrsson, F. Ingman and S. Johansson, Talanta, 23 (1976) 769, 781; 24 (1977) 79.
13 L. M. Doane, J. T. Stock and J. D. Stuart, Anal. Chem., 56 (1979) 415.
14 Ch. R. Martin and H. Freiser, Anal. Chem., 51 (1979) 803.
15 T. Nishikawa, I. Ogasawara and T. Harada, Anal. Chim. Acta, 133 (1981) 463.
16 S. Ebel, J. Hocke and B. Reyer, Fresenius Z. Anal. Chem., 308 (1980) 437; 312 (1982) 346.
17 J. C. Smit and H. C. Smit, Anal. Chim. Acta, 143 (1982) 45.
18 G. D. Owens and R. J. Eckstein, Anal. Chem., 54 (1982) 2347.
19 J. Boelema, Ph.D. Thesis, University of Groningen, 1982.
20 F. L. Hahn and G. Weiler, Fresenius Z. Anal. Chem., 69 (1926) 417.
21 G. Gran, Acta Chem. Scand., 4 (1950) 559; Analyst, 77 (1952) 661.
22 G. F. Tubbs, Anal. Chem., 26 (1954) 1670.
23 E. Bishop, Anal. Chim. Acta, 26 (1962) 397; 27 (1962) 253.
24 W. E. Wentworth, J. Chem. Educ., 42 (1965) 96.
25 N. Ingri, W. Kakołowicz, L. G. Sillen and B. Warnqvist, Talanta, 14 (1967) 1261.
26 D. Dyrssen, D. Jagner and F. Wengelin, Computer Calculations of Ionic Equilibria and Titration Procedures, Almqvist and Wiksel, Stockholm, 1968.
27 J. A. Goldman and L. Meites, J. Electroanal. Chem., 14 (1967) 373; 16 (1968) 47; 18 (1968) 41; 19 (1968) 204; Anal. Chim. Acta, 28 (1963) 472.
28 D. Midgley and C. McCallum, Talanta, 21 (1974) 723.
29 P. Gans, Coord. Chem. Rev., 19 (1976) 99.
30 M. Bos, Anal. Chim. Acta, 81 (1976) 21; 90 (1977) 61; 122 (1980) 193.
31 G. Arena, E. Rizzarelli, S. Sammartano and C. Rigano, Talanta, 26 (1979) 1.
32 Å. Olin and B. Wallén, Talanta, 25 (1978) 720.
33 R. A. Stairs, J. Chem. Educ., 55 (1978) 99.
34 H. N. J. Poulisse, Anal. Chim. Acta, 112 (1979) 361.
35 R. Rosset, D. Bauer and J. Desbarres, Labo-Pharma, 303 (1980) 833; Chimie Analytique des Solutions et Micro-informatique, Masson, Paris, 1979.
36 H. Narasaki, Talanta, 27 (1980) 409.
37 T. F. Brown and S. D. Brown, Anal. Chem., 53 (1981) 1410.

38 A. D. Zuberbühler and T. A. Kaden, Talanta, 29 (1982) 201.
39 Ch. Willis, J. Chem. Educ., 58 (1981) 659.
40 F. Gaizer and A. Puskás, Talanta, 28 (1981) 565.
41 L. Meites, Anal. Lett., 15 (1982) 507.
42 R. T. Shrager and R. W. Hendler, Anal. Chem., 54 (1982) 1147.
43 W. E. Gordon, J. Phys. Chem., 83 (1979) 1365; Anal. Chem., 54 (1982) 1595.
44 A. Avdeef, D. L. Kearney, J. A. Brown and A. R. Chemotti, Jr., Anal. Chem., 54 (1982) 2322.
45 S. Ebel, E. Glaser, R. Kantelberg and B. Reyer, Fresenius Z. Anal. Chem., 312 (1982) 604.

Analytica Chimica Acta, 158 (1984) 113—117
Elsevier Science Publishers B.V., Amsterdam — Printed in The Netherlands

Short Communication

PULSED PHOTOACOUSTIC SPECTROMETRY FOR SELECTIVE DETERMINATION OF SORBED AND DISSOLVED PRASEODYMIUM SPECIES

SARAH C. RUTAN and STEVEN D. BROWN*

Department of Chemistry, Washington State University, Pullman WA 99164-4630 (U.S.A.)

(Received 19th August 1983)

Summary. Pulsed photoacoustic spectroscopy is used to monitor the adsorption of praseodymium at a montmorillonite clay surface in situ. Observation of the photoacoustic transient response shows that the signals from solid and solution are temporally resolved, allowing spectra of praseodymium in solution and on the clay surface to be obtained.

An understanding of the interaction of solution species with solid substrates is important in many areas of chemistry. One area of particular interest is the uptake of aqueous metal species by clays and other substrates. In many cases, adsorption processes control the availability of metal species in natural aqueous environments [1]. Despite the importance of these processes, few methods are available which are capable of identifying adsorbed species at the liquid/solid interface. Information on the nature of the adsorbed species is of considerable value in understanding adsorption processes.

In the past several years, photoacoustic spectroscopy (p.a.s.) has emerged as a promising technique for studying light-absorbing material at solid/liquid interfaces. Previous studies have utilized a photoacoustic detector which is coupled directly to the solid material [2, 3]. This communication reports a method by which pulsed p.a.s. is used to monitor a lanthanide species adsorbed at the solid/liquid interface, where the p.a.s. transducer is coupled to both the solid and liquid phases. This detection scheme allows solution and sorbed species to be selectively monitored. Preliminary results are given for the photoacoustic detection of praseodymium species adsorbed at a montmorillonite clay/aqueous solution interface.

Experimental

The photoacoustic spectrometer, cell geometry, and computer used for these studies have been described previously [4].

The solid/liquid interface studied consisted of plate glass cut to 1 cm × 5 cm slides and coated with a Belle Fourche, South Dakota montmorillonite clay (Wards, Rochester, NY). The clay was suspended in deionized water and

0003-2670/84/$03.00

subsequently coated on the solid surface to yield a loading of 0.2 mg cm^{-2}. The coated slide was placed in a cell containing 3.00 ml of 0.1 M potassium nitrate. Successive 20-μl additions of 0.20 M praseodymium nitrate were made, and photoacoustic transient and spectral responses were recorded.

Results and discussion

The time required for the acoustic pulse to reach the detector depends on the velocity of sound in the various media through which the pulse must travel to reach the detector. Sam and Shand [5] demonstrated that for a system in which both a solid and a liquid are coupled to the photoacoustic detector, the acoustic pulses arising from the bulk absorption of both the liquid and the solid may be distinguished by the difference in their arrival times at the detector.

Table 1 shows the velocities of sound and the distances for the various media through which the acoustic pulse must propagate to reach the detector. From these data, arrival times for solid and solution pulse propagation were calculated and compared to the experimental arrival times observed in the photoacoustic transient, as shown in Fig. 1. The first two positive excursions (A and C) appear only in the transients obtained when the solid substrate was present. The time at which the first maximum (A) arrives at the detector corresponds well to the travel time calculated for an acoustic pulse propagating through a solid substrate. The third maximum in Fig. 1 (E) is that due to the acoustic pulse which propagates through the solution; again, the arrival time agrees reasonably well with the calculated propagation time. The responses occurring at later times in the photoacoustic transient are due to acoustic reflections within the sample cell.

Spectra were constructed by monitoring the magnitude of the photoacoustic transient oscillations as a function of wavelength. Differences between maxima and minima were calculated in order to discriminate against low-frequency noise. The spectra generated are shown in Fig. 2. The spectra

TABLE 1

Acoustic pulse propagation time

Material	Velocity ($cm\ s^{-1}$)	Solid		Solution	
		Distance (cm)	Time (μs)	Distance (cm)	Time (μs)
Water	1.5×10^5	0.05	0.3	1.3	8.7
Plate glass	5.0×10^5	1.3	2.3	—	—
Quartz	6.0×10^5	0.1	0.2	0.1	0.2
Glycerol	1.7×10^5	0.05	0.3	0.05	0.3
Quartz	6.0×10^5	0.2	0.3	0.2	0.3
Theoretical total	—	—	3.4	—	9.5
Experimental total	—	—	3.4	—	10.7

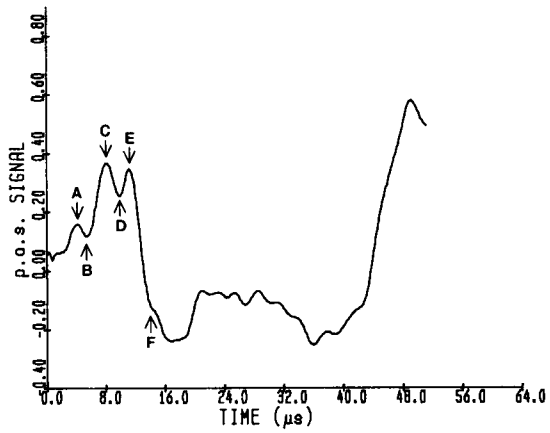

Fig. 1. Typical photoacoustic transient at 600.0 nm.

were obtained from measurements on a solution to which successive additions of praseodymium were made while the solution remained in contact with the clay-coated substrate. For the spectra constructed from the early deviation (occurring at 4.2 μs, A—B in Fig. 1), additions of praseodymium caused an increase in the signal at longer wavelengths, until a limiting value was reached (Fig. 2a). This increase is attributed to the absorption of light by praseodymium species complexed at the clay surface. When the surface sites are filled, the spectrum remains constant. Spectrum B in Fig. 2(a) represents an unsaturated surface, probably caused by kinetic rather than equilibrium effects. When the third deviation at 11.5 μs (E—F in Fig. 1) is monitored, a typical spectrum of praseodymium in solution is obtained with increasing praseodymium concentration [4] (Fig. 2b). The sorbed praseodymium spectrum is shifted to longer wavelengths, relative to the solution spectrum; this shift is similar to the shift observed for complexed praseodymium species is solution [4].

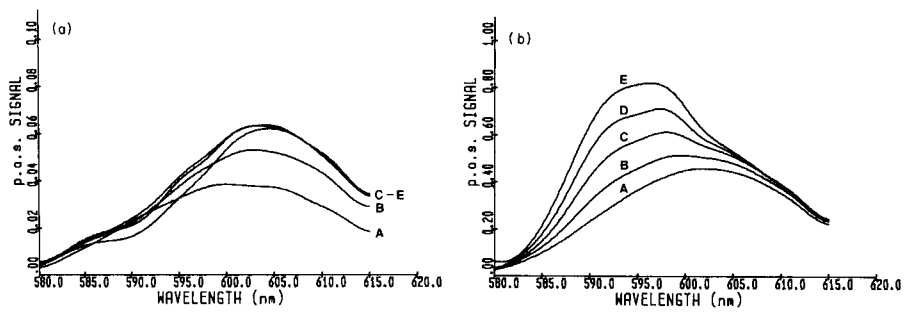

Fig. 2. Photoacoustic spectra constructed by calculating differences: (a) difference between the maximum at 4.2 μs and the minimum at 5.5 μs (A—B in Fig. 1); (b) difference between the maximum at 11.5 μs and the minimum at 14.0 μs (E—F in Fig. 1). Curves: (A) background spectrum; (B—E) successive additions of praseodymium.

It is important to note that even at early times in the transient, the contribution of the praseodymium species in solution is not completely eliminated. When increasing amounts of praseodymium are added to the solution, there is a negative contribution at shorter wavelengths where the aqueous praseodymium species absorb light. This happens because the acoustic wave propagating through the solution interferes destructively with the solid acoustic wave at the detector, causing a decrease in amplitude when increasing amounts of praseodymium solution species are present (Fig. 2a). By increasing the distance through which the acoustic pulse must propagate in solution, the negative contribution from the solution species to the surface spectra can be minimized. The response of species in solution can be seen to have a small contribution from the sorbed species (Fig. 2b). This may be due to the interference of solid and solution acoustic pulses (in this case, constructive interference), or it may be due to the acoustic signal generated by the surface species propagating through both the liquid and solid phases. The contribution of the sorbed species to the solution spectra is small, however, because the number of moles of praseodymium in the region of the solution illuminated by the laser is much greater than the number of moles illuminated on the surface of the clay.

In order to measure the amounts of species in solution and sorbed onto the substrate, several features must be considered. The amplitude of the signal for species in solution depends on the presence as well as the exact orientation of the glass slide. With fixed, reproducible geometry for the cell and glass slide, a simple calibration curve can be used to obtain the concentrations of solution species. Direct measurement of the sorbed surface species is hindered, as for all surface spectroscopic techniques, by the need for reliable standards in similar matrices.

An alternative approach applicable to the system studied here is to construct a titration curve for praseodymium with the clay adsorbent. This method was used with these preliminary data by subtracting the background spectrum (A in Fig. 2b) from spectra B—E (Fig. 2b). The p.a.s. signal at 592.5 nm was plotted as a function of the total praseodymium concentration, and a linear relationship with a slope of $(9.60 \pm 0.04) \times 10^{1}$ M^{-1}, a y-intercept of $(-2.65 \pm 0.11) \times 10^{-2}$, and an x-intercept of $(2.76 \pm 0.15) \times 10^{-4}$ M was obtained, where the reported errors are the 95% confidence limits. The correlation coefficient was 1.0000. The x-intercept value should represent the equivalence point of the praseodymium-clay reaction, given the minimal spectral contributions from sorbed praseodymium species. It should be noted that the detection limit for solution-based praseodymium species found in previous experiments was 4×10^{-5} M [4] well below the value observed for the equivalence point. This equivalence point value corresponds to about 10^{-9} mol of praseodymium on the portion of the surface that is illuminated. From this equivalence point value, an ion-exchange capacity for the clay was calculated to be approximately 0.9 mmol g^{-1}, which is a reasonable value for a lanthanide ion interacting with a clay [6]. This value should

be viewed with caution, however, because no measurements were made in the vicinity of the equivalence point.

At present, the experimental design is limited by the reproducibility of the geometry of the sample cell/solid substrate. An improved cell is currently being constructed, which should alleviate this problem. Better measurements can then be made to characterize the praseodymium/clay reaction curve. It is important to note, however, that the value of this technique lies in its ability to monitor the spectral responses of the solution and sorbed species selectively in the same experiment.

The support of the Division of Analytical Chemistry of the American Chemical Society in the form of a Summer Fellowship for S. C. R. is gratefully acknowledged.

REFERENCES

1 T. M. Florence and G. E. Bately, CRC Crit. Rev. Anal. Chem., (1980) 219.
2 M. Wun-Fogle, D. J. Milgaten and W. C. Hwang, Appl. Opt., 21 (1982) 121.
3 R. E. Malpas and A. J. Bard, Anal. Chem., 52 (1980) 109.
4 S. C. Rutan and S. D. Brown, Anal. Chem., 55 (1983) 1707.
5 C. L. Sam and M. L. Shand, Opt. Commun., 31 (1979) 174.
6 S. E. Miller, G. R. Heath and R. D. Gonzalez, Clays Clay Miner., 30 (1982) 111.

Analytica Chimica Acta, 158 (1984) 119—124
Elsevier Science Publishers B.V., Amsterdam — Printed in The Netherlands

Short Communication

DETERMINATION OF URANIUM IN SEA WATER AND BIOLOGICAL MATERIALS BY NEUTRON ACTIVATION AFTER SELECTIVE PRECONCENTRATION WITH 1-(2-PYRIDYLAZO)-2-NAPHTHOL

H. BEM[a], and D. E. RYAN*

Trace Analysis Research Centre, Department of Chemistry, Dalhousie University, Halifax, Nova Scotia B3H 4J1 (Canada)

(Received 19th October 1983)

Summary. Uranium is preconcentrated from sea water, tap water, and solutions obtained by digestion of biological samples, by coprecipitation with 1-(2-pyridylazo)-2-naphthol (PAN). Coprecipitation is most effective at pH 4.5—6.5 with a recovery of 85—94%. In the presence of 0.1 M 1,2-cyclohexylenedinitrilotetraacetic acid (CyDTA) as a masking agent, the method is highly selective for uranium. After neutron activation of the precipitate, uranium can be quantified via the ^{239}U nuclide with a relatively low background in the region of interest (74 keV). Detection limits are 3—4 ng kg^{-1} for 500-ml water samples and 5 μg kg^{-1} for 0.5-g biological samples (after digestion). The method can be applied to most environmental samples, as shown by the results for sea water and three standard reference materials.

The uranium content in natural waters and biological material is often below 0.1 ppb and methods with low detection limits are needed to obtain results of reasonable accuracy. For sea water, where the uranium content is at least 10 times higher, the high concentrations of the alkali metals and the halogens represent additional difficulty for most quantitative techniques.

Neutron activation methods are very often applied for the determination of uranium because of the low detection limits for this element. Delayed neutron counting has been used for the determination of uranium in natural water [1] and it is applicable to NBS biological standard reference materials after elimination of the matrix effect [2]. Most activation methods are based on the measurement of the 74-keV γ-rays from ^{239}U ($t_{1/2}$ = 23.5 min) produced by ^{238}U (n, γ) ^{239}U reaction after short reactor irradiation. However, very few attempts have been made to activate water samples without preconcentration of uranium. In that case, because of the high Compton background around 74 keV, a rapid postirradiation separation of uranium by extraction [3] or ion-exchange chromatography [4] was necessary. Because of low natural levels of uranium in environmental samples, a preconcentration step is normal despite the risk of contamination. All of the proposed

[a]On leave from Technical University of Lodz, Poland.

0003-2670/84/$03.00

methods, such as adsorption of uranium complexes on charcoal [5—7], co-precipitation with lead phosphate [8], colloid flotation on hydrous iron oxide [9], or ion-exchange chromatography on Chelex-100 resin [10] lack selectivity for uranium and were applied to multielement measurements. In addition to nonquantitative recovery of uranium, the presence of other elements in the preconcentrated sample increases background in the low-energy region and increases the detection limit of uranium. Coprecipitation of trace elements with organic chelating reagents is attractive for neutron activation because of low induced activities in the matrix and low blanks (after proper purification of chelating compounds).

1-(2-Pyridylazo)-2-naphthol (PAN) reacts with many heavy metals [11] and has been applied for the preconcentration of metals from natural waters and sea water in conjunction with x-ray fluorescence spectrometry [12—14]. It has also been reported that in an alkaline solution containing strong complexing agents such as EDTA and cyanide, only uranium precipitates with PAN [15]. Subsequently, PAN was recommended as a selective, extractive spectrophotometric reagent for uranium in the presence of masking agents [16, 17].

In the present study, PAN was investigated for preconcentration of uranium from different environmental samples for rapid neutron activation/γ-spectrometry via the ^{239}U radionuclide. This is particularly important for biological samples, in which the presence of large amounts of sodium and manganese makes it impossible to measure low uranium concentrations after short irradiation; uranium can then be detected only after long epithermal irradiation and a long waiting period via its daughter radionuclide ^{239}Np ($t_{1/2}$ = 2.35d) [18].

Experimental

Reagents and samples. A 1% solution of PAN (Baker) in acetone (ACS Spectro-grade Caledon) was used. An atomic absorption standard solution of uranium (Alfa-Ventron) was used to establish the optimum conditions for preconcentration of uranium. The masking agent, 1,2-cyclohexylenedinitrilotetraacetic acid (CyDTA), was used as an aqueous 0.1 M solution. For pH adjustment, a mixed solution of potassium phthalate and potassium hydroxide was used. All other chemicals were reagent grade (Fisher).

The sea water was from the Northwest Arm, Halifax, Nova Scotia and was taken directly from a tap in the Oceanography Laboratory of the University; the water is filtered through sand before entering the building. It was further filtered through a Metricel filter, pore size 0.45 μm (Gelman Sci.).

Samples (0.5 g) of National Bureau of Standards standard reference materials SRM 1573 (Tomato Leaves), SRM 1575 (Pine Needles) and International Atomic Energy Agency-Calcined Animal Bone A3-74 were used to evaluate the accuracy of the developed method.

Preconcentration procedure. Because of the relatively high concentration of uranium in sea water ($\approx$3 μg kg^{-1}), 200 g of sea water sufficed. To each

sample was added 2 ml of 0.1 M CyDTA and the pH was adjusted to 4.5 with phthalate buffer. The solution was rapidly stirred and 2 ml of the PAN solution was added slowly. The solution was heated at 80°C for 1 h, allowed to cool, and then filtered under suction through Metricel filter (pore size 0.45 μm). The filter containing the precipitate was dried and transferred to a small polyethylene irradiation vial.

The same procedure was applied for tap water except that 500-g samples of tap water were needed and 3 ml of the PAN solution was added for precipitation.

Solid biological SRM's 1573 and 1575 were ashed by heating at 500°C for 8 h in a porcelain crucible. The residue was partially dissolved by addition of 2 ml of concentrated hydrochloric acid; the mixture was transferred to a teflon vial, and 0.5 ml of hydrofluoric acid and 1 ml of 30% hydrogen peroxide were added. The solution was evaporated to dryness and the dry residue was redissolved by addition of 0.1 ml of concentrated hydrochloric acid and 5 ml of distilled water. This solution was transferred to 200 ml of distilled water.

The 0.5-g samples of IAEA Calcined Animal Bone were dissolved in 5 ml of a 1:1 mixture of perchloric and nitric acids by heating at 60°C for 3 h followed by addition of 1 ml of hydrogen peroxide and further heating for 1 h. The solution was evaporated to about 3 ml and transferred to 200 ml of distilled water. The pH was adjusted to 4.5 by addition of solid potassium hydroxide and phthalate buffer.

The remainder of the preconcentration procedure for all solid SRM's was as for sea water except for the addition of 5 ml of 0.1 M CyDTA solution to avoid coprecipitation of traces of calcium and other metals.

Apparatus. All samples were irradiated in an inner site of the SLOWPOKE reactor at a flux of 5×10^{11} n cm^{-2} s^{-1} for 10 min. After a decay time of 1 min, the samples were counted for 10 min using a Canberra Ge (Li) detector with a 9.5% relative efficiency and 1.9-keV resolution at 1332 keV. The lead shielding was removed from the Ge(Li) detector to eliminate the interfering lead x-rays at 74 keV.

Results and discussion

Uranium is known to be present in natural waters, mainly in the hexavalent state, as uranyl carbonate complexes, $UO_2(CO_3)_2^{2-}$, but uranium also forms stable complexes with organic matter in water (humic and fulvic acids) [19]. These organic complexes can influence formation of complexes with chelating reagents and consequently the recovery of uranium in the precipitate. Ultraviolet irradiation can be used to reduce the effect of organic material in natural waters on the recovery of uranium [20] and the necessity of sea water pretreatment was therefore checked. Recovery of uranium from sea-water samples depended on the time of heating after precipitation. For example, after 20-min heating, the recovery was only about 67% but it was almost quantitative (94%) after heating for 1 h. Pretreatment of sea-water

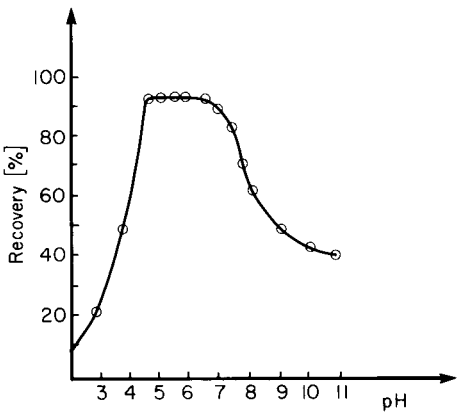

Fig. 1. pH profile for the coprecipitation of uranium with PAN.

samples (200 g) by addition of 5 ml of nitric acid or of 50 mg of hydrazine dihydrochloride and heating for 1 h or u.v. irradiation for 3 h prior to precipitation resulted in the same high recovery (90—94%) after heating for 20 min but the total preconcentration time was longer. Heating of the mixture for 1 h at 80°C after precipitation, without any sample pretreatment, was therefore chosen as a standard procedure.

The stability of uranium-PAN complexes may be influenced by pH and the presence of masking agents. Figure 1 illustrates the effect of pH on coprecipitation of uranium. It is evident that for maximum recovery the pH of coprecipitation should be between 4.5 and 7. At pH values above 5, PAN can collect several other elements, especially manganese [14], and a pH of 4.5 was used for precipitation.

The influence of several masking agents on the recovery is shown in Table 1. Potassium cyanide cannot be used at pH 4.5 and EDTA and citric acid seriously affect the recovery of uranium. Up to 5 ml of 0.1 M CyDTA did not affect recovery and showed no influence on the pH profile. In addition, CyDTA strongly complexes several cations at pH 4.5 and can be applied as a masking agent for the preconcentration of uranium [17, 21, 22].

TABLE 1

Influence of different complexing compounds on recovery of uranium

Complexing solution	Volume added (ml)	Recovery (%)	Complexing solution	Volume added (ml)	Recovery (%)
0.1 M citric acid	2	1.5	0.1 M CyDTA	1	93
1% KCN (pH 7)	2	90	0.1 M CyDTA	2	93
0.1 M potassium phthalate	2	92.5	0.1 M CyDTA	3	93
0.1 M potassium phthalate	5	90	0.1 M CyDTA	4	92
0.1 M EDTA	2	66	0.1 M CyDTA	5	91

TABLE 2

Determination of uranium in different samples after selective preconcentration with PAN

Sample	Uranium recovery (%)	Uranium found (μg kg^{-1})		Detection limit (μg kg^{-1})
		This work	Reported values	
Tap water (500 g)	94	0.04 ± 0.005	—	0.004
Sea water (200 g)	93	3.3 ± 0.08	3.08 [9]	0.003
Sea water (300 g)	92.5	3.2 ± 0.08	3.2 [8]	0.003
Sea water (500 g)	91	3.25 ± 0.07		0.003
Pine Needles	85	22 ± 1.8	20[a]	4.5
Tomato Leaves	86	59 ± 1.2	60[a]	4.5
Calcined Bone	93	<5		5.0

[a]Certified values.

The detection limit of uranium depends also on the blank irradiated, and, because this is connected with the amount of irradiated precipitate, the influence of the amount of PAN used on the recovery of uranium was investigated. It was shown that 20 mg (2 ml of 1% solution in acetone) of PAN was sufficient for preconcentration from 200 ml of sea water; for 0.5 kg of tap water, 30 mg of PAN was required. The blank was equivalent to $\leqslant$3 ng of uranium.

The accuracy of the developed method for uranium was evaluated for sea water and some biological SRM's. The results are presented in Table 2. The good agreement between determined values and those certified or reported by others confirms the suitability of the method. Recoveries were determined by measuring the uranium concentration before and after standard addition (1—10 μg of uranium). Detection limits were calculated on the basis of 3 times the square root of the background; their values are close to the blank introduced during preconcentration. The higher values for Pine Needles and Tomato Leaves are caused by traces of sodium and manganese adsorbed by the surface of the precipitate. For calcined bone, traces of calcium and magnesium phosphates also coprecipitated at pH 4.5 and the limit of detection was almost twice that for sea water.

The results show that this method permits determination of concentrations of uranium in natural waters as low as 4 ng kg^{-1}. For biological samples, the detection limit is 5 μg kg^{-1}.

REFERENCES

1 R. J. N. Brits and M. C. B. Smit, Anal. Chem., 49 (1977) 67.
2 E. S. Gladney, D. R. Perrin and W. K. Hensley, J. Radioanal. Chem., 59 (1980) 249.
3 E. Steinnes, Radiochem. Radioanal. Lett., 16 (1973) 25.
4 E. S. Gladney, J. W. Owens and J. W. Starner, Anal. Chem., 48 (1976) 973.
5 H. A. van der Sloot, R. Massee and H. A. Das, J. Radioanal. Chem., 25 (1975) 99.

6 K. H. Lieser, W. Calmano, E. Heuss and V. Neitzert, J. Radioanal. Chem., 37 (1977) 717.
7 J. Holzbecher and D. E. Ryan, Anal. Chim. Acta, 119 (1980) 405.
8 J. Holzbecher and D. E. Ryan, J. Radioanal. Chem., 74 (1982) 25.
9 R. S. S. Murthy and D. E. Ryan, Anal. Chem., 55 (1983) 682.
10 R. R. Greenberg and H. M. Kingston, J. Radioanal. Chem., 71 (1982) 147.
11 K. L. Cheng and R. H. Bray, Anal. Chem., 27 (1955) 782.
12 R. Puschel, Talanta, 16 (1969) 351.
13 H. Watanabe, S. Berman and D. S. Russell, Talanta, 19 (1972) 1363.
14 M. G. Vanderstappen and R. E. Van Grieken, Talanta, 25 (1978) 653.
15 K. L. Cheng, Anal. Chem., 30 (1958) 1027.
16 S. Shibata, Anal. Chim. Acta, 22 (1960) 479.
17 K. L. Cheng, Talanta, 9 (1962) 739.
18 K. Kostadinov and R. Djingova, J. Radioanal. Chem., 63 (1982) 5.
19 W. C. Li, D. M. Victor and C. L. Chakrabarti, Anal. Chem., 52 (1980) 520.
20 G. S. Caravajal, K. I. Mahan and D. E. Leyden, Anal. Chim. Acta, 135 (1982) 205.
21 Z. Sulcek and P. Povondra, Collect. Czech. Chem. Commun., 32 (1967) 3140.
22 P. Pakalns, Anal. Chim. Acta, 120 (1980) 289.

Analytica Chimica Acta, 158 (1984) 125—129
Elsevier Science Publishers B.V., Amsterdam — Printed in The Netherlands

Short Communication

A GENERALIZED APPROACH FOR THE CALCULATION AND AUTOMATION OF POTENTIOMETRIC TITRATIONS
Part 2. Redox Titrations

J. STUR, M. BOS and W. E. VAN DER LINDEN*

Department of Chemical Technology, Twente University of Technology, Enschede (The Netherlands)

(Received 14th September 1983)

Summary. The very fast calculation procedure described earlier is applied to calculate the titration curves of complicated redox systems. The theory is extended slightly to cover inhomogeneous redox systems. Titrations of iodine or 2,6-dichloroindophenol with ascorbic acid are described. It is shown that correspondence between theory and practice is good as long as the relevant stability constants and redox potentials are known with sufficient accuracy.

In a previous paper [1], a generalized approach for the calculation of titration curves was presented. Based on the rapidity of the calculation, a sophisticated, automated titration procedure was introduced. The examples given in that paper were confined to pure acid-base reactions, although the calculation procedure was based essentially on the simultaneous change of both pH and redox potential of the system. The present paper deals with redox systems in which the pH also changes.

With respect to practical performance, redox titrations differ in some aspects from acid-base titrations. First, proton transfer is generally very fast, whereas many reactions involving electron transfer are slow. This can apply to the chemical reaction in the bulk of the solution as well as to the electrochemical reaction at the indicator electrode surface. It can be difficult to maintain the appropriate kinetic conditions and to control the reaction rates; moreover, if the solution is only moderately buffered, unstable signals will be observed and sometimes rather long waiting times have to be adopted. But it is in exactly such situations that automation can offer advantages. Secondly, most redox titrations show more pronounced end-points than acid-base titrations. This is partly due to the large difference in redox potentials between the substances in the sample solution and a properly selected titrant, but is also due to the fact that samples will normally contain fewer reducible or oxidizable substances than protolytes. Therefore, fewer potential jumps have to be accommodated on a larger voltage span. Further, the existence of different valency states in redox systems will mean that errors will be larger if activity coefficients are neglected.

0003-2670/84/$03.00

Although the previous treatment of redox equilibria [1] seems to be universal as far as protolytic reactions are concerned, it does not provide for situations where the coefficients for the oxidized and the reduced form are not equal for one of the substances participating in the reaction. Bishop [2] introduced the expression "inhomogeneous" for such reactions. This requires a short extension of the theory.

Theory

Two situations will be considered. First, a system is examined in which the coefficients of the oxidized (ox) and reduced (red) forms occur in the ratio 2:1; then, a system with the ratio 1:2 is considered.

Ratio 2:1. The redox reaction, e.g., $Hg_2^{2+} \rightleftharpoons 2Hg^{2+} + 2e^-$, has the following form

$$z_R Y_2^{red} + z_Y R^{ox} \rightleftharpoons 2z_R Y^{ox} + z_Y R^{red}$$

From the mass-balance equation, the concentration of Y^{ox} can be calculated

$$[Y^{ox}] = \tfrac{1}{4}\exp[\phi_Y]\ \{-1 + (1 + 8C_Y[V_0/(V_0 + V)]\ \exp[-\phi_Y])^{1/2}\} \quad (1)$$

where $\phi_Y = z_Y F(E - E_Y^0)/RT$, $C_Y = 2[Y^{red}] + [Y^{ox}]$ (analytical concentration of Y), V_0 is the initial volume, and V is the volume of titrant added.

Further, the following implicit equation in V must be valid:

$$V = 1/8[(V_0 + V)/C_R]\ (1 + \exp[\phi_R])(z_Y/z_R)\ \exp[\phi_Y]$$
$$\times\ \{-1 + (1 + 8C_Y[V_0/(V_0 + V)]\ \exp[-\phi_Y])^{1/2}\} \quad (2)$$

Ratio 1:2. The overall reaction, e.g., $2I^- \rightleftharpoons I_2 + 2e^-$ or sulfhydryl systems can be written as $2z_R Z^{red} + z_Z R^{ox} \rightleftharpoons z_R Z^{ox} + z_Z R^{red}$ and similarly to Eqn. 1 the concentration of Z^{ox} can be expressed as

$$[Z^{ox}] = 1/8\{4C_Z[V_0/(V_0 + V)] + \exp[-\phi_Z]$$
$$\times\ \{1 - (1 + 8C_Z[V_0/(V_0 + V)]\ \exp[\phi_Z])^{1/2}\}\} \quad (3)$$

The implicit equation for V is

$$V = (V_0 + V)(1 + \exp[\phi_R])\ z_Z\{[4C_Z V_0/(V_0 + V)] + \exp[-\phi_Z]$$
$$\times\ \{1 - [1 + 8C_Z V_0 \exp[\phi_Z]/(V_0 + V)]^{1/2}\}\}/8C_R z_R \quad (4)$$

It can be concluded that for solutions containing Y or Z systems, the extended redox equation can be presented in the form

$$V = \{(V_0 + V)(1 + \exp[\phi_R])/z_R C_R\}[\sum_{i=1}^{l} z_{Xi} C_{Xi} V_0/\{(1 + \exp[-\phi_{Xi}])(V_0 + V)\}$$
$$+ \sum_{i=1}^{m} 0.125\, z_{Yi} \exp[\phi_{Yi}]\ \{-1 + [1 + (8C_{Yi} V_0 \exp[-\phi_{Yi}])/(V_0 + V)]^{1/2}\}$$
$$+ \sum_{i=1}^{n} 0.125\, z_{Zi}\{4C_{Zi} V_0/(V_0 + V) + \exp[-\phi_{Zi}]$$

$$\times \{1 - (1 + 8C_{Zi}V_0 \exp[\phi_{Zi}]/(V_0 + V))^{1/2}\}] \quad (5)$$

where X indicates a redox substance that can be considered as a homogeneous system and l, m and n denote the total number of the three kinds of species, respectively.

Experimental

Chemicals. All chemicals were of analytical reagent-grade purity. Ascorbic acid solutions (0.1 M and 0.02 M) were prepared from the acid (Baker) in deionized-distilled water. The solution was standardized against the iodine solution [3]. Iodine solution (0.05 M) was prepared from Titrisol ampoules (Merck). 2,6-Dichloroindophenol solution (0.001 M) was prepared from the sodium salt (Merck) by dissolving the salt in deionized-distilled water, filtering through a Millipore filter (AAWP 02500) and diluting to the appropriate volume. This solution was standardized photometrically, as proposed by Armstrong [4].

Apparatus. The equipment, which was basically the same as described before [1], was extended with a platinum electrode, a silver/silver chloride reference electrode (Ingold C 373 M-NS) and a mV-meter (Knick Type DIN). The redox electrode system was tested simultaneously with the pH-measuring system by means of several buffers saturated with quinhydrone. All measurements were done under nitrogen. The solutions were usually deaerated by bubbling nitrogen; for the iodine-containing solutions, nitrogen was only passed over the solution.

Computer program. The extensions dealing with inhomogeneous redox reactions, as presented in the theoretical part, were incorporated in the program described in Part 1 [1]. Because the square-root terms in the equations can produce values that exceed the capacity of the computer, especially if the expressions $\exp[\pm\phi]$ have very small values, a value of 1 can be obtained for this square root which yields concentrations equal to zero. In order to circumvent this problem, the program switches automatically in such cases to the approximation $(1 + x)^{1/2} \simeq 1 + x/2$.

The program for the calculation of redox titrations is again presented as a choice of options for the selection of data input, correction and print out. Different kinds of calculation are possible. For instance, there is the option of faster calculation by omitting the iterative process for the calculation of activity coefficients. Although the variations of the differential quotients caused by changes in the activity coefficients are not taken into account, these variations are usually so small that the number of iterations needed to achieve the desired precision does not increase. The program offers the additional possibility of calculating the formal potentials of a system at each pH value by using the "absolute" standard potential as defined in Part 1.

Results and discussion

To illustrate the possibilities of the above approach, titrations of iodine and 2,6-dichloroindophenol with ascorbic acid were examined. In both cases, the pH drops during the titration, causing a slight change in the formal potential. However, there is a difference between the two systems. In titrations of iodine, a significant decrease in pH is observed at the beginning, whereas the pH remains approximately constant after the equivalence point. In titrations of 2,6-dichloroindophenol, a large drop in pH occurs just after the equivalence point, leading to an increase in the formal potential.

The results for the iodine titration are given in Fig. 1, which also shows the theoretical curves calculated with and without consideration of the inhomogeneity of the reaction. The large influence of this factor is clear. The titration proceeds quickly and reproducibility is very good.

The second example deals with 2,6-dichloroindophenol, which is used in its oxidized state as an indicator in titrations with ascorbic acid. When reduced in unbuffered solutions with ascorbic acid, the compound shows characteristic changes in both pH and redox potential (Fig. 2). For the theoretically calculated curves, the constants used first were those determined by Gibbs et al. [5] and summarized in Clark's classic work [6] and in a monograph [7] (see Table 1). The experimental values did not fit

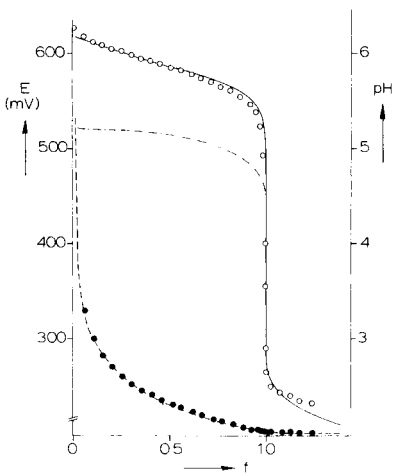

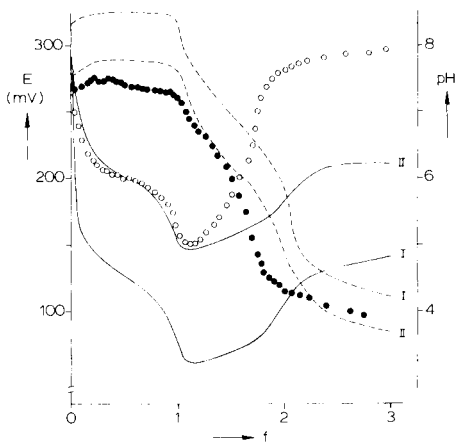

Fig. 1. Titration curves of iodine with ascorbic acid in unbuffered aqueous solution (C_{I_2} = 0.02 M; V_0 = 40 ml). pH change: (———) calculated; (•) measured. Potential change: (—·—) calculated without accounting for the inhomogeneity of the system; (——) calculated with inhomogeneity taken into account; (○) measured.

Fig. 2. Titration curves of 2,6-dichloroindophenol (sodium salt) with ascorbic acid in unbuffered aqueous solution (C_{DCIP} = 0.008 M; V_0 = 40 ml). pH change: (———) calculated with constants of Table 1; (•) experimental values. Potential change: (——) calculated; (○) experimental values. Curves: (I) calculated with constants in first row of Table 1; (II) calculated with constants in last row of Table 1.

TABLE 1

Relevant protonation constants and standard potentials for 2,6-dichloroindophenol and ascorbic acid

2,6-Dichloroindophenol					Ascorbic acid		
E_0 (V)	pK_{ox}	pK_{red1}	pK_{red2}	Ref.	E_0 (V)	pK_1	Ref.
0.669	5.7	7	10.1	5—7	0.3895	4.1	3
0.700	3.95	4.5	9.4	8			
—	6.02	—	—	4			
0.73	3.95	6.2	9.4	—	0.3895	3.1	—

the theoretical curves (Fig. 2; curves I); the experimental pH curve seems to be shifted to lower pH values, whereas the experimental potentials are shifted to higher values. However, for values of the titration parameter (f) lower than 1.2, the shapes of the theoretical and experimental curves agree fairly well. For larger values of f, the calculated pH values are too high leading to low redox potentials. With regard to these discrepancies, it has to be stressed that the relevant stability constants and redox potentials for many redox indicators in the literature are uncertain [7]. Table 1 gives some other, more recent values of some of the constants. No better correspondence was obtained with these values. Recalculation with the set of constants denoted by II yields a good fit in the first part of the titration curve. No set of constants could be found to improve the correspondence for $f > 1$. Probably this discrepancy has to be attributed to kinetic effects; the ascorbate/dehydroascorbate redox couple is irreversible [9].

It was not the goal of this work to verify or to determine values of the stability constants of this complicated system, but to show that in unbuffered redox systems such pH changes can occur during titrations that the change in potential can be inverted. Even for such complicated systems, the calculation of a complete titration curve takes only several minutes.

REFERENCES

1 J. Stur, M. Bos and W. E. van der Linden, Anal. Chim. Acta, 158 (1984) 93.
2 E. Bishop, Anal. Chim. Acta, 26 (1962) 397; 27 (1962) 253.
3 L. Erdey and G. Svehla, Ascorbinometric Titrations, Akad. Kiadó, Budapest, 1973.
4 J. McD. Armstrong, Biochim. Biophys. Acta, 86 (1964) 191.
5 H. D. Gibbs, B. Cohen and R. K. Cannan, Public Health Rep. (U.S.), 40 (1925) 649.
6 W. M. Clark, Oxidation-Reduction Potentials of Organic Systems, Williams and Wilkins, Baltimore, MD, 1960.
7 J. M. Ottaway, in E. Bishop (Ed.), Indicators, Pergamon, Oxford, 1972, p. 484.
8 O. S. Ksenzhek, S. A. Petrova and M. V. Kolodyazhny, Bioelectrochem. Bioenerg., 4 (1977) 346.
9 L. Erdey and G. Svehla, Z. Anal. Chem., 150 (1956) 407.

Analytica Chimica Acta, 158 (1984) 131—136
Elsevier Science Publishers B.V., Amsterdam — Printed in The Netherlands

Short Communication

MINIMIZATION OF MATRIX INTERFERENCES IN THE DETERMINATION OF ALUMINIUM IN SILICON BY ELECTROTHERMAL ATOMIC ABSORPTION SPECTROMETRY WITH THE L'VOV PLATFORM

M. TADDIA

"G. Ciamician" Chemical Institute of the University, I-40126 Bologna (Italy)

(Received 22nd September 1983)

Summary. The pyrolytic L'vov platform in a pyrolytically-coated graphite tube was successful in eliminating the suppressive interference by silicon (≤ 10 mg ml^{-1}) on the aluminium signal, thus allowing ≥ 0.2 μg Al g^{-1} to be determined without preliminary separation.

The routine determination of aluminium in silicon is necessary in the chemical characterization of material used for solar cells. A previous paper described a method based on electrothermal atomic absorption spectrometry (a.a.s.) in an uncoated graphite tube [1]. The relatively poor sensitivity of this method was due to the depressive effect of the silicon matrix on the aluminium signal. Various possibilities for decreasing or eliminating matrix interferences in electrothermal a.a.s. have been reviewed recently [2, 3]. The best approach to adopt usually depends on both the interference and mechanism, but matrix effects tend to be of composite nature so that preliminary tests are normally needed.

Matrix problems encountered in the determination of aluminium in silicon can be explained by the chemical reactions that occur during the determination of silicon in graphite-furnace a.a.s. [4, 5]. The formation of a refractory material such as silicon carbide could play a key role in the process; different coatings were therefore tried to protect the graphite surface. Standard pyrolytically-coated tubes gave some encouraging results, but reliable data were obtained only by incorporating the L'vov platform, which minimized the matrix interference without sacrifice of precision of the measurements. The benefits provided by the platform are well known [6—8]. The time lag between the heating of the tube and the platform causes the vaporization and atomization processes of the sample to be delayed. The atomic vapour enters an environment almost at constant temperature, so that the analyte signal is less matrix-dependent.

0003-2670/84/$03.00

Experimental

Apparatus. The atomic absorption spectrometer was a Perkin-Elmer 372 model equipped with a HGA-500 graphite furnace atomizer and a Leeds-Northrup 681A chart recorder. An Intensitron aluminium hollow-cathode lamp (25 mA, 309.3 nm) was used at a spectral bandwidth of 0.7 nm. Pyrolytically-coated graphite tubes (Perkin-Elmer No. 091504) and pyrolytic graphite L'vov platforms (Perkin-Elmer No. 121091) were used. The proper adjustment of the platform was inspected visually by ensuring that the sample solution was uniformly distributed on the platform depression. Some experiments were done both with standard uncoated tubes and also by treating the inner surface of the furnace with carbide-forming elements. Lanthanum and molybdenum coatings were obtained by following known procedures [9—11]. Argon provided the inert atmosphere within the furnace.

Samples (10 μl) were injected manually. Deuterium background correction was found to be unnecessary. Furnace conditions for sampling from the pyrolytically-coated tube wall and from the platform are given in Table 1. When the platform was used the cooling time was prolonged by 20 s to allow the whole system to return to room temperature. Conditions for sampling from uncoated tubes have already been reported [1].

Reagents. The stock aluminium solution was 1000 mg Al l^{-1} (aluminium chloride, Merck standard solution). More dilute standards in 0.2% (w/v) nitric acid were prepared daily. The hydrofluoric and nitric acids were of electronic grade (J. T. Baker and C. Erba, respectively).

Procedure. Introduce the sample (20—100 mg, ground to a fine powder) into a polymethylpentene test tube, add 1 ml of 65% nitric acid and 5 ml of 5 M hydrofluoric acid, and mix thoroughly. Place the covered tube on a bath at 100°C to complete dissolution. Allow to cool and dilute to 10 ml with redistilled water. Determine aluminium by using a standard addition technique. After measuring the absorbance of three or four replicates, repeat after the addition of 50, 100 and 150 μl of a standard containing 10 μg Al ml^{-1}. Read the absorbance in the peak-height mode.

TABLE 1

Operating parameters for the graphite furnace

	Wall (pyrolytic tube)			Platform		
	Temp. (°C)	Ramp (s)	Hold (s)	Temp. (°C)	Ramp (s)	Hold (s)
Dry	120	8	20	120	8	20
Ash 1	250	2	8	250	2	8
Ash 2	1200	10	60	1200	10	40
Atomize[a]	2600	1	5	2600	1	6
Clean-out	2700	1	3			
Cool	—	—	—	20	1	20

[a] Argon flow through the tube was 50 ml min^{-1} during the atomization stage.

Results and discussion

In early attempts to find a suitable coating to protect the graphite surface, the performance of lanthanum- and molybdenum-treated tubes was tested for standard and samples. The results were unsatisfactory. The lanthanum treatment, resulting in the formation of oxide or carbide or both, initially improved the sensitivity by a factor of 2.2, but after a few cycles the initial conditions had been restored. The discrepancy between the present results and those obtained by other authors [9, 11] can be explained by the lower atomization temperatures used (1950°C, 2000°C), compared with the boiling point of lanthanum trioxide (4200°C). The molybdenum treatment gave a more stable coating, improved sensitivity (enhancement factor 1.2) and precision (r.s.d. 1.1% for 0.2 ppm Al), but failed to decrease the silicon interference. Probably it was the formation of molybdenum silicides that destroyed the effectiveness of the treatment.

The literature data concerning the determination of aluminium by using injection into pyrolytically-coated tubes were not very favourable [12]. Both precision and sensitivity were reported to be poorer than those for uncoated tubes. In spite of this, the pyrolytic graphite coating was expected to preclude the formation of silicon carbide, so permitting matrix volatilization before the atomization step. Initial experiments were encouraging. By using pyrolytic graphite tubes, 80—100% of the original aluminium signal was restored, in the presence of 10 mg Si ml^{-1}. Unfortunately, the peak-height sensitivity was significantly affected by the presence of nitric acid and abruptly declined during the lifetime of the tube. The destructive effect of the nitric acid on the pyrolytic coating was probably responsible for such effects. Thus, use of the L'vov platform was expected to alleviate deterioration in performance.

Interference studies. A comparison was made of the effects of nitric acid, hydrofluoric acid and silicon on the absorbance of aluminium, injected onto various surfaces in the furnace. In each case, the concentration of concomitant was varied while the analyte concentration was kept constant. A series of blank analyses was performed; the signals reported, therefore, are the net ones. Figure 1(a) shows the effect of various amounts of nitric acid on the aluminium signal. A rather sharp enhancement of the signal was observed when the sample was injected onto the wall of a pyrolytic graphite tube. An uncoated tube, or pyrolytic tube and platform, showed a much smaller effect. The increase in signal between the uncoated tube and the pyrolytic tube with platform was about 60% over the range of nitric acid concentrations examined. Figure 1(b) shows the effect of hydrofluoric acid on the absorbance of aluminium. The platform again gave higher sensitivity. As the acid concentration increased, the signal from uncoated tubes tended to decrease.

To study the overall matrix effect, solutions obtained by dissolving increasing amounts of silicon were measured by using uncoated tubes, pyrolytic tubes and platforms. The ratio of the slope of the standard addition plot in

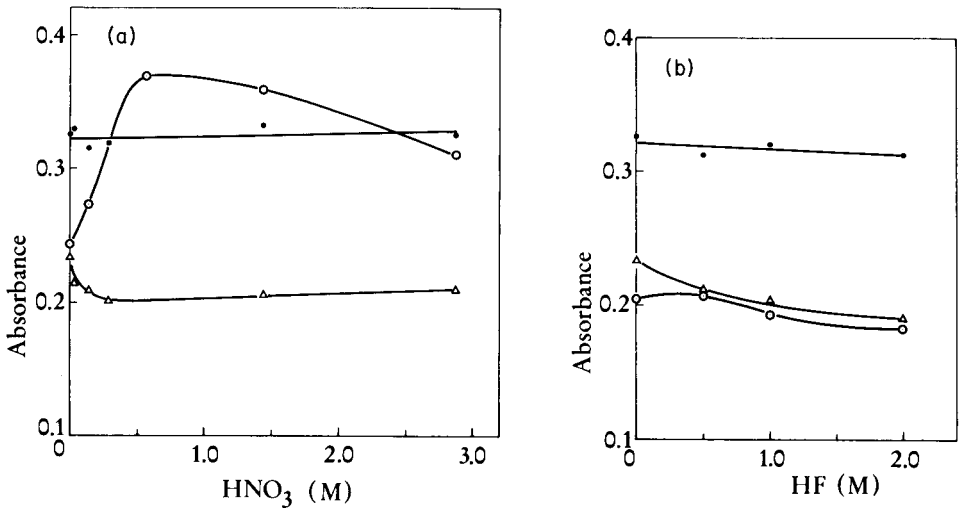

Fig. 1. Effect of (a) nitric acid and (b) hydrofluoric acid on the peak absorbance for 0.2 μg Al ml^{-1}: (△) uncoated graphite; (○) pyrolytically-coated graphite; (•) platform.

the presence of the matrix to the slope for solutions in 0.2% nitric acid gives a measure of the interference (Fig. 2). With uncoated tubes, the aluminium signal was severely suppressed (up to 80%) by 10 mg Si ml^{-1}; peak-height and peak-area measurements gave similar results. The determination was

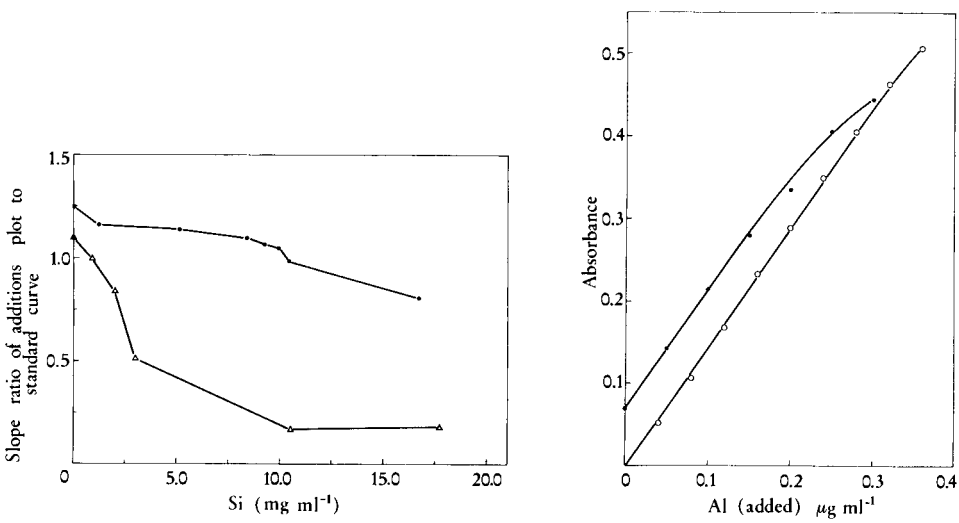

Fig. 2. The silicon interference on aluminium response in: (△) uncoated graphite tube; (•) pyrolytically-coated tube with pyrolytic platform.

Fig. 3. Calibration graphs for aluminium in: (○) 0.2% nitric acid; (•) silicon solution (5 mg ml^{-1}).

practically free from interference when a platform and pyrolytic tube were used; up to 17 mg Si ml^{-1} then had a <20% suppressive effect. An enhanced signal, i.e., a ratio greater than 1.0 in the absence of silicon, was obtained from a standard addition plot for a mixture of nitric and hydrofluoric acids. The composition (0.4 M HF, 1.0 M HNO_3) corresponded to the calculated excess of the two acids in the sample solution. The results obtained by using pyrolytic tubes without a platform, showed dramatic changes during the lifetime of the tubes, so that the data are not reliable enough to be reported.

Ashing stage. The effect of the final ashing temperature on the aluminium signal, in the presence of 8.0 mg Si ml^{-1}, is constant up to ca. 1200°C. There is a slight increase in signal with increasing ashing time at this recommended temperature. The same optimum ashing temperature was previously observed in the absence of silicon [1]. In contrast, the effect of ashing temperature in the presence of silicon, when uncoated tubes were used [1], was different, and the optimum temperature was 1400—1500°C. These facts help to explain the matrix effect. Silicon is primarily present in the decomposed sample solution as hexafluorosilicic acid and polymeric species. Despite the high volatility of silicon tetrafluoride, it seems reasonable not to exclude the retention of a certain amount of the silicon matrix in various chemical forms. When uncoated graphite tubes are used, conditions may favour the formation of silicon carbide. Equilibrium calculations for the silicon-carbon-oxygen system [4] have shown that silicon carbide may be formed at an extremely low partial pressure of oxygen, this being governed by the extent of the reaction between carbon and oxygen. Other studies, including kinetic measurement [5], show that silicon carbide is formed in uncoated tubes at above ca. 1700°C.

The physical occlusion of the analyte in this "new" matrix may retard the liberation of the atomic vapour. This is indicated by the change in the optimum ashing temperature and by the peak tailing observed with uncoated tubes. The pyrolytic coating prevents the formation of the carbide so that any silicon can be volatilized as the tetrafluoride. The platform decreases the extent of the interference and improves the reproducibility by decreasing the destructive effect of the acids on the tube wall.

Calibration graphs, detection limits and analytical results. Figure 3 shows the calibration graphs obtained for 0.2% nitric acid solutions and by standard addition to a silicon sample having a low aluminium concentration (ca. 7 $\mu g\ g^{-1}$). The original level of aluminium has not been subtracted from the sample readings. The linear range extends to about 0.30 $\mu g\ ml^{-1}$ in the absence of silicon. The two calibration graphs are almost parallel over a moderate concentration range, indicating the absence of any matrix effect. An important advantage of the platform is that it shows adequate performance in minimizing silicon interference after 250—300 firings. This is emphasized by Fig. 3. The calibration in 0.2% nitric acid was obtained by using a new platform, but that in the presence of silicon was obtained

TABLE 2

Limits of detection and recoveries for the determination of aluminium in silicon

	Detection limit[a] (μg Al g^{-1})	Relative standard deviation[b] (%)	Recovery (%)
Uncoated tube	1.2	7.2	98 ± 6
Pyrolytic tube and platform	0.2	2.2	102 ± 4

[a] 3 × standard deviation of the blank. [b] Calculated from 5 measurements of 0.2 μg Al ml^{-1} in the presence of 10.4 mg Si ml^{-1}.

after 300 firings. The slope ratio differs only by about 14% from that measured by using a new platform. Detection limits, precision and recoveries are listed in Table 2. Comparative results for uncoated tubes and platforms are given.

p-Type silicon, of declared resistivity 15—20 ohm cm^{-1}, was analyzed by the proposed procedure. The aluminium content was found to be 8.0 ± 0.8 μg g^{-1} (n = 8). The relative standard deviation was 10%, significantly worse than the peak-to-peak reproducibility (2.2%). One reason for this was the uncontrollable fluctuations of the blank values caused by environmental aluminium.

The author thanks Professor P. Lanza for valuable discussions. This work was supported by the National Research Council (C.N.R.), under a contract related to the "Progetto Finalizzato per la Chimica Fine e Secondaria". It was presented at the 23rd CSI/10th ICAS, Amsterdam, June, 1983.

REFERENCES

1 M. Taddia, Anal. Chim. Acta, 142 (1982) 333.
2 J. P. Matousek, Prog. Anal. At. Spectrosc., 4 (1981) 247.
3 W. Slavin and D. C. Manning, Prog. Anal. At. Spectrosc., 5 (1982) 243.
4 W. Frech and A. Cedergren, Anal. Chim. Acta, 113 (1980) 227.
5 G. Müller-Vogt and W. Wendl, Anal. Chem., 53 (1981) 651.
6 E. J. Hinderberger, M. L. Kaiser and S. R. Koirtyohann, At. Spectrosc., 2 (1981) 1.
7 D. C. Manning, W. Slavin and G. R. Carnrick, Spectrochim. Acta, Part B, 37 (1982) 331.
8 I. Havezov and E. Ivanova, Fresenius Z. Anal. Chem., 315 (1983) 26.
9 K. C. Thompson, K. Wagstaff and K. C. Wheatstone, Analyst (London), 102 (1977) 310.
10 D. C. Manning and W. Slavin, Anal. Chem., 50 (1978) 1234.
11 J. H. Runnels, R. Merryfield and H. B. Fisher, Anal. Chem., 47 (1975) 1258.
12 W. Slavin, D. C. Manning and G. R. Carnrich, Anal. Chem., 53 (1981) 1504.

Analytica Chimica Acta, 158 (1984) 137—141
Elsevier Science Publishers B.V., Amsterdam — Printed in The Netherlands

Short Communication

CHEMICALLY MODIFIED RETICULATED VITREOUS CARBON ELECTRODE WITH IMMOBILIZED ENZYME AS A DETECTOR IN FLOW-INJECTION DETERMINATION OF GLUCOSE

HENRY J. WIECK[a], GEORGE H. HEIDER, Jr. and ALEXANDER M. YACYNYCH*
Department of Chemistry, Rutgers, the State University of New Jersey, New Brunswick, NJ 08903 (U.S.A.)

(Received 4th April 1983)

Summary. The construction and response of a chemically modified electrode in which glucose oxidase (E.C. 1.1.3.4) is covalently attached to the surface of reticulated vitreous carbon is reported. Hydrogen peroxide produced by the oxidation of glucose is consumed at the electrode surface, which is held at +0.9 V vs. a saturated calomel reference electrode. The hydrodynamic and electrochemical properties of the reticulated vitreous carbon electrode substrate make the electrode attractive for use in flow systems. The current varies nonlinearly with glucose concentration throughout most of the range examined (10^{-1}—10^{-4} M). At concentrations of 2.5—10 mM, response is approximately linear with concentration, with a sensitivity of about 400 nA mM^{-1}. Relative standard deviation for five samples at 10 mM^{-1} is less than 2%.

The expanding field of immobilized enzymes has been reviewed by Carr and Bowers [1]. Immobilized enzymes have been utilized in a variety of electrodes. In the commonest version of such electrodes, a layer of trapped enzyme is held against an electrode surface where the products of the enzymatic reaction are sensed [2]. The products can be detected by either potentiometric or amperometric techniques. Although these electrodes combine the specificity of enzyme/substrate reactions with electrochemical detection, electrodes which are constructed with thick immobilized enzyme layers generally have long response times because of the time necessary for the electroactive species to diffuse through the enzyme layer, and there is a "memory effect" which often requires extensive rinsing in order to return to baseline response. Recently, chemically modified electrodes (c.m.e.) with immobilized enzymes have been constructed in which enzymes are covalently attached directly to the surface of carbonaceous electrodes [3, 4]. Ianniello et al. [5, 6] have shown that direct covalent immobilization of enzymes on chemically modified electrode surfaces yields devices having both superior response times and linear ranges.

Reticulated vitreous carbon (RVC) physically resembles a sponge with

[a]Present address: Department of Chemistry and Physics, Kean College of New Jersey Union, NJ 07083, U.S.A.

0003-2670/84/$03.00

small pores. The electroanalytical uses of this versatile material were recently reviewed by Wang [7]. The use of RVC in flowing systems has been advocated by Strohl and Curran [8]. This type of carbon has been produced in a number of forms, including RVC-S (which has a surface similar in electrochemical properties to glassy carbon), RVC-A which has a much larger activated surface area, and various compressed RVC derivatives; RVC-S is presently available in various porosities, ranging from 10 to 100 pores per inch. The preparation of a c.m.e. with immobilized enzyme based on RVC has been reported briefly [9]. The dynamic electrochemical response of this type of electrode is presented here for an electrode constructed of RVC-S to which glucose oxidase (E.C.1.1.3.4) is attached. Hydrogen peroxide produced by the enzymatic oxidation of glucose is detected amperometrically by its oxidation at the electrode surface. The electrode is used to quantify glucose in a flow-injection system [10].

Experimental

Reagents. Glucose oxidase was type II from *Aspergillus niger* (Sigma Chemical Co.). The water-soluble carbodiimide used was 1-cyclohexyl-3-(2-morpholinoethyl)-carbo-metho-*p*-toluene sulfonate (biochemical grade; Fluka). All other chemicals were of reagent grade, and only distilled/deionized water was used.

Preparation of the immobilized enzyme electrode. A slight alteration of the earlier method [9] was used. Cylinders (3-mm diameter, 15 mm long) of RVC were cut from a block of the material with a number 1 cork borer. The cylinders were washed in 6 M hydrochloric acid overnight and then washed with water until the effluent was neutral. The RVC was extracted overnight with anhydrous methanol in a Soxhlet apparatus, which was followed by oven-drying (110°C). The cylinders were then press-fitted into a plexiglas housing. Electrical connection was made through a hole in the plexiglas housing by bonding a piece of pencil lead (epoxy-bonded graphite, Grade RX, Dylon Industries, Cleveland, OH) to the RVC using conducting graphite epoxy. The cell design is shown in Fig. 1. The cell was then attached to a peristaltic pump and the RVC surface was activated by passing a 40 g l^{-1} solution of the water-soluble carbodiimide in pH 5.1 acetate buffer (0.05 M) through the cell for 30 min at a flow rate of 5 ml min^{-1}. The cell was then flushed with the same buffer (0°C) for 10 min. A solution of glucose oxidase in the same buffer (300 mg of enzyme per 50 ml of buffer) was maintained at 0°C while it was recirculated through the cell for 3 h. The cell was then flushed a second time for 10 min with the cold buffer. While the modified RVC prepared by this method exhibited less enzymatic activity than the previously reported modified RVC, this method always led to a successful attachment.

Apparatus. The potentiostat (Princeton Applied Research Model 364) was used in the d.c. mode. The output was recorded on a strip-chart recorder (Omniscribe; Houston Instruments). A Rainin peristaltic pump (Rainin

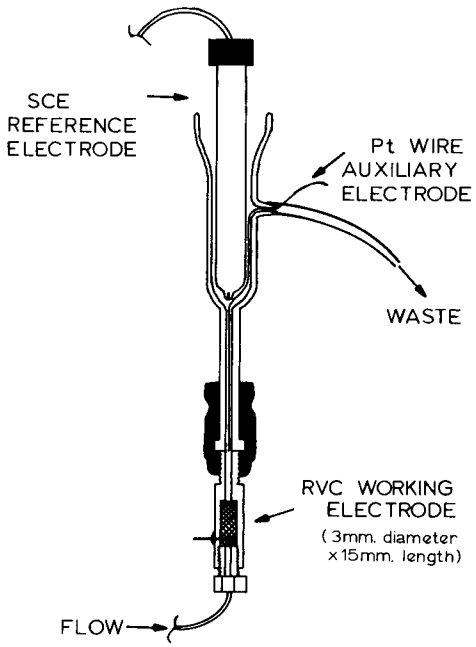

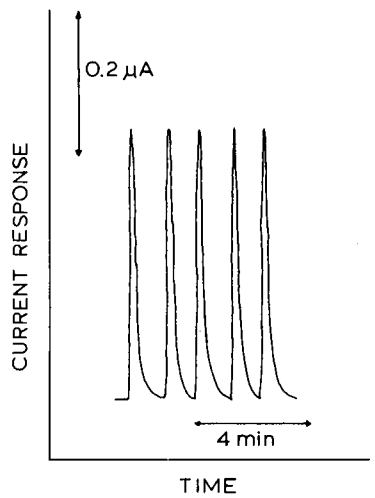

Fig. 1. Reticulated vitreous carbon flow cell showing the working, reference, and auxiliary electrodes.

Fig. 2. Typical electrode response to 100 μl of 10 mM glucose at a flow rate of 2.0 ml min^{-1}.

Instruments Rabbit) was used. The sample was introduced into the system through a Rheodyne injection valve, using a 100-μl sample loop. The auxiliary and reference electrodes were positioned downstream from the working electrode in a custom-built glass chamber (see Fig. 1). Samples were prepared in the same buffer (pH 6.5, 0.1 M phosphate buffer) that was used in the flow stream.

Results and discussion

Five peaks are presented in Fig. 2 to demonstrate the reproducibility of peak shape and peak height. The response of the electrode to the sample plug is essentially instantaneous, yielding the slightly tailing peaks normally encountered in flow-injection systems. The peak width (baseline to baseline) is about 48 s at a flow rate of 2.0 ml min^{-1} but increases to about 108 s at 0.5 ml min^{-1}. This indicates a sample throughput of 30—75 samples per hour, although the upper limit of useful flow rates has not been approached. The relative standard deviation (r.s.d.) of this set of peak heights is less than 2%.

Dispersion in flow-injection systems has been classified into three ranges, limited (D = 1—3), medium (D = 3—15) and large (D >15), where D is the

ratio of the sample concentration before and after the dispersion takes place. The dispersion found for the system in Fig. 2 (D = 8) falls within the medium range. In systems where one or several chemical reactions must occur, a medium degree of dispersion is desirable [11]. In this case, the small pores of the RVC insure that the sample is mixed efficiently with the carrier stream in a reproducible fashion. The electrode has a void volume of 0.095 cm^3 and can be thought of as consisting of many small, interconnected chambers.

The effect of varying the flow rate on the current response of the system, is shown in Fig. 3. The response decreases with increasing flow rate, first rapidly and then gradually.

Figure 4 shows the response of the working electrode to solutions of various concentrations of glucose. Similar results were obtained when peak areas were used. Reasons why curves level off at higher concentrations were not evaluated but probably include saturation of the enzyme with substrate. The response in the range of 2.5—10 mM, is approximately linear with a slope of 400 nA mM^{-1}. The choice of flow rate involves a compromise between sensitivity and sample throughput.

Electrodes which had been stored at 2°C in buffer for 40 days retained 30% of their initial activity. This far exceeds the lifetime of the free enzyme in solution [2].

This electrode system has faster response than a previously described electrode [12], and the overall flow system with the proposed detector appears to offer advantages relative to flow systems that include enzymes in the flow stream or immobilized in a packed column [13, 14]. The electrode construction may be useful in microdetectors described recently [15].

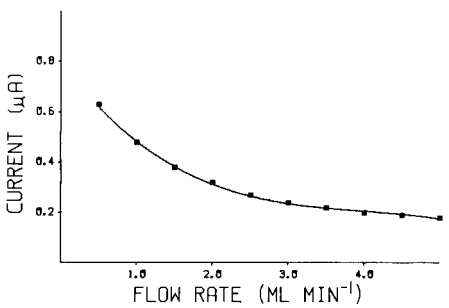

Fig. 3. Effect of flow rate on the response of the RVC electrode with immobilized enzyme. Injection volume 100 μl; 5 mM glucose.

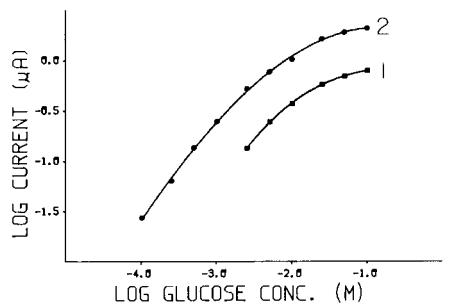

Fig. 4. Working curves showing the response (peak currents) of the RVC electrode with immobilized enzyme to various concentrations of glucose. Flow rates (1) 2 ml min^{-1}, (2) 0.5 ml min^{-1}.

A. M. Y. thanks the National Science Foundation (grant number CHE 8022237) for research support. This work was presented in part, as paper number 876, at the 1983 Pittsburgh Conference and Exposition on Analytical Chemistry and Applied Spectroscopy, Atlantic City, NJ.

REFERENCES

1 P. W. Carr and L. D. Bowers, Immobilized Enzymes in Analytical and Clinical Chemistry, Wiley-Interscience, New York, NY, 1980.
2 G. Rechnitz, Chem. Eng. News, January 27, 1975, Vol. 53, No. 4, p. 29.
3 C. Bourdillon, J. Bourgeois and D. Thomas, J. Am. Chem. Soc., 102 (1980) 4231.
4 R. Kamin and G. Wilson, Anal. Chem., 52 (1980) 1198.
5 R. M. Ianniello and A. M. Yacynych, Anal. Chem., 53 (1981) 2090.
6 R. M. Ianniello, T. J. Lindsay and A. M. Yacynych, Anal. Chem., 54 (1982) 1980.
7 J. Wang, Electrochim. Acta, 26 (1981) 1721.
8 A. Strohl and D. Curran, Anal. Chem., 51 (1979) 1045.
9 H. J. Wieck, C. Shea and A. M. Yacynych, Anal. Chim. Acta, 142 (1982) 277.
10 J. Růžička and E. H. Hansen, Flow Injection Analysis, Wiley-Interscience, New York, NY, 1981.
11 A. Ramsing, J. Růžička and E. Hansen, Anal. Chim. Acta, 129 (1981) 1.
12 W. Blaedel and J. Wang, Anal. Chem., 52 (1980) 1426.
13 E. H. Hansen, J. Růžička and B. Rietz, Anal. Chim. Acta, 89 (1977) 241.
14 J. Růžička, E. H. Hansen, A. K. Ghose and H. A. Mottola, Anal. Chem., 51 (1979) 199.
15 J. Růžička, Anal. Chem., 55 (1983) 1040A.

Analytica Chimica Acta, 158 (1984) 143—146
Elsevier Science Publishers B.V., Amsterdam — Printed in The Netherlands

Short Communication

PHOTOMETRIC TITRATION OF TOTAL IODINE AT TRACE LEVELS IN CONCENTRATED CHLORIDE SOLUTIONS

MARIA PESAVENTO* and RAFFAELA BIESUZ

Istituto di Chimica Generale e Inorganica, Università di Pavia, Viale Taramelli 12, 27100 Pavia (Italy)

(Received 1st June 1983)

Summary. The method is based on reduction of total iodine (10^{-7}—10^{-5} M), to iodide with sulphite in acidic solution. The excess of sulphur dioxide is removed by bubbling with nitrogen, and the resulting solution is titrated spectrophotometrically with a standard solution of iodate, the absorbance being measured at 230 nm. Some Italian table salts, iodized or common, were analyzed for their iodide and total iodine content.

It has been shown [1] that traces of iodide (2×10^{-7}—2×10^{-5} M) can be determined by a spectrophotometric titration with iodate in 0.5—5 M hydrochloric acid. The reaction is that of the Andrews—Jamieson titration, which is quantitative even at low iodide concentrations, and in 0.5 M hydrochloric acid [1]. This was not completely unexpected, for Swift [2] showed that the Andrews titration of iodide is quantitative even in 1 M hydrochloric acid, if the titrant is allowed to react for long enough; he attributed to kinetic reasons the earlier observations that quantitative oxidation of I^- to I^+ was impossible in hydrochloric acid less concentrated than 4—5 M. In the previous work [1], the reactions of I^- and I_2 with iodate were found to be rapid in 0.5—5 M hydrochloric acid. The slow step must therefore be the extraction of iodine from the organic phase, which is used to detect the endpoint in the Andrews—Jamieson titration.

The method proposed earlier [1] can be applied to many different samples, but its most interesting use is in the determination of traces of iodide in the presence of high concentrations of chloride. It is therefore suitable for the determination of iodide in table salt, and offers some advantages compared to that proposed by Sadusk and Ball [3], which is substantially accepted by the AOAC [4] for the determination of iodide in iodized table salt. The Sadusk and Ball procedure is based on the oxidation of iodide to iodate with bromine, removal of the excess of bromine and iodimetric titration of the iodate. Many interferences can be expected, e.g., from iron ions and atmospheric oxygen, as discussed by Sadusk and Ball [3]. Further, only 5 g of sodium chloride should be present in 100 ml if accurate results are to be achieved, which limits correct use of the method to >20 mg kg^{-1} iodide in the salt though its sensitivity is actually better.

0003-2670/84/$03.00

The spectrophotometric titration [1] is suitable for lower iodide concentrations (>0.08 mg kg^{-1}) and is applicable to common as well as iodized table salt. It is faster and chloride does not interfere. Some oxidants, e.g., nitrite, chromate and iodate, interfere at very low concentrations; iodate is particularly important, because it is present in sea water [5, 6] and can therefore be expected in table salt; it may also be added to iodized salt. It is shown here that such interferences can be eliminated by reduction with excess of sulphite in 0.5—5 M hydrochloric acid. Iodine, in all its oxidation states, is simultaneously reduced to iodide; excess of sulphite is then removed with a stream of inert gas (nitrogen or carbon dioxide) and iodide is titrated spectrophotometrically with iodate solution.

Experimental

The sample solution is prepared by dissolving a suitable amount of salt in water, and adding concentrated hydrochloric acid. The amount of acid added depends on the salt concentration required; the solubility of sodium chloride is about 30 g/100 ml in 0.5 M hydrochloric acid, but only 3 g/100 ml in 5 M acid. Thus, for small concentrations of iodide in table salt, a final hydrochloric acid solution 0.5 M is particularly suitable.

For the determination of very low amounts of iodide, a sample of about 30 g of table salt is dissolved in 100 ml of 0.5 M hydrochloric acid. Freshly prepared 0.1 M sodium sulphite solution (1 ml) is added. After about 1 min, nitrogen is bubbled through the solution for 30—60 min. Quantitative removal of sulphur dioxide is checked by measuring the absorbance of the solution at 230 nm at regular intervals; a steady absorbance (within ±0.002) is reached when the gas has been completely removed [1].

The titration is done with standard potassium iodate solution, obtained by diluting a 0.1 M stock solution. In order to titrate 100 ml of very dilute iodide solution (2×10^{-7}—2×10^{-6} M), 10^{-4} M iodate solution is suitable; the total volume of titrant needed is 0.1—1.1 ml. Analogously, a 10^{-3} M iodate solution is suitable for 2×10^{-6}—2×10^{-5} M iodide solutions. The titrant is added with a micropipette, so as to obtain at least five points before and three points after the end-point. The absorbance at 230 nm is recorded after each iodide addition, and the end-point is obtained graphically. The end-point corresponds to the reaction

$$2I^- + IO_3^- + 6H^+ \rightarrow 3I^+ + 3H_2O$$

where I^+ indicates all possible iodine chloride complexes (ICl, ICl_2^-, ..., $I_x Cl_y^{(x-y)}$ [1]).

Dilute iodate solutions ($\leqslant 10^{-4}$ M) must be prepared daily. The composition of the very dilute iodate solutions can be checked by titrating them in 0.5 M hydrochloric acid with standard iodide solutions. A two-step reaction takes place

$$IO_3^- + 2I^- + 6Cl^- \rightarrow 6I^+ + 3H_2O; \; I^+ + I^- \rightarrow I_2$$

and the titration can be followed spectrophotometrically at 230 nm. The first end-point is sharp enough even with 2×10^{-7} M iodate concentrations; the second is detectable only at concentrations $>2 \times 10^{-6}$ M, because of iodine(0) disproportionation [1].

Results and discussion

Several samples of commercial Italian table salt, iodized to different degrees or not iodized, were analyzed as described above. The results are reported in Table 1. All the samples were analyzed by the spectrophotometric titration with standard iodate both for iodide (i.e., without reduction with sulphite) and for total iodine as described above.

The freshly prepared solutions mostly show only a small difference between the two determinations. The results indicate that iodine is present mainly as iodide in these table salts, the difference between the two determinations never exceeding about 8%. In a few cases (e.g., sample 6), the difference is significant, so that the reduction procedure is useful. Some of the samples were spiked with iodide or iodate in order to check the recoveries.

TABLE 1

Results obtained for Italian commercial table salts[a]

Sample No.	Sample	Iodine added	I^- found[b]	Total iodine found	
				Proposed method	AOAC method [4]
1	Iodized	—	1.66 ± 0.05	1.81 ± 0.05	2.4
	marine salt	1.69[c]	<0.08	3.47 ± 0.06	
		—[d]	<0.08	1.81 ± 0.05	
2	Iodized	—	<0.08	<0.08	3.7
	marine salt[e]	0.85[c]	<0.08	<0.86 ± 0.03	
		0.34 (as I^-)	0.38 ± 0.02	0.36 ± 0.02	
3	Iodized salt[f]	—	0.49 ± 0.03	0.53 ± 0.03	
		—	<0.08[g]	0.54 ± 0.04[g]	
4	Common salt	—	6.18 ± 0.08	6.60 ± 0.10	6.3
		1.69[c]	2.37 ± 0.06	8.29 ± 0.09	
		—	5.93 ± 0.08[h]	6.60 ± 0.08[h]	
5	Iodized salt[i]	—	7.06 ± 0.07	7.62 ± 0.08	9.5
6	Iodized	—	5.08 ± 0.07	6.53 ± 0.07	9.0
	marine salt	—	3.30 ± 0.06[h]	6.52 ± 0.07[h]	
7	Iodized salt[j]	—	1.35 ± 0.04	1.47 ± 0.05	2.4
		0.85 (as I^-)	2.25 ± 0.05	2.42 ± 0.05	
		—	<0.08[h]	1.42 ± 0.05[h]	
8	Marine salt	—	<0.08	<0.08	
		0.34 (as I^-)	0.42 ± 0.03	0.51 ± 0.03	
		0.17 (as I^-)	0.25 ± 0.03		
9	NaCl	—	<0.08	<0.08	
	(RPE C. Erba)	0.34 (as I^-)	0.41 ± 0.03	0.45 ± 0.03	
		0.17 (as I^-)	0.25 ± 0.03	0.25 ± 0.03	

[a]All the concentrations in the salts are expressed as iodine in mg kg^{-1}. The results given are mean values with standard deviation on three determinations. [b]Ref. 1. [c]As iodate. [d]With 39.2 mg ml^{-1} $K_2Cr_2O_7$ added. [e]Declared content: ⩾15 mg kg^{-1}. [f]Declared content 0.49 mg kg^{-1}. [g]Two days after preparation of the solution. [h]One day after preparation of the solution. [i]Declared content: 12.7 mg kg^{-1}. [j]From Sardinia.

Recoveries of added iodide were generally good (samples 2, 7, 8, 9). When iodate was added and iodide was present, of course iodide was not recovered, whereas recovery of the total iodine by the reduction method was not affected (samples 1, 4). Strong oxidants, such as dichromate (sample 1), caused low recovery of iodide but did not affect the determination of total iodine, if sulphite was added in sufficient excess. Some solutions were also analyzed 1—2 days after their preparation. In such cases the iodide determination gave variable results (samples 3, 4, 6), but the total iodine concentration remained constant.

Samples with iodine contents exceeding 1 mg kg^{-1} were also analyzed by the AOAC method [4]; in most cases, the iodine concentrations found were higher (Table 1). The result for sample 2 is particularly high; this sample contained 9.2 mg kg^{-1} total iron, which oxidized to iron(III) by bromine and then releases iodine in the iodimetric titration [4], thus accounting for the high result.

The total iodine found was almost always less than that declared by the manufacturers (samples 2, 3, 5). The samples had been stored for 6—12 months before the analysis, and it is well known that the iodine content of iodized salts decreases with time [3, 7].

As iodide concentrations as low as about 2×10^{-7} M can be detected by this method, an attempt was made to analyze directly a sea-water sample collected at the surface of the Ligurian sea (Italy), near the shore line. Only an upper limit could be determined (<26 $\mu g\ l^{-1}$). Therefore, a 500-ml aliquot was evaporated to 50 ml on a boiling water bath, and the procedures for iodide and total iodine were applied. The results were 14 $\mu g\ l^{-1}$ and 21 $\mu g\ l^{-1}$, respectively; these are meaningless in terms of distribution between the different oxidation states of iodine in the original water, but the value for total iodine appears to be a reasonable estimate, consistent with values reported earlier for sea water [5, 6].

We thank the Istituto Richerche Siturezza Industriale—Milano for financial support to R. B.

REFERENCES

1 M. Pesavento, Anal. Chim. Acta, 153 (1983) 249.
2 E. H. Swift, J. Am. Chem. Soc., 52 (1930) 894.
3 T. F. Sadusk and E. G. Ball, Ind. Eng. Chem., Anal. Ed., 5 (1933) 386.
4 AOAC Methods, No. 33147, (1980), p. 566.
5 A. D. Mattheus and J. P. Riley, Anal. Chim. Acta, 51 (1970) 295.
6 M. M. Schnepfe, Anal. Chim. Acta, 58 (1972) 83.
7 P. W. F. Fisher and M. L'Abbé, Can. Inst. Food Sci. Technol. J., 13 (1980) 103.

0003-2670/84/$03.00

Printed in The Netherlands

VOL. 158 No. 1 ANALYTICA CHIMICA ACTA APRIL 1, 1984

CONTENTS

(Abstracted, Indexed in: Anal. Abstr.; Biol. Abstr.; Chem. Abstr.; Curr. Contents Phys. Chem. Earth Sci.; Life Sci.; Index Med.; Mass Spectrom. Bull.; Sci. Citation Index; Excerpta Med.)